

Dynamics of Advanced Polymer Systems studied by Dielectric Spectroscopy and Rheology: From Binary Glass Formers to Nanocomposites

Von der Universität Bayreuth
zur Erlangung des Grades eines
Doktors der Naturwissenschaften (Dr. rer. nat.)
genehmigte Abhandlung

von
Fathia Mohamed
geboren am 27.09.1984 in Kalyobiya, Egypt

1. Gutachter: Prof. Dr. Ernst Rößler
2. Gutachter: Prof. Dr. Roland Böhmer

Tag der Einreichung: 02. 03. 2018

Tag des Kolloquiums: 04. 06. 2018

Table of Contents

I. Abstract	5
II. Kurzdarstellung.....	7
1. Introduction	10
2. Neat glass formers	12
2.1. Properties of the Liquid - quantities of interest	12
2.2. Relaxation processes in molecular glass formers: simulation and experiment	14
2.3. Generic features of polymer dynamics.....	18
3. Experiments.....	22
3.1 Dielectric spectroscopy	22
3.2. Shear experiment	25
3.3 Polymer models.....	27
4. Dynamics of binary mixtures	30
4.1 State-of-the-art.....	30
4.2 Results	33
4.2.1 Mixtures studied.....	33
4.2.2 Main relaxations	34
4.2.2.1 Neat system	34
4.2.2.2. Mixtures.....	36
4.2.3 Discussion	44
4.3 Secondary process in binary glass formers	46
4.3.1 Results	46
4.3.3 Discussion	48
5. Dynamics of linear polymers.....	49
5.1 State-of-the-art.....	49
5.2 Results	50
5.2.1 Polymers studied	51
5.2.2 Polymer dynamics studied by dielectric spectroscopy	51
5.2.3 Discussion	56
5.3 Viscoelastic properties of PI and PB	56
5.3.1 Testing FTS	58
5.3.2 Scaling analysis	63
5.3.3 Discussion	65
6. Dynamics of polymer nanocomposites	70

6.1 State-of-the-art.....	70
6.2 Results	71
6.2.1 Systems investigated	71
6.2.2 Dielectric spectroscopy	73
6.3 Rheology	80
6.3.1 Comparison of the rheological and dielectric Master curves	81
6.3.2 Discussion	83
7. Dynamics of Dendrimers.....	87
7.1 State-of-the-art.....	87
7.2 Results	88
7.2.1 Systems measured	88
7.2.2 DS results in PPI dendrimers.....	89
7.2.3. Discussion	92
References	95
Appendix	116
List of Publications.....	117
Acknowledgments	118

I. Abstract

In this thesis, the dynamics of molecular as well as polymeric glass formers is investigated by measuring their dielectric (DS) and rheological response. The temperature evolution of primary (α) and secondary (β) relaxations of binary glass formers, linear polymers, and dendrimers is one focus. Another objective is to gain insight into the collective dynamics of polymer melts and its change in the presence of nanoparticles.

Two asymmetric binary glass formers with large T_g contrast of their components ($\Delta T_g = 176$ K and 222 K) are analyzed by DS. They are made from organophosphates (m-TCP or TPP) as low- T_g components and especially synthesized spirobichroman derivatives (DH379 or SBC) as high- T_g components. Two main relaxations are observed for all concentrations. The slower (α_1) process is assigned to the dynamics of the high- T_g component and the faster (α_2) process to that of the low- T_g component (additive). Consequently two distinct T_g values (T_{g1} and T_{g2}) are obtained. The α_2 -process broadens with decreasing concentration (c_{add}) of the additive as well as frequency-temperature superposition (FTS) fails. The relaxation time $\tau_{\alpha_2}(T)$, and thus T_{g2} , increases with decreasing c_{add} , reflecting the anti-plasticizer effect. At low c_{add} , $\tau_{\alpha_2}(T)$ crosses over from a super-Arrhenius ($T > T_{g1}$) to an Arrhenius temperature dependence ($T \leq T_{g1}$) (fragile-to strong-transition). This crossover leads to a re-decrease of T_{g2} at low c_{add} , resulting in a maximum of $T_{g2}(c_{\text{add}})$. As proven by NMR in this regime, the additive molecules perform an isotropic (liquid-like) motion in an arrested matrix of the high- T_g component. In contrast to the α_2 -process, the α_1 -process only weakly broadens with increasing c_{add} , showing features similar to that of neat glass formers. By inspecting the dielectric relaxation strength, indications are found that a fraction of the additive molecules are participating in the α_1 -process. All features observed are similar to those previously reported for polymer-plasticizer systems. Furthermore, the secondary (β -) relaxation in the binary mixture (TPP /SBC) is investigated at $T < T_{g2}$. This process resembles that of neat TPP and does not show any concentration dependence. NMR results suggest that the TPP molecules enslave the SBC molecules to participate in the β -process.

The rheological relaxation spectra of linear poly(isoprene) (PI), and poly(butadiene) (PB) were measured in a wide temperature as well as wide molar mass M (up to $M = 1000$ kg/mol) range. By applying FTS, master curves $G''(\omega\tau_\alpha)$ and $G'(\omega\tau_\alpha)$ for a large frequency range are obtained showing the polymer relaxation, while a single spectrum displays the α -process.

Thereby, the entire frequency range of 12 decades is covered. In order to identify the different power law regimes along their characteristic exponents of $G''(\omega\tau_\alpha) \propto \omega^\varepsilon$, a derivative method is applied. The method offers several advantages compared to conventional analyses of $G''(\omega\tau_\alpha)$. The exponent $\varepsilon(\omega\tau_\alpha)$ is highly similar among polymers. For the polymer part, the exponent $\varepsilon(\omega\tau_\alpha)$ exhibits subtle features from which the Rouse regime exponent and entanglement time τ_e are disclosed. The exponent $\varepsilon(\omega\tau_\alpha)$ characterizing the high-frequency flank of the terminal relaxation process $\varepsilon_{eCLF} = -0.21 \pm 0.01$ is found which is close to the prediction of the tube reptation model including contour length fluctuation CLF. At lower frequencies a second regime with lower $\varepsilon(\omega\tau_\alpha)$ is revealed signaling the crossover to coherent reptation. All features provided by the derivative method agree well with those suggested by Likhtman-McLeish (LM) theory. Moreover, the exponent $\varepsilon(\omega\tau_\alpha)$ describing the low-frequency flank of the α -process deviates from that of the simple liquid, from which an onset frequency of the polymer dynamics may be defined. Furthermore, the M dependency of τ_{\min} describing the minimum in $G''(\omega\tau_\alpha)$ and the terminal relaxation time τ_t is revealed.

After studying neat PI, coated nanoparticles PI@PbS, and its polymer nanocomposites PNCs (PI@PbS/PI), were investigated by means of DS and shear rheology. The α -process and the normal mode (n) relaxation observed in neat PI are rediscovered in PI@PbS. The dielectric relaxation times $\tau_n(T)$ and $\tau_\alpha(T)$ of PI@PbS particles slightly increase compared to those of the corresponding neat PI. The spectral shape of the α -process does not change, while the n-mode relaxation broadens, in particular, on its high-frequency flank of $\varepsilon'' \propto \nu^{-\gamma}$. In addition, a slow “composite mode” is identified by DS and rheology. This mode is more separated from the n-mode in the case of PI@PbS containing short PI chains and becomes more pronounced. The composite mode leads to a strong increase of viscosity. Furthermore, in the PNCs of PI@PbS/PI, the value of the exponent γ decreases with increasing the PI@PbS weight fraction w . Also, the strength of the composite mode decreases with decreasing w .

Finally, the dynamics of the poly (propyleneimine) (PPI) dendrimers of generations G (2-5) were investigated. In addition to the α -process, two secondary processes ($T < T_g$) are identified. The relaxation time of the α -process, extended to higher temperatures by including those from field cycling (FC) NMR, changes only weakly with G . The DS findings are similar to those observed in hyperbranched polymers.

II. Kurzdarstellung

In dieser Arbeit wird die Dynamik von niedermolekularen und polymeren Glassbildnern mit Hilfe der dielektrischen Spektroskopie (DS) und Rheologie untersucht. Die Temperaturentwicklung von primärer (α) und sekundärer (β) Relaxation binärer Gläser, linearer Polymere und Dendrimere werden in den Fokus gerückt. Ein weiteres Ziel der Arbeit ist, Einblick in die kollektive Dynamik von Polymerschmelzen zu erhalten und die Veränderung bei Zugabe von Nanopartikeln zu studieren.

Zwei asymmetrische binäre Glasbildner mit großem T_g -Kontrast der Komponenten ($\Delta T_g = 176$ K and 222 K) wurden mit Hilfe der DS untersucht. Als Komponenten wurden Organophosphate (mTCP oder TPP) als Additiv mit niedrigem T_g , und speziell hergestellte Spirobichroman-Derivate (DH379 oder SBC) als hoch- T_g Komponente gewählt. Zwei Primärrelaxationen werden für alle Konzentrationen beobachtet. Der langsamere (α_1) Prozess wird der Dynamik der Hoch T_g - Komponente zugeschrieben, der schnellere (α_2) Prozess der Additivkomponente. Somit erhält man zwei unterscheidbare T_g - Werte (T_{g1} and T_{g2}). Der α_2 Prozess verbreitert sich mit abnehmender Konzentration des Additivs (c_{add}), gleichzeitig schlägt das Frequenz-Temperatur-Superpositionsprinzip (FTS) fehl. Die Relaxationszeit $\tau_{\alpha_2}(T)$ nimmt mit abnehmender Konzentration c_{add} zu, und damit auch T_{g2} , den Anti-Weichmachereffekt widerspiegelnd. Bei kleinen Konzentrationen c_{add} geht die Relaxationszeit von einer superarrhenius- ($T > T_{g1}$) zu einer arrheniusförmigen ($T \leq T_{g1}$) Temperaturabhängigkeit über (fragile-to- strong transition). Dieser Übergang führt zu einer Wiederabsenkung von T_{g2} bei kleiner Konzentration c_{add} , was zu einem Maximum von T_{g2} (c_{add}) führt. Wie NMR-Experimente in diesem Bereich zeigen, führen die Additivmoleküle eine isotrope (flüssigkeitsartige) Bewegung in einer starren Matrix der Hoch- T_g Komponente aus. Im Gegensatz zum α_2 -Prozess verbreitert sich der α_1 -Prozess nur schwach mit zunehmender Konzentration c_{add} und zeigt Merkmale reiner Glassbildner. Indem die Stärke der dielektrischen Relaxation untersucht wurde, konnten Hinweise gefunden werden, die auf eine teilweise Beteiligung der Additivmoleküle am α_1 -Prozess hindeuten. Alle beobachteten Eigenschaften sind ähnlich zu den Beobachtungen, die vorher für Polymer/Weichmacher-Systeme dokumentiert wurden. Weiterhin wurde die sekundäre (β) Relaxation in der binären Mischung (TPP/SBC) für Temperaturen $T < T_{g2}$ untersucht. Dieser Prozess ähnelt dem von reinem TPP und zeigt keinerlei Konzentrationsabhängigkeit. NMR-Ergebnisse legen nahe, dass die TPP Moleküle die SBC Moleküle dazu versklaven am β -Prozess teilzunehmen.

Die rheologischen Relaxationsspektren von linearem Poly(isopren) (PI) und Poly(butadien) (PB) wurden in einem großen Temperatur- und molaren Massebereich (bis zu $M = 1000$ kg/mol) gemessen. Durch FTS erhält man Masterkurven $G''(\omega\tau_\alpha)$ und $G'(\omega\tau_\alpha)$ für einen großen Frequenzbereich, der die Polymerrelaxation zeigt, während ein einzelnes Spektrum die α -Relaxation zeigt. Damit, kann der gesamte Frequenzbereich von 12 Dekaden abgedeckt werden. Um die verschiedenen Potenzgesetzabschnitte mit ihren charakteristischen Exponenten $G''(\omega\tau_\alpha) \propto \omega^\varepsilon$ zu identifizieren, wurde eine Ableitungsmethode angewandt. Diese Methode bietet einige Vorteile verglichen mit herkömmlichen Auswertungen von $G''(\omega\tau_\alpha)$. Der Exponent $\varepsilon(\omega\tau_\alpha)$ ist sehr ähnlich zwischen verschiedenen Polymeren. Für den Polymerteil zeigt $\varepsilon(\omega\tau_\alpha)$ subtile Merkmale, aus denen der Rouseexponent und die Entanglementzeit τ_e hervorgehen. Der Exponent $\varepsilon(\omega\tau_\alpha)$ der hoch frequenten Flanke des terminalen Relaxationsprozesses $\varepsilon_{eCLF} = -0.21 \pm 0.01$ wurde gefunden. Dieser Wert ist nah an der Vorhersage des Reptationsmodells unter Berücksichtigung von Konturlängenfluktuationen (CLF). Bei kleineren Frequenzen wird ein zweiter Bereich mit kleinerem $\varepsilon(\omega\tau_\alpha)$ ersichtlich, den Übergang zu kohärenter Reptation anzeigend. Alle Merkmale die durch die Ableitungsmethode bestimmt sind, stimmen mit den Vorraussagen der Likhtman-McLeish (LM) Theorie überein. Ferner weicht der Exponent $\varepsilon(\omega\tau_\alpha)$ an der Niederfrequenzflanke des α -Prozesses von einer einfachen Flüssigkeit ab. Das Abweichen kann als die Einsetzfrequenz der Polymerdynamik definiert werden. Weiterhin wird die M Abhängigkeit von τ_{\min} , welche das Minimum in $G''(\omega\tau_\alpha)$ beschreibt, und der terminalen Relaxationszeit τ_i aufgedeckt.

Nachdem reines PI studiert wurde, konnten ummantelte Nanopartikel PI@PbS und deren Polymernanokomposite (PI@PbS/PI) mit Hilfe von DS und Scheerreologie untersucht werden. Der α -Prozess und die Normalmode (n), die in reinem PI beobachtet wurden, werden in PI@PbS wiedergefunden. Die dielektrischen Relaxationszeiten $\tau_n(T)$ und $\tau_\alpha(T)$ der PI@PbS Partikel sind gegenüber dem entsprechendem reinen PI leicht erhöht. Die spektrale Form des α -Prozesses verändert sich nicht, die Normalmode hingegen verbreitert sich, insbesondere auf ihrer hochfrequenten Flanke von $\varepsilon'' \propto \nu^{-\gamma}$. Zusätzlich wird eine langsame „Kompositmode“ dielektrisch und rheologisch erkannt. Diese Mode ist für PI@PbS mit kurzen PI Ketten stärker von der Normalmode separiert und ist dort deutlich ausgeprägt. Die Kompositmode führt zu einem starken Anstieg der Viskosität. Zudem nimmt in den PI@PbS mit steigendem Gewichtsanteil w der Wert des Exponenten γ ab. Außerdem nimmt die Stärke der Kompositmode mit abnehmendem w ab.

Schließlich wird die Dynamik der Poly-(propylenimin)-(PPI)-dendrimere der Generationen G (2-5) untersucht. Zusätzlich zum α -Prozess werden zwei Sekundärprozesse ($T < T_g$) bestimmt. Die Relaxationszeit des α -Prozesses, bei hohen Temperaturen durch Feldzyklus-NMR-Messungen ergänzt, ändert sich nur schwach mit G. Diese DS Ergebnisse sind ähnlich zu den Beobachtungen in hyperverzweigten Polymeren.

1. Introduction

Glasses are used by mankind since prehistoric times, and are nowadays of paramount technological interest as they are found everywhere in our daily life, e.g., architecture, optical fibers, medicines, and so on. Many varieties of matter can form a glass, e.g. silica based materials, ionic liquids, polymers, ceramics, plastics and almost all simple liquids.

When rapidly cooling a liquid below its melting point T_m , giving it not sufficient time to crystallize, a super-cooled liquid is formed. Further cooling leads to a glass. Super-cooling is accompanied by a tremendous increase of the viscosity from 10^{-3} Pa·s ($T > T_m$, with T_m being the melting temperature) to 10^{12} Pa·s ($T < T_m$). In other words, the liquid solidifies on the experimental time scale and thus it is unable to flow. Consequently, the time required by the system to equilibrate its structure gradually increases on the order of minutes or even years. The glass transition point T_g is conventionally defined as the temperature at which the structural relaxation time τ_α reaches a value $\tau_\alpha = 100$ s. In the glassy state ($T < T_g$) often a secondary (β -) relaxation is found which merges with the structural (α -) relaxation at $T > T_g$.

The properties of glass formers can be adjusted by mixing with each other. If the T_g values of both components are close to each other, a dynamically homogeneous mixture is formed. In contrast, mixing two components of highly different T_g values results in a complex dynamical behavior. Such "asymmetric" mixtures may exhibit two distinct T_g values. This behavior was intensively studied in polymer blends or polymer-additive mixtures. Up to now, it is not clear whether the measured effects are controlled by the polymer-nature or by the high " T_g contrast" of the components. The question is addressed in this work by studying two binary glass formers with a high T_g contrast which are of non-polymeric nature. Specially synthesized molecular high- T_g glass formers are mixed with simple liquids as low- T_g component and they are investigated by DS and the results are compared with those reported by nuclear magnetic spectroscopy (NMR).

A relaxation scenario more complex than that of low-molecular glass formers emerges in polymers. In addition to α - and β -relaxations, the polymer chains perform breathing motions described by the Rouse model at low molar mass M . Above a critical mass (M_c) the chains are entangled and the tube-reptation (TR) model applies. The TR model describes the chain as being confined in a virtual tube made by its neighbors performing a snake-like motion. In the present work, the dynamics of neat polymers is investigated by a combined study of dielectric

spectroscopy and rheology. Furthermore, polymer dynamics in blends with nanoparticles, so-called polymer nanocomposites (PNCs) are of interest. In particular, the inorganic nanoparticles are coated by the polymer in order to avoid aggregation. Finally, dendrimers, which are repetitively branched polymers with a functional core in the center, are addressed in the course of this work.

The thesis is structured as follows. Chapter 2 gives a brief introduction about the relaxation features of glass formers as well as polymers. Chapter 3 provides information on the theoretical and experimental aspects of dielectric and mechanical spectroscopy. In chapter 4, the state-of-the-art on the main relaxation in binary glass formers (section 4.1) is given, and followed by the experimental results obtained in the course of this work on asymmetric binary mixtures (section 4.2). The experimental results collected on the secondary relaxation in binary glass formers as well as in polymers are discussed in section 4.3. Chapter 5 presents the dielectric and rheological response for linear polymers and their comparisons to each other. Furthermore, the dielectric and rheological response for the PNCs is presented and discussed in chapter 6. Finally, chapter 7 deals with the dielectric response of poly(propyleneimine) dendrimers.

2. Neat glass formers

2.1. Properties of the Liquid - quantities of interest

A liquid is a form of condensed matter, i.e. an ensemble of particles (e.g. atoms, molecules, monomeric units of polymer chains or particles of colloidal suspensions) with inter-particle distances on the order of the particle size [1]. In contrast, gases show much larger inter-particle distances. Liquids exhibit no long range order, contrary to crystals. This is reflected in the radial distribution function $g(r)$ showing damped oscillations, which vanish at long distance r [2]. Alternatively, one can define a liquid as a dense ensemble of particles which is able to flow, i.e. the shear modulus vanishes.

By cooling the liquid below its melting temperature T_m and avoiding crystallization a super-cooled liquid is formed. The thermodynamical variables like the thermodynamic potential, the heat capacity or the specific volume undergo only small changes, while the viscosity η or the reciprocal of the diffusion coefficient D^{-1} and consequently the structural relaxation τ increase continuously over decades until they reach values of a typical solid [3]. Further cooling leads to a transition from a super-cooled liquid to a glass below T_g characterized by structural arrest on the time scale of the experiment. Although many theories have been invoked, the underlying physical phenomenon of the glass transition is not fully understood yet [5,7]. The most intriguing theory is the mode coupling theory (MCT) which explains the phenomenon assuming a dynamical phase transition [1,8].

Experimentally, different techniques are used to study the relaxation response of glass formers (*cf.* Figure 1). The most important techniques covering the range from picoseconds to nanoseconds are neutron scattering (NS) [9-12], light scattering applying double monochromator combined with Fabry-Perot interferometer (DM/FPI) [13-17], optical Kerr effect (OKE) [18-20], and in some cases dielectric spectroscopy (DS) [21,22]. Below T_m (super-cooled liquid) or at times $t > 10^{-9}$ s, DS [23-25], NMR [26-31] including field cycling NMR relaxometry [32, 33], and photon correlation spectroscopy (PCS) [34-37] give valuable information about the dynamical processes in liquids and polymers. Among all these techniques, DS provides the widest dynamical range. Furthermore, DS has a large resolution, a dielectric loss of $\epsilon'' \sim 10^{-4}$ can still be accurately measured. Yet, DS is unselective unlike NMR, which can follow the dynamics of distinct molecules in a mixture or distinct bonds in the molecules. Besides all mentioned techniques, shear experiments provide dynamical

information on macroscopic scale which may be connected to the microscopic dynamics revealed by NMR, NS, DS [38, 39]. Altogether, 14 decades have to be covered to monitor the response of a glass former.

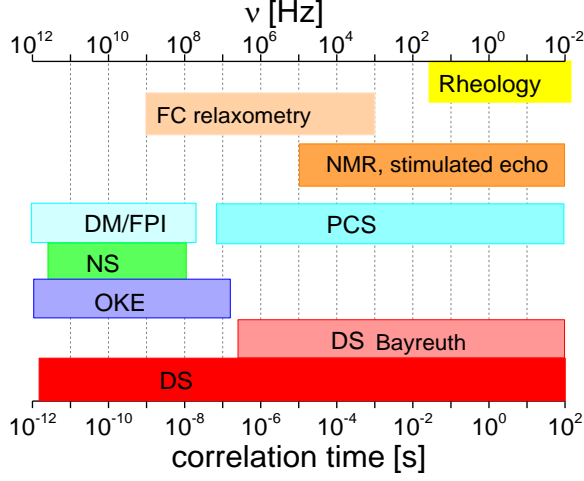


Figure 1: Time window of the most important experimental methods studying molecular dynamics: neutron scattering (NS), double monochromator / Fabry-Perot interferometer (DM/FPI), photon correlation spectroscopy (PCS), Optical Kerr effect (OKE), field cycling (FC) relaxometry and two dimensional NMR.

The essence of detecting molecular motion is to measure the fluctuations in the thermal equilibrium which are characterized by a time correlation function of the relevant physical quantities, defined as,

$$C_A(t) = \langle A(0) \cdot A(t) \rangle \quad (1)$$

$A(t)$ is the fluctuating quantity, and $\langle \rangle$ denotes an ensemble average [40]. The Fourier transform of a correlation function gives the spectral density $J_A(\omega)$ according to the Wiener-Khintchine theorem [41, 42],

$$J_A(\omega) = \frac{1}{2} \int_{-\infty}^{\infty} C_A(t) \exp[-i\omega t] dt. \quad (2)$$

A correlation time τ can be defined as,

$$\int_0^{\infty} C_A(t) dt = J_A(0) = \tau \quad (3)$$

In some experiments, the correlation function or the spectral density are directly probed, e.g. in scattering and NMR experiments. In other experiments like in dielectric spectroscopy or rheology, a macroscopic response to a small external perturbation, is probed. Assuming linear response, the macroscopic response can be linked to the corresponding correlation function by the Fluctuation Dissipation Theorem (FDT) [40]. Thus, the spectral density $J_A(\omega)$ and the corresponding (dynamic) susceptibility $\hat{\chi}(\omega)$ are connected along,

$$\text{Im} [\widehat{\chi}_A(\omega)] = \chi_A''(\omega) = \chi_0 \frac{\omega}{k_B T} J_A(\omega) \quad (4)$$

with χ'' being the imaginary (loss) part of the complex susceptibility, and χ_0 denotes their static part.

For the rheological measurement, the stress (off-diagonal) tensor autocorrelation function $G(t)$ is probed,

$$G(t) = \frac{V}{k_B T} \langle \sigma_{ab}(t) \sigma_{ab}(0) \rangle \quad (5)$$

with σ_{ab} being the off-diagonal component of the stress-tensor.

In the case of dielectric spectroscopy, the autocorrelation function of the macroscopic polarization \vec{P} is probed, [43]

$$C_P(t) = \frac{\langle \vec{P}_{or}(0) \vec{P}_{or}(t) \rangle}{\langle \vec{P}_{or}(0) \vec{P}_{or}(0) \rangle} \approx C_\mu(t) = \frac{1}{N\mu^2} \sum_{i=1}^N \left\langle \vec{\mu}_i(0) \vec{\mu}_i(t) \right\rangle \cong \frac{1}{\mu^2} \langle \vec{\mu}(0) \vec{\mu}(t) \rangle \quad (6)$$

with P_{or} is the orientational polarization which is defined as the sum of all N molecular dipoles μ_i in a given volume V , $P = \frac{1}{V} \sum_i \mu_i$. In the right identity negligible cross-correlation

terms are assumed, and thus the autocorrelation function of the macroscopic polarization is identical to the microscopic dipole-dipole autocorrelation function [43].

A characteristic property of many susceptibilities of a liquid is that frequency-temperature superposition (FTS) holds, i.e. the spectral shape of $\chi_A''(\omega)$ is temperature independent. Thus, by applying a temperature dependent frequency shift factor a_T , a master curve can be built; the idea is well established in rheology,

$$\chi''(\omega) \equiv \widetilde{\chi}''(\omega a_T) \quad (7)$$

In many cases instead of a_T the structural relaxation τ_α is taken.

2.2. Relaxation processes in molecular glass formers: simulation and experiment

Molecular dynamic (MD) simulations of a supercooled liquid can be described by introducing the (incoherent) intermediate scattering function $F_s(q, t)$ which reflects the autocorrelation of the position of a tagged particle. Figure 2 shows $F_s(q, t)$ of a Lennard-Jones (LJ) liquid at different temperatures and constant q (wave vector). At high temperatures, the function decays exponentially. Upon cooling down, the decay shifts to longer time and a shoulder appears. With further cooling, the shoulder is more extended and the long time decay becomes non-exponential (stretched). Thus, the relaxation behavior exhibits a two-step decay

function which is a characteristic of glassy dynamics [44,45]. The slower process is the structural (α -) process and the faster process is simply denoted “fast dynamics”. It was demonstrated that FTS holds for the α -process in many cases [45].

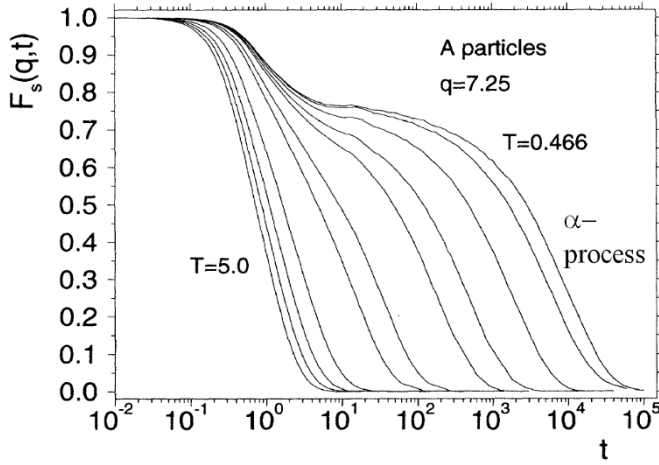


Figure 2: The incoherent intermediate scattering function $F_s(q,t)$ of LJ liquid with $q = q_{\max} = 7.25$ for different temperatures as indicated. Reprinted with permission from (Kob, W.; Andersen, H.C. *Phys. Rev. E*, 51, 4626-4641, 1995) Copyright (1995) by the American Physical Society.

Experimentally, the depolarized light scattering (DLS) measuring the orientational autocorrelation function $C^2(t)$ of the rank-two Legendre polynomial [17,46] shows similar findings as MD simulations. For example, the susceptibility obtained from DLS of o-terphenyl OTP in the GHz regime is presented in Figure 3a measured at temperatures well above the melting temperature $T_m = 330$ K. In a range of 100 GHz–5000 GHz, the so-called boson peak and microscopic dynamics appear, weakly changing with temperature. In the low-frequency range, the α -process is revealed. It gets faster with increasing temperature and finally approaches the boson peak around 500 GHz at high temperatures. At low temperatures, a minimum is observed around 50 GHz due to the interplay of the high-frequency tail of the α -relaxation and the fast dynamics [46]. The latter is attributed to a kind of “rattling in a cage” of the molecules [8,47]. In the time domain, the correlation function $C^2(t)$ is presented in Figure 3b which is extended by the results from PCS. At low temperatures, a two-step function is observable and vanishes at high temperatures; similar to that from MD simulation (*cf.* Figure 2).

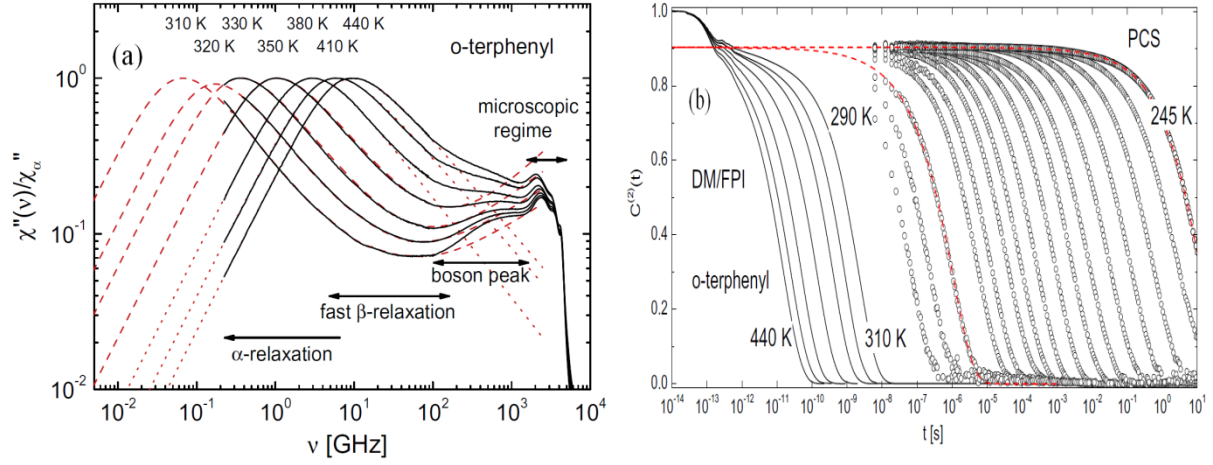


Figure 3: Normalized susceptibility of OTP obtained in GHz regime by light scattering. (b) The corresponding time correlation function $C^2(t)$ for the data shown in (a) obtained by Fourier transformation (solid lines); data from photon correlation spectroscopy (PCS) is added (symbols). Dashed lines: fit using a Kohlrausch function. Reprinted with permission from *J Chem. Phys.* 2010, 133, 124512. Copyright (2010) AIP Publishing.

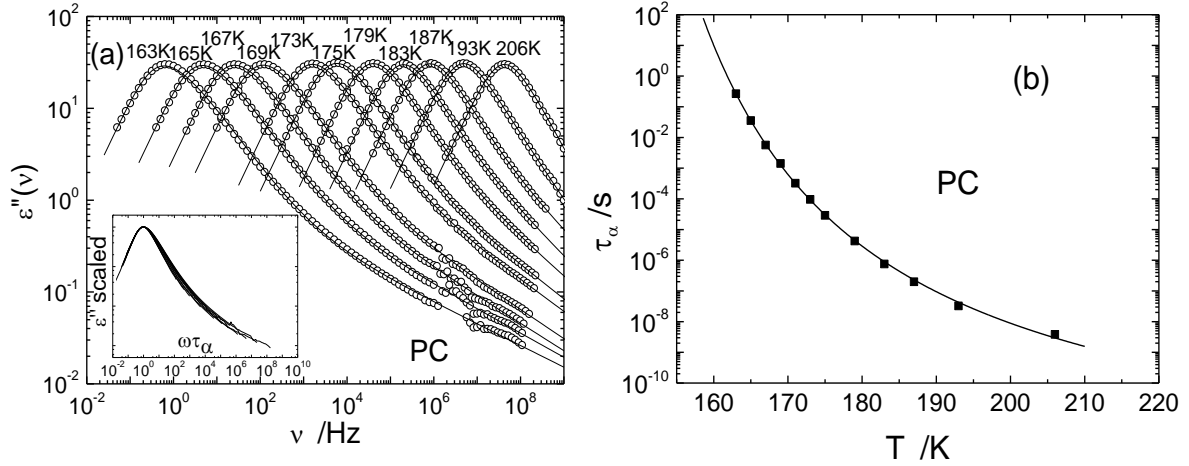


Figure 4: (a) Dielectric susceptibility of propylene carbonate (PC). Inset: data scaled to maximum and position of the α -process. (b) Relaxation time constants $\tau_\alpha(T)$ of α -process of PC. Reprinted with permission from (Kudlik, A.; Benkhof, S.; Blochowicz, T.; Tschirwitz, C.; Rössler, E. *J. Mol. Struct.* 1999, 479, 201-218), Elsevier.

Qualitatively, similar spectral features can be seen by analyzing the dielectric response. Figure 4a shows the DS spectra of propylene carbonate (PC $T_g = 158\text{K}$). The α -relaxation is observed and shifts to lower frequencies upon cooling. Its spectral shape is essentially temperature independent as is demonstrated in the inset in Figure 4a, where the data are

shifted to the position of the α -process. Again, FTS holds in good approximation. The α -relaxation displays an asymmetric (a non-Debye) spectral shape [48, 49].

Another feature of the α -relaxation is that the relaxation time $\tau_\alpha(T)$ shows a super-Arrhenius temperature dependence as it is presented in Figure 4b. According to Angell et al., glass formers are classified into “strong” (e.g. SiO_2) and “fragile” (e.g. OTP) [4, 50]. The latter exhibits $\tau_\alpha(T)$ often described by a Vogel-Fulcher-Tammann (VFT) [51-52] function, while that of the former almost follows an Arrhenius law.

In the case of PC, the exponent of the power law of the high-frequency flank of the α -relaxation changes to a smaller value at higher frequencies (*cf.* Figure 4a). A so-called “excess wing” is observable [22,54,55]. In some glass formers, instead of an excess wing, a secondary β -relaxation peak is observed at temperatures close to T_g ; it survives in the glassy state ($T < T_g$), e.g., as seen in the DS spectra of toluene displayed in Figure 5a. Moreover, in some cases both excess wing and secondary relaxation are observed; see the case of 3-fluoro aniline Figure 5b. According to these findings, glass formers were classified into two types: type A glass formers with no discernable β -process, and type B glass formers where a β -process is recognizable [23].

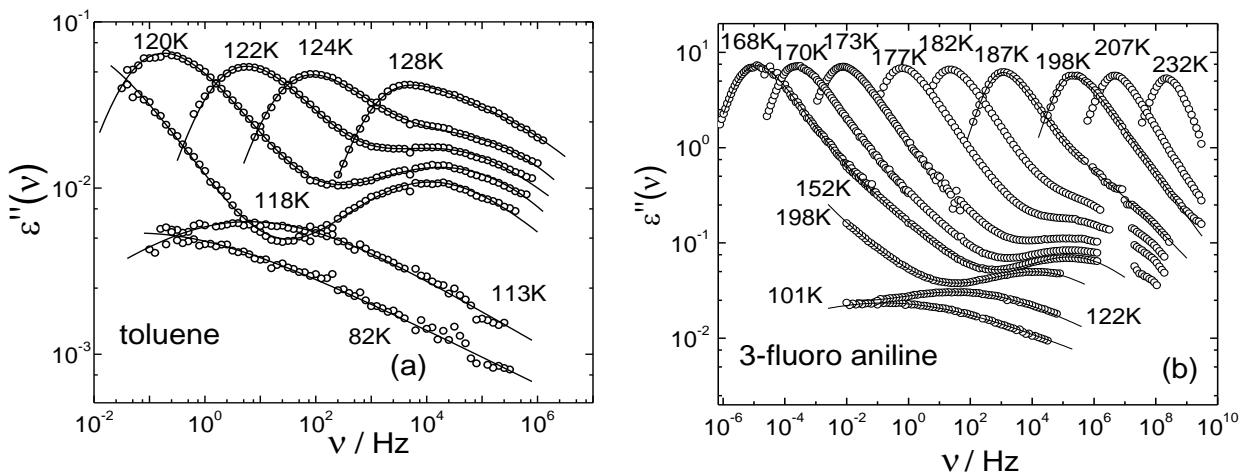


Figure 5: Dielectric loss of (a) toluene ($T_g = 117\text{K}$) and (b) 3-fluoroaniline ($T_g = 172\text{K}$) as type B glass formers. Reprinted with permission from (Kudlik, A.; Benkhof, S.; Blochowicz, T.; Tschirwitz, C.; Rössler, E. *J. Mol. Struct.* 1999, 479, 201-218), Elsevier.

In contrast to the α -process, the relaxation time of the β -process follows an Arrhenius law ($T < T_g$), i.e. the process is thermally activated. Moreover, its spectral width is temperature dependent while the relaxation strength weakly depends on temperature ($T < T_g$), albeit, it increases strongly at $T > T_g$ [23,55,60]. Activation energies in the range $E/R = 11 - 26 T_g$ and an attempt time of $\tau_0 = 10^{-18} - 10^{-13}$ s are typically found [23,60].

The β -process was first suggested to be caused by intramolecular dynamics. For example, the motion of side groups in polymers was thought to be one of its origin [38]. Yet, Johari and Goldstein [61,62] showed that the secondary process exists in systems consisting of small rigid molecules and stated that this process is an intrinsic feature of the glassy state. In most cases, DS is applied as a probe, in a few cases also mechanical relaxation or neutron scattering is applied [38,39]. Until today, the underlying nature of the β -process is not completely understood. Johari and Goldstein proposed “islands of mobility”, i.e. some molecules have higher mobility compared to others suggesting that the glass state is dynamically inhomogeneous [61]. In contrast, NMR revealed that essentially all molecules take part in spatially highly restricted reorientations. A “wobbling-on-a-cone” model with an opening angle smaller than $\pm 10^\circ$ was able to reproduce the NMR observables [63,64].

By doing aging experiment or pressure dependent experiments, the excess wing was regarded as a special hidden secondary relaxation [56,57] or as an intrinsic spectral feature of the α -process, respectively [58,59].

2.3. Generic features of polymer dynamics

Polymers are macromolecules constructed from covalently bonded units (monomers). Polymers appear in different topologies, e.g. linear, stars, hyperbranched, dendrimer, grafted polymer, copolymer, etc. [65]. An important feature of linear polymers is disclosed by the mean square displacement $\langle r^2(t) \rangle$ obtained from MD simulations when compared to that of a simple (LJ) liquid (cf. Figure 6). The polymer dynamics are similar to that of the (LJ) fluid at short times, where both show a ballistic regime ($\langle r^2(t) \rangle \propto t^2$) followed by the “cage effect” ($\langle r^2(t) \rangle \cong \text{constant}$). The LJ liquid crosses directly from the cage regime to a behavior of the normal diffusion ($\langle r^2(t) \rangle \propto t^1$). In contrast, a polymer exhibits a sub-diffusive behavior ($\langle r^2(t) \rangle \propto t^{0.63}$) at intermediate times, reflecting Rouse dynamics. Only at longer times normal diffusion is observed [67].

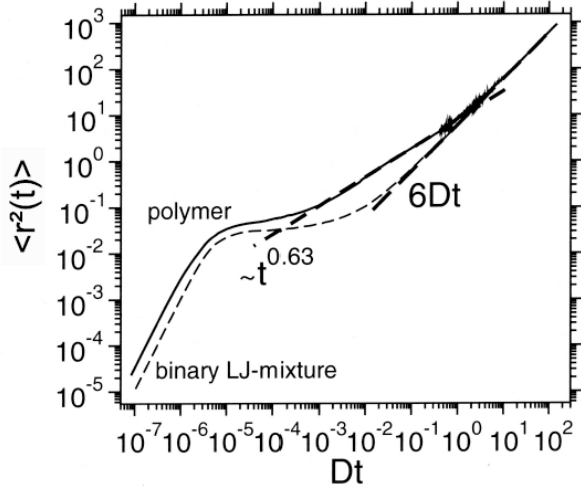


Figure 6: The mean square displacement $\langle r^2 \rangle$ versus time scaled by the diffusion coefficient D is shown for a binary Lennard-Jones mixture (dashed line) and for a polymer (solid line). Reprinted with permission from (Baschnagel, J.; Bennemann, C.; Paul, W.; Binder, K. *J. Phys.: Condens. Matter* 2000, 12, 6365–6374). Copyright of IOP Publishing.

Dielectric spectroscopy is an important method to study also polymer dynamics. According to *Stockmayer* [68], polymers are classified into type A (with dipole moment parallel to the chain contour) and type B (with dipole moment perpendicular to the chain contour) polymers. Type A polymers exhibit a dielectric relaxation called normal mode relaxation which reflects the fluctuations of the end-to-end-vector of the chain. In type B polymers only information about the segmental dynamics is given. Yet, pure type A polymers do not exist. For example, the DS spectra of polyisoprene (PI) which is known as a type A polymers show in addition to a normal mode relaxation (at low frequencies) a segmental relaxation (at high frequencies) [69-73]; as is shown in Figure 7a for different M of PI [74]. The normal mode relaxation slows down with increasing M , reflecting the M dependence of $\tau_n/\tau_a(M)$ (cf. Figure 7b). The $\tau_n/\tau_a(M)$ plot shows three power law regimes along $\tau_n/\tau_a \propto M^a$ with different exponent a . For $M < M_c$ ($M \cong 10k$ for PI), an exponent $a = 2.6$ is found (regime I), which is close to the Rouse prediction for the unentangled polymer ($a = 2$) [67]. For $M > M_c$, the entanglement regime is found. Two different regimes can be distinguished; regime II occurs at $M_c < M < M_{rep}$ with an exponent of $a = 4.0$ being larger than that predicted by tube-reptation (TR) theory (M^3) [75,76]. This behavior was explained by taking contour length fluctuations (CLF) and constraint release (CR) into account [77] (cf. section 5). For $M > M_{rep}$, an exponent of $a = 3.0$ is found which indicates pure reptation. Similar behavior is also found in the M dependency of the zero shear viscosity [78]; see below.

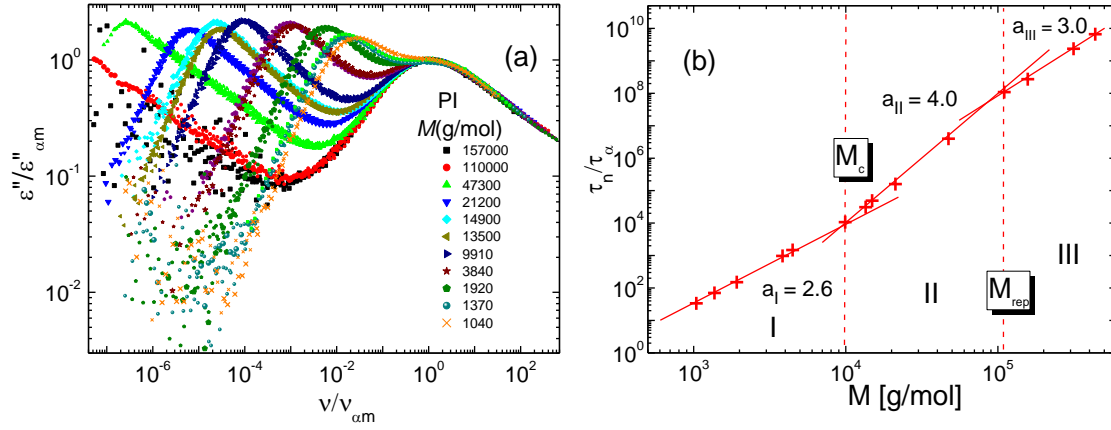


Figure 7: (a) Dielectric master curves for different M of PI scaled to the α - process. (b) The τ_n/τ_α ratio as function of M obtained from the data on (a). Reprinted with permission from (Abou Elfadl, A.; Kahlau, R.; Herrmann, A.; Novikov, V. N.; Rössler, E. A. *Macromolecules* 2010, 43 , 3340). Copyright (2010) American Chemical Society.

Rheology is the most important method to study polymer dynamics. The stress relaxation function $G(t)$ is recorded after applying a small shear deformation. Only in rare cases the complex shear $\hat{G}(\omega)$ modulus was measured down to temperature close to T_g (glassy dynamics). For example, master curves of storage G' and loss G'' moduli for poly(butadiene) PB are shown in Figure 8 [78]. By assuming FTS to hold, master curves were constructed covering polymer dynamics as well as the glassy dynamics. At lowest reduced frequencies (longest time), the terminal power laws of $G''(\omega) \propto \omega^1$ and $G'(\omega) \propto \omega^2$ are found, which reflect Newtonian liquid flow of the polymer melt. At higher frequency, the (entangled) polymer melts temporarily behave like an elastic (Hookean) solids showing a rubber plateau in $G'(\omega)$. This rubber plateau is a characteristic feature of the polymer entanglements (*cf.* chapter 5). While the rubber plateau is prominent in $G'(\omega)$, $G''(\omega)$ shows a power law of $G''(\omega) \propto \omega^{-(-0.2)}$. This exponent is smaller than that expected from the TR model ($\omega^{-0.5}$). Again, this deviation has been discussed by taking additional effects (CLF and CR) into account [77]. At high frequencies, the Rouse regime of $G''(\omega) \propto G'(\omega) \propto \omega^{-0.7}$ is defined. At highest frequencies, $G''(\omega)$ shows α -relaxation, while $G'(\omega)$ approaches a frequency independent glass plateau G_0 .

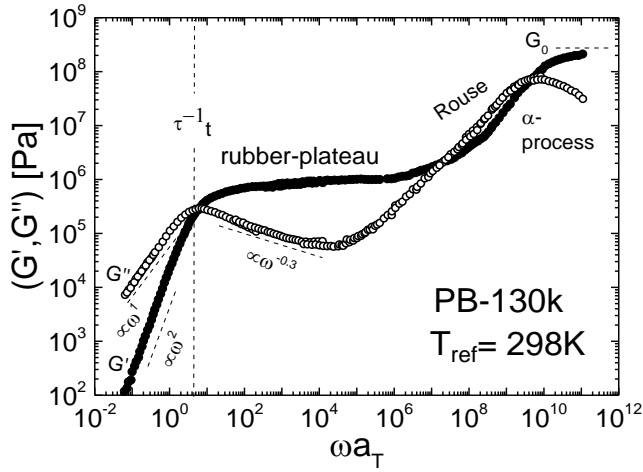


Figure 8: The shear loss G'' (open symbols) and storage G' (filled symbols) as a function of reduced frequency $\omega\tau_\alpha$ for poly (butadiene) of $M = 130k$. Adapted with permission from (Colby, R. H.; Fetters, L. J.; Graessley, W. W. *Macromolecules* 1987, 20, 2226). Copyright (1987) American Chemical Society.

Analogous to the $\tau_n/\tau_\alpha(M)$, the M dependency of the zero shear viscosity $\eta_0(M)$ displays three different regimes, as shown in Figure 9 for PI and PB [80,81]. First, a crossover from unentangled to entangled regimes for $M < M_c$ with $\eta_0 \propto M^1$ [67]. Then the entangled regime $M > M_c$ crosses from $\eta_0 \propto M^{3.3}$ (PB) or $\eta_0 \propto M^{3.8}$ (PI) to $\eta_0 \propto M^{3.0}$ at $M > M_{rep}$ [81].

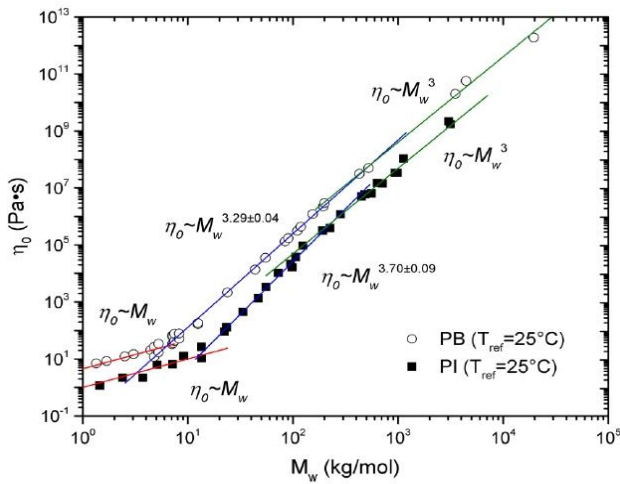


Figure 9: Zero shear viscosity as function of M for PI and PB obtained at the temperature $T = 25^\circ\text{C}$. Reprinted with permission from (Unidad, H.J.; Goad, M.A.; Bras, A.R.; Zamponi, M.; Faust, R.; Allgaier, J.; Pyckhout-Hintzen, W.; Wischniewski, A.; Richter, D.; Fetters, L.J. *Macromolecules* 2015, 48, 6638). Copyright (2015) American Chemical Society.

3. Experiments

3.1 Dielectric spectroscopy

In the dielectric experiment, the dipolar material is subjected to an external electric field and the time or frequency dependent macroscopic response is measured.

The Static Case

When a static electric field \vec{E} is applied to a dipolar material, it causes a polarization \vec{P} response. They are related by the static dielectric susceptibility χ_s along,

$$\vec{P} = \epsilon_0 \tilde{\chi}_s \vec{E} \quad (8)$$

which is a tensorial quantity, and with ϵ_0 being the vacuum permittivity. A restriction to isotropic media is considered and thus, χ_s is treated as a scalar quantity.

The polarization response consists of two components: one due to the orientation of the permanent dipoles $P_{or} = \Delta\chi E$, and the other due to the induced dipole moments $P_{in} = \chi_\infty E$.

$$P = \epsilon_0 \chi_s E = P_{or} + P_{in} = \epsilon_0 (\Delta\chi + \chi_\infty) E \quad (9)$$

With $\Delta\chi = \chi_s - \chi_\infty$ defines the relaxation strength.

The scalar nature of χ may suggest perfect orientation of the microscopic dipoles along the field direction. Yet, thermal fluctuations lead to non-perfect orientation of the dipoles and a quantitative assessment of the temperature dependence of $\Delta\chi$ is given by the Curie law [82],

$$\Delta\chi = \frac{N\mu^2}{3\epsilon_0 V k T} \quad (10)$$

The Curie law holds without any problem for gases, while in condensed matter, some corrections must be considered regarding the interaction among the dipoles as well as the effect of the local field. Several theoretical attempts have been made in this regard, based on the local Lorentz field (Clausius-Mosotti relation), or the influence of a dipole on the surrounding “continuum” by calculating a correction factor (Onsager reaction field) [82, 83]. Moreover, a correlation factor g was introduced by *Kirkwood* and *Fröhlich* considering static

orientational correlations in the liquid due to intermolecular dipolar interactions [82]; explicitly:

$$\Delta\chi = \frac{N\mu^2}{3\varepsilon_0 V kT} \cdot g \quad (11)$$

The dynamic response

In the dynamic response, a time dependent electric field is considered. The $P_{in}(t)$ contribution relaxes on times on the order of 10^{-13} s or even shorter, i.e. it is regarded as “instantaneous”, while the $P_{or}(t)$, closely related to the molecular reorientation. In a linear isotropic medium, the $P_{or}(t)$ reads, [84]

$$P_{or}(t) = P(t) - P_{in}(t) = \varepsilon_0 \chi_{or} \int_{-\infty}^t E(t') \phi(t-t') dt' \quad (12)$$

Here, the polarization at time t is determined by field $E(t')$ applied at $t' \leq t$. The quantity $\phi(t)$ is called the pulse response function. The function $\phi(t)$ is connected to the step-response function which describes the polarization response after switching off the field [40],

$$\phi(t) = -d/dt \psi(t) \quad (13)$$

In equilibrium, the response will decay to zero at longer time, i.e., $\phi(t \rightarrow \infty) = 0$. According to the FDT [40], the step-response function $\psi(t)$ is identical to the autocorrelation of the macroscopic polarization $C_P(t)$ given in Eq.(6) (cf. section 2.1).

In the case of an oscillating (harmonic) electric field $\hat{E}(\omega, t) = E_0 \exp(i\omega t)$, the orientational polarization defined in Eq. (12) reads,

$$\hat{P}_{or}(\omega, t) = \varepsilon_0 E_0 \exp(i\omega t) \Delta\chi \int_0^\infty \phi(\tau) \exp(-i\omega \tau) d\tau \quad (14)$$

with introducing $\tau = t - t'$.

Thus,

$$\hat{P}(\omega, t) = \varepsilon_0 \hat{\chi}(\omega) \hat{E}(\omega, t) \quad (15)$$

with the complex susceptibility $\hat{\chi}(\omega) = \chi'(\omega) - i\chi''(\omega)$ which is defined as:

$$\frac{\hat{\chi}(\omega) - \chi_\infty}{\Delta\chi} = \int_0^\infty \phi(t) \exp(-i\omega t) dt = 1 - i\omega \int_0^\infty \psi(t) \exp(-i\omega t) dt \quad (16)$$

Considering the dielectric displacement ($\widehat{D}(\omega, t) = \varepsilon_0 \widehat{E}(\omega, t) + \widehat{P}(\omega, t) = \varepsilon_0 \widehat{\varepsilon} \widehat{E}(\omega, t)$) instead of the polarization one gets,

$$\widehat{\varepsilon}(\omega) = 1 + \widehat{\chi}(\omega) \quad (17)$$

The complex dielectric permittivity $\widehat{\varepsilon}(\omega)$ is related to the autocorrelation of the step response function $\phi(t)$ by [43],

$$\widehat{\varepsilon}(\omega) = \varepsilon'(\omega) - i\varepsilon''(\omega) = \varepsilon_\infty - \Delta\varepsilon \int_0^\infty \frac{d\phi}{dt} \exp(-i\omega t) dt \quad (18)$$

where $\Delta\varepsilon$ is the dielectric strength and ε_∞ is the high frequency permittivity. The most common quantity discussed in the literature is $\varepsilon''(\omega)$, which is then called *dielectric loss*.

In the simplest case, the step response function $\phi(t)$ is a single exponential decay function (Debye). Several phenomenological fit functions can be used to describe a non-exponential relaxation, e.g., the Kohlrausch function:

$$\phi(t) = \exp\left(-\left(\frac{t}{\tau_k}\right)^\beta\right) \quad (19)$$

with a stretching parameter $0 < \beta \leq 1$, and an average relaxation time defined as $\langle \tau \rangle = \frac{\tau_k}{\beta_k} \Gamma\left(\frac{1}{\beta_k}\right)$. In the frequency domain, a Cole-Davidson (*CD*) function [43] or even a generalized function, which combines a Kohlrausch and a *CD* function [85] can be used. In some cases, a Havriliak-Negami (*HN*) function is suited as well, which is defined by [43, 86],

$$\widehat{\varepsilon}(\omega) - \varepsilon_\infty = \frac{\Delta\varepsilon}{(1 + (i\omega\tau)^{1-a})^b} \quad (20)$$

where a and ab are the power law exponents of the low- and high-frequency flank of $\varepsilon''(\omega)$, respectively.

Regarding the β -relaxation, Blochowicz et al. [84] introduced a distribution of correlation times $G_\beta(\ln \tau)$ used to describe a relaxation caused by a thermally activated process (observed at $T < T_g$),

$$G_\beta(\ln \tau) = N_\beta(a, b) \frac{1}{b \left(\frac{\tau}{\tau_m}\right)^a + \left(\frac{\tau}{\tau_m}\right)^{-ab}} \quad (21)$$

with the normalization factor,

$$N_{\beta}(a, b) = \frac{a(1+b)}{\pi} b^{\frac{b}{1+b}} \sin\left(\frac{\pi b}{1+b}\right) \quad (22)$$

and τ_m being the time constant at the maximum of $G_{\beta}(\ln \tau)$. The parameter a controls the symmetric broadening of the susceptibility, while b is the “asymmetry” part [84]. By using the $G_{\beta}(\ln \tau)$ distribution, the underlying temperature independent distribution of activation energies can be formulated.

In the case of polymer dynamics revealed by type A polymers, the step-response function of the normal mode relaxation, $\phi(t) = \phi_n(t)$ is given by the autocorrelation function of the end-to-end vector R of the chain [86]

$$\phi_n(t) = \frac{\langle R(0)R(t) \rangle}{\langle R(0)^2 \rangle} \quad (23)$$

3.2. Shear experiment

In the shear experiment, the thermal equilibrium of the material is perturbed by applying shear deformation or shear stress. A macroscopic response is detected which reflects the microscopic molecular rearrangements of the material. Most commonly, a time-dependent shear deformation $\gamma(t)$ is applied and a time-dependent shear stress $\sigma(t)$ is measured (*cf.* Figure 10a). The constitutive equation of the shear-stress relaxation in limits of the linear response regime (small deformation) is given by [79,87,88],

$$\sigma(t) = \int_{-\infty}^t G(t-t') \dot{\gamma}(t') dt' \quad (24)$$

with $G(t-t')$ being the stress response function or the time dependent shear modulus, which is identical with the stress (off-diagonal) tensor autocorrelation function $G(t)$ defined in Eq. (5) (*cf.* section 2.2).

In an oscillatory shear experiment, a sinusoidal strain is applied $\gamma(t) = \gamma_0 \sin(\omega t)$, with ω is the angular frequency, thus Eq. (24) becomes,

$$\sigma(t) = \gamma_0 \omega \int_0^{\infty} G(\bar{t}) \cos \omega(t-\bar{t}) d\bar{t} = \gamma_0 \omega R \left\{ e^{i\omega t} \int_0^{\infty} G(\bar{t}) e^{-i\omega \bar{t}} d\bar{t} \right\} \quad (25)$$

where R in the right identity represents the real part of the complex expression in the bracket. Assuming an exponential decay function $G(t)$ relaxing in the time τ , $G(\bar{t}) = G_0 e^{-\bar{t}/\tau}$, thus the integral in Eq. (25) reads,

$$\int_0^{\infty} G(t) e^{-i\omega t} dt = G_0 \left(\frac{\tau}{1+\omega^2\tau^2} \right) - iG_0 \left(\frac{\omega\tau^2}{1+\omega^2\tau^2} \right) \quad (26)$$

which yields,

$$\sigma(t) = \gamma_0 G'(\omega) \sin(\omega t) + \gamma_0 G''(\omega) \cos(\omega t) \quad (27)$$

with $G'(\omega)$ and $G''(\omega)$ being the real part “storage modulus“, and imaginary part “loss modulus” of the complex shear modulus:

$$G'(\omega) = \omega \int_0^{\infty} G(\bar{t}) \sin(\omega \bar{t}) d\bar{t} = G_0 \left(\frac{\omega^2 \tau^2}{1+\omega^2 \tau^2} \right),$$

$$G''(\omega) = \omega \int_0^{\infty} G(\bar{t}) \cos(\omega \bar{t}) d\bar{t} = G_0 \left(\frac{\omega \tau}{1+\omega^2 \tau^2} \right) \quad (28)$$

They are presented graphically in Figure 10b. The ratio of the loss and storage defines the tangent of the lag angle δ between the strain and the stress, $\tan \delta = G''(\omega)/G'(\omega)$.

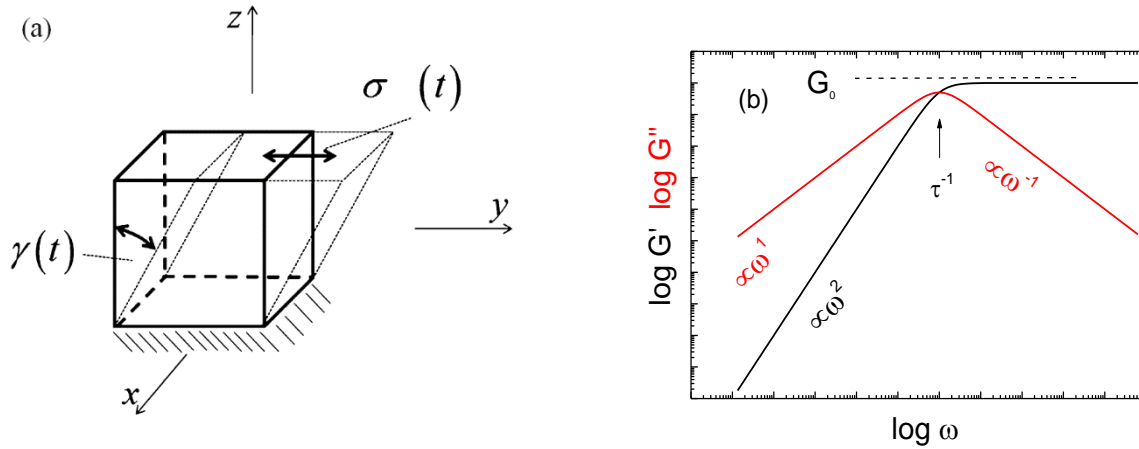


Figure 10: (a) Illustration of the time-dependent functions characterizing shearing of a volume element (b) Sketch represents the low- and high-frequency limits for the dynamical loss $G''(\omega)$ and storage $G'(\omega)$ modulus as a function of frequency ω according to Eq. (28).

3.3 Polymer models

In the present section, the stress correlation function of a polymer melts predicted by Rouse model or the Doi/Edwards will be described.

If the polymer molar mass M is smaller than a critical mass $M_c \cong 2M_e$, unentangled polymers, (M_e is entanglement molar mass), the dynamics can be described by the Rouse model [67]. In a coarse-grained description, a chain consists of N Kuhn segments (beads) of length b , connected together by $(N-1)$ entropic springs with a force constant, $k = 3k_B T b^{-2}$. By solving the equation of motion for an overdamped oscillator, the correlation functions of the p^{th} Rouse normal modes $X_p(t)$ can be calculated; [87]

$$C_p(t) = \langle X_p(t)X_p(0) \rangle = \frac{N_k b^2}{2\pi p^2} \exp(-p^2 t / N^2 \tau_s) \quad (29)$$

with $p = 1, \dots, N-1$, and $\tau_s = \frac{\zeta b^2}{3\pi^2 k_B T}$ expressing the shortest time where ζ is the frictional coefficient. The relaxation time of the p^{th} mode is $\tau_p = \frac{N^2}{p} \tau_s$.

Thus, the longest Rouse relaxation time ($p = 1$),

$$\tau_R = N^2 \tau_s \quad (30)$$

Concerning the stress correlation function, it is given by the sum over all normal modes;

$$G_R(t) = G_0 \sum_{p=1}^{N-1} \exp\left(-\frac{p^2 t}{\tau_R}\right) \quad (31)$$

with $G_0 = \rho N_A k_B T / M$ being the static modulus. In the frequency domain the loss and storage will be,

$$G'(\omega) \propto \begin{cases} G_0(\omega\tau_R)^{\frac{1}{2}} \\ G_0(\omega\tau_R)^2 \end{cases} \quad \text{and} \quad G''(\omega) \propto \begin{cases} G_0(\omega\tau_R)^{\frac{1}{2}} & \omega < \tau_R^{-1} \\ G_0(\omega\tau_R) & \omega > \tau_R^{-1} \end{cases} \quad (32)$$

For $M > M_c$, the Rouse model is insufficient to describe the dynamics of chains any more. The tube reptation (TR) model is accepted to be applied [75,76]. In the model, a tagged chain is constraint by its neighbors in a virtual tube of diameter $a = bN_e^{1/2}$, (N_e is entanglement number

which corresponds to M_e by $N_e = M_e/M_0$; M_0 is mass of the Kuhn monomer) and performs a snake-like motion (*cf.* Figure 11).

On short times ($t < \tau_e$), the segments do not feel the restrictions of the tube and perform a Rouse-like motion with a maximal relaxation time τ_e (entanglement time) (*cf.* Figure 11), similar to Eq. (30) τ_e reads,

$$\tau_e = N_e^2 \tau_s \quad (33)$$

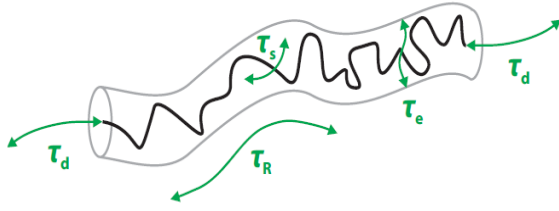


Figure 11: Sketch represents a tagged polymer chain confined in a virtual tube as well as the characteristic time constants along the tube-reptation model.

In the TR model, the stress correlation function is described by a multi-exponential decay [75,76], where $G(t)$ is determined by two relaxation regimes: the Rouse and the entanglement regime. The latter is described by the tube-segment occupation function $\mu(t)$ at $t > \tau_e$.

$$G(t) = G_N^{(0)} \mu(t) = G_N^{(0)} \sum_{p=odd} \frac{8}{p^2 \pi^2} \exp\left(\frac{-t p^2}{\tau_t}\right) \quad (34)$$

with $G_N^{(0)}$ being the entanglement rubber plateau modulus, and the $\tau_t = \tau_d$ being the terminal relaxation time.

Different relaxation regimes delimited by different relaxation time are defined as follow. At short times $G(t)$ is given by a stretched exponential decay with an exponent 0.5, and at longer time $t > \tau_t$, $G(t)$ shows a transition to an exponential decay, constituting the terminal relaxation. In the frequency domain it reads,

$$\begin{aligned} G''(\omega) &\cong \frac{\sqrt{2}}{\pi} G_N^0 (\omega \tau_t)^{-1/2} & \frac{1}{\tau_t} << \omega << \frac{1}{\tau_R} \\ G''(\omega) &\cong \frac{\pi^2}{12} G_N^0 \omega \tau_t & \omega << \frac{1}{\tau_t} \end{aligned} \quad (35)$$

where $\tau_t = \tau_e N^3$. These predictions along the original TR model (reptation regime (III and IV) are sketched in Figure 12 together with those from the Rouse and glassy relaxation regime as dashed line.

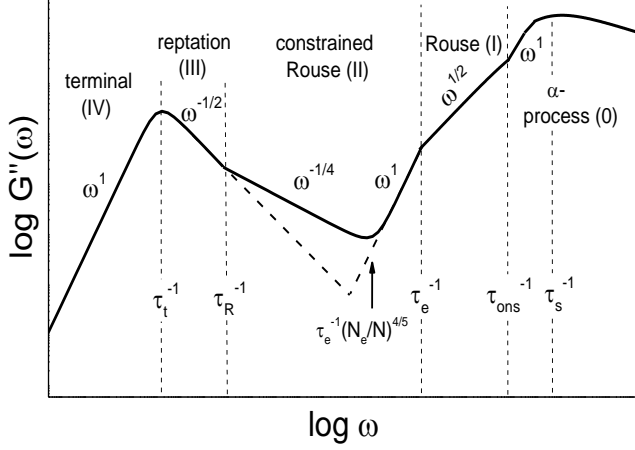


Figure 12: Loss modulus $G''(\omega)$ as predicted by the original TR model, schematically (dashed line) and by incorporating contour length fluctuations (solid line). Relaxation regimes and crossover frequencies/times are indicated.

Experimentally the original TR model cannot reproduce the viscoelastic data. The model has been modified by Likhtman and McLeish (LM) [77]. Several additional effects were taken into account; contour length fluctuation CLF (as free ends of the chain were considered) and constraint release CR (the motion of the surrounding chains). By taking CLF into account, the $G''(\omega)$ reads [89],

$$G''(\omega) \propto \frac{N_e}{N} \frac{G_N^0}{(\omega \tau_e)^{1/4}} \cdot \quad 1/\tau_R \ll \omega \ll 1/\tau_{\min} \quad (36)$$

where $1/\tau_{\min} = \omega_{\min}$ is the frequency of the minimum in $G''(\omega)$ which delimits the CLF regime due to the fact that at higher frequencies $\omega_{\min} \ll \omega \ll 1/\tau_e$ the loss modulus $G''(\omega)$ grows proportional to ω (solid lines in Figure 12), explicitly [89],

$$G''(\omega) \propto G_N^0 \omega \tau_e \quad 1/\tau_{\min} \ll \omega \ll 1/\tau_e \quad (37)$$

At $\omega = \omega_{\min}$, Eq. (36) and Eq. (37) can be equated and a prediction of the N dependence of ω_{\min} can be derived [89],

$$\omega_{\min} \propto \frac{1}{\tau_e} \left(\frac{N_e}{N} \right)^{4/5} \quad (38)$$

These are the expected different regimes which will be studied experimentally in chapter 5.

4. Dynamics of binary mixtures

4.1 State-of-the-art

The properties of glass formers can be tuned by mixing them with other glass formers. The most intriguing findings are that the mixing often enhances the vitrification ability and that it changes the glass transition temperature T_g (plasticizer effect). The concentration dependence of T_g in mixtures was studied in a variety of systems [90]. In some mixtures, e.g. sorbitol ($T_g = 265$ K) in glycerol ($T_g = 191$ K) [91], or propylene glycol PG ($T_g = 165$ K) in 2-ethylhexamine ($T_g = 138$ K) [92], a single main (α -) relaxation was identified. Its relaxation time $\tau_\alpha(T)$ follows a non-Arrhenius temperature dependence. Correspondingly, only single concentration dependent T_g was found.

In other mixtures with a large “ T_g contrast” of their components, so-called “asymmetric” mixtures, two T_g values, T_{g1} and T_{g2} , were found by DSC measurements (*cf.* refs. 93, 94). Correspondingly, two primary relaxations were observed by DS [95-97]. They were assigned to the dynamics of each component. For example, DS spectra of 20% of tripropyl phosphate (TPP) in polystyrene (PS), with a T_g contrast of about 200 K, are presented in Figure 13a [95]. The process (α_2) at high-frequencies was assigned to the dynamics of TPP (low- T_g component or additive) while that at low-frequencies (α_1) to the dynamics of PS (high- T_g component). The former broadens with decreasing TPP concentration (*cf.* Figure 13b), i.e. a broad distribution of relaxation times $G(\ln\tau_{\alpha_2})$ is found, compared to neat TPP. This broadening reflects increasing dynamic heterogeneities in the mixture [98, 99]. In contrast, the α_1 -relaxation only weakly broadens, and resembles the α -relaxation in neat systems [95, 96].

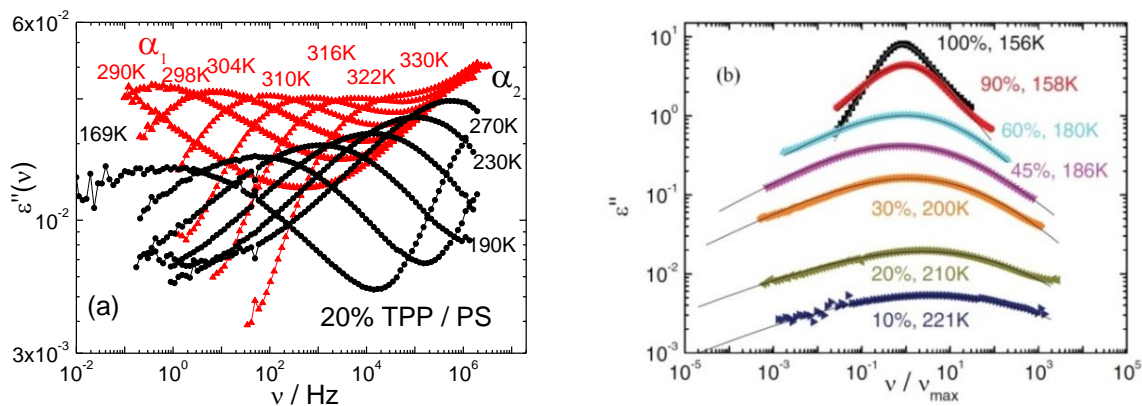


Figure 13: (a) Dielectric spectra for TPP/PS for $c_{\text{TPP}} = 20\%$ [adapted with permission from *J Chem. Phys.* 2014, 140, 044509. Copyright (2014) AIP Publishing]. (b) DS spectra comparing the α_2 -relaxation for different concentrations of TPP [Reprinted with permission from *J Chem. Phys.* 2014, 140, 094505. Copyright (2014) AIP Publishing].

The relaxation time $\tau_{\alpha 1}(T)$, reflecting the dynamics of high- T_g component, decreases with increasing the additive concentration (c_{TPP}) and follows a non-Arrhenius temperature dependence (cf. Figure 14a). This leads to a decrease of the corresponding T_g value $T_{g1}(c_{\text{TPP}})$, and reflects the plasticizer effect, as it is shown in Figure 14b. In contrast, the relaxation time $\tau_{\alpha 2}(T)$, displaying the dynamics of low- T_g component, increases upon decreasing c_{TPP} yielding an increase of the corresponding T_g value $T_{g2}(c_{\text{TPP}})$ which reflects the anti-plasticizer effect [95] (cf. Figure 14b). The temperature dependence of $\tau_{\alpha 2}(T)$ changes from a non-Arrhenius at high additive concentration to an Arrhenius behavior at low additive concentrations (cf. Figure 14a). This feature is known as a “fragile-to-strong” transition [100]. The transition occurs around T_{g1} (the T_g of the high- T_g component). Similar findings were also reported in water/polymer mixtures [101-103]. Accordingly, a maximum was discussed in the concentration dependence of T_{g2} at low additive concentrations (cf. Figure 14b) [95,98]. Such a maximum was not discussed by Blochowicz et al. [97] by considering different mixtures (PS of different molar masses in M-THF) with different T_g contrast (cf. Figure 15). Below T_{g1} , the additive component performs an isotropic motion in an arrested matrix of the high- T_g component as confirmed by NMR [98].

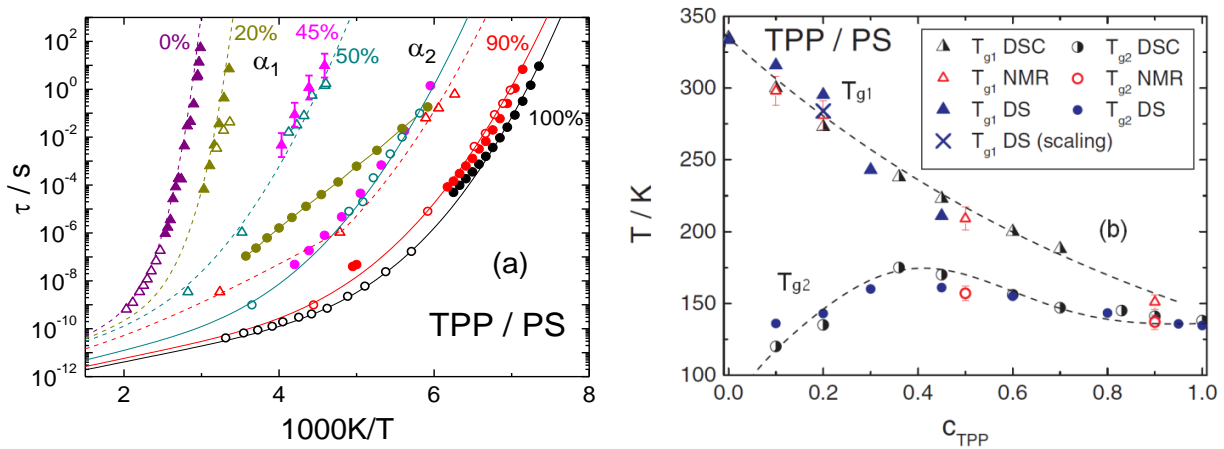


Figure 14: (a) Time constants $\tau_{\alpha 1}(T)$ (triangles) and $\tau_{\alpha 2}(T)$ (circles) for different additive concentrations of $c_{\text{TPP}} = 0\%$, 20% , 45% , 50% , 90% , and 100% in the TPP/PS mixtures as obtained by DS (full symbols) and NMR (open symbols). (b) T_{g1} and T_{g2} as a function of the TPP concentration in TPP/PS. Reprinted with permission from *J Chem. Phys.* 2014, 140, 044509. Copyright (2014) AIP Publishing.

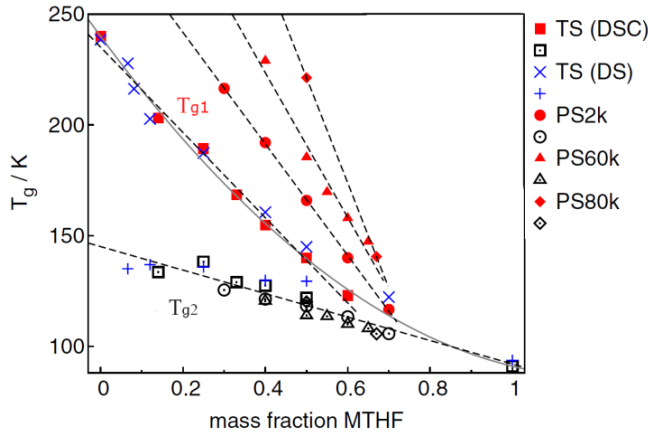


Figure 15: T_{g1} and T_{g2} values as a function of the MTHF mass fraction obtained in the mixtures MTHF/tristyrene and MTHF/PS of different molar masses as indicated. Adapted Figure 1 with permission from [Blochowicz, T.; Schramm, S.; Lusceac, S.; Vogel, M.; Stühn, B.; Gutfreund, P.; Frick, B. *Phys. Rev. Lett.* 109, 035702, 2012] Copyright (2012) by the American Physical Society.

Discussing the dielectric strength in asymmetric mixtures, Blochowicz et al. [97] concluded that the additive component takes part in the dynamics of both processes: one fraction performs the faster (α_2) process which is controlled by intrinsic confinement effects and the other one participates in the slower (α_1 -) process. These findings were also found in TPP/PS mixtures (*cf.* Figure 16) [95]. The strength of the α_2 -relaxation increases with temperature while that for the α_1 -relaxation decreases, and at a distinct temperature (T_c) it reaches the expected value of neat PS. Thus, the participation of the additive in the slow (α_1 -) process ceases at high temperature.

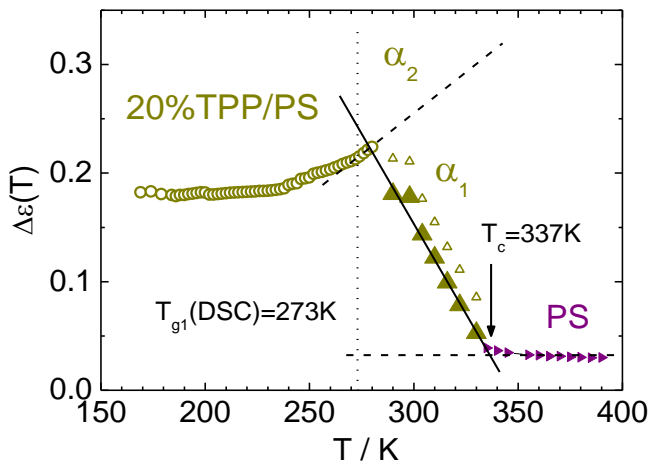


Figure 16: Dielectric strength as a function of temperature in $c_{TPP} = 20\%$ of TPP/PS. Reprinted with permission from *J Chem. Phys.* 2014, 140, 044509. Copyright (2014) AIP Publishing

The dynamics of asymmetric binary mixtures was also studied by MD simulations and interpreted by MCT [104-107]. Systems consisting of particles with a “size disparity” δ which is defined as the particles diameter ratio were studied [107]. The studies revealed that as the size disparity increases, the dynamics of the components become more and more decoupled (*cf.* Figure 17). The intermediate scattering function for the small particle (filled symbols) dynamics shows an unusual relaxation feature with increasing δ : The intermediate plateau

describing the cage effect is not found at high δ and the correlation functions become highly stretched. For the large particle (open symbols), the cage effect remains unchanged. A scenario that the small particles move in an arrested matrix of the large particles is proposed.

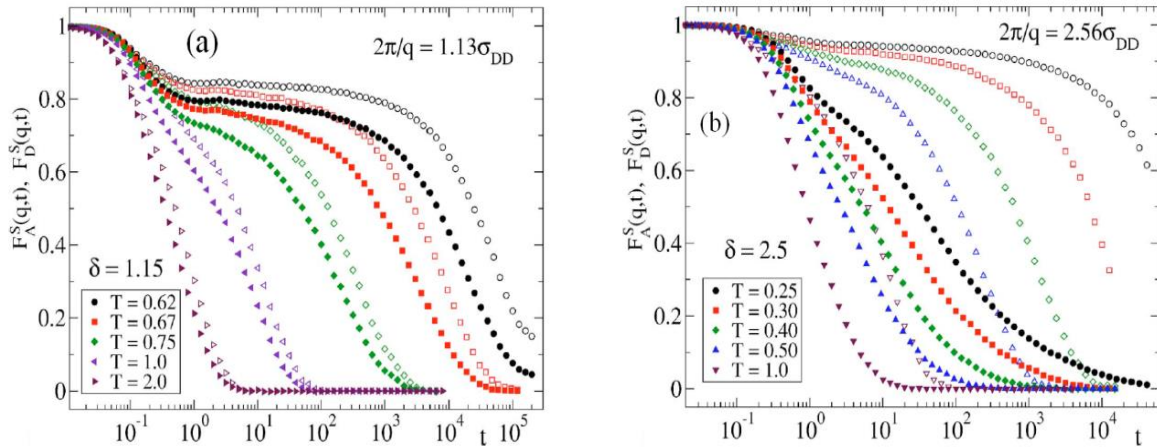


Figure 17: Intermediate scattering function from MD simulation of binary mixtures with particles of different size ratio δ (a) $\delta = 1.15$ (b) $\delta = 2.5$ (large to small). Filled symbols: small particle; open symbol: large particle. Adapted with permission from *J Chem. Phys.* 2006, 125, 164507. Copyright (2006) AIP Publishing.

Until now, these dynamical features were only investigated in polymer-additive mixtures. The question arises whether similar features are found in asymmetric binary mixtures consisting of two “non-polymeric” components. Is the T_g contrast alone responsible for these dynamical heterogeneities explained above? These questions are the subject of the present chapter.

4.2 Results

4.2.1 Mixtures studied

In order to investigate mixtures of non-polymeric nature, two spirobichroman derivatives as high- T_g components, hereafter called DH379 ($T_g = 382$ K) and SBC ($T_g = 356$ K) were specially synthesized in cooperation with *MC I, Universität Bayreuth*. As low- T_g components m-tri-cresyl phosphate (m-TCP, $T_g = 206$ K) and tripropyl phosphate (TPP, $T_g = 134$ K) were selected. Thus, a T_g contrast of $\Delta T_g = 176$ K for the mixture *I* (m-TCP/DH379) and 222 K for the mixture *II* (TPP/SBC) was reached. The chemical formulae of both systems are listed in Table 1.

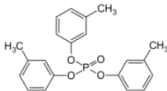
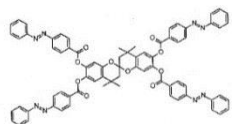
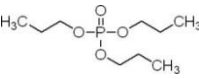
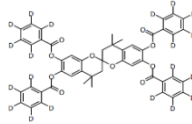
System	Low- T_g	High- T_g
mixture <i>I</i> $\Delta T_g = 179\text{K}$	m-tri-cresyl phosphate (m-TCP)  $M_{\text{mol}} = 368.4 \text{ g/mol}$ $T_g = 206 \text{ K}$	DH379  $M_{\text{mol}} = 1205.3 \text{ g/mol}$ $T_g = 385 \text{ K}$
mixture <i>II</i> $\Delta T_g = 222 \text{ K}$	tripropyl phosphate (TPP)  $M_{\text{mol}} = 224.23 \text{ g/mol}$ $T_g = 134 \text{ K}$	SBC  $M_{\text{mol}} = 809.0 \text{ g/mol}$ $T_g = 356 \text{ K}$

Table 1. The chemical formulae and T_g values of the components of mixture *I* and mixture *II*.

For the mixtures, the concentration is defined by the mass percentage of the low- T_g component, $c_{\text{low-}T_g}$. In the case of the mixture *I*, a wide concentration range was dielectrically measured: $c_{\text{m-TCP}} = 20, 34, 46, 56, 66, 73$, and 80% . In the case of the mixture *II* due to crystallization, the measurements were limited to the concentrations $c_{\text{TPP}} = 66, 70$, and 85% .

The present section is organized in three parts: First, the dynamics of the neat components will be characterized (section 4.2.2.1). Then; the main relaxation in the mixtures will be discussed (section 4.2.2.2). The dynamics at $T < T_{g2}$ will be discussed in section 4.3.

4.2.2 Main relaxations

4.2.2.1 Neat system

The dielectric spectra of the neat components are presented in Figures 18 and 19. At high temperatures, the main α -relaxation is well recognized which slows down upon cooling. Here and in the upcoming section, the dc conductivity contribution was subtracted along $\epsilon''(\nu) = \epsilon_0 \sigma_{\text{dc}} / \nu$. The relaxation time $\tau_\alpha(T)$ is extracted via the condition $(\omega_{\text{max}} \tau_\alpha) = 1$, and displayed in Figure 20. A super-Arrhenius temperature dependence of the relaxation time is observed which is typical of molecular glass formers. The temperature at $\tau_\alpha(T) = 100 \text{ s}$ defines T_g (cf. Table 1). In the case of m-TCP, the high-frequency flank of the α -relaxation crosses over to another power law known as “ excess wing”, revealing that m-TCP is a type A glass former (not displaying a β -relaxation), while the high- T_g component DH379 shows a well-defined β -relaxation (type B glass former) [23]. By contrast, both components of mixture *II* show a

well-defined β - relaxation at $T < T_g$ which will be discussed in section 4.3. As demonstrated below, FTS holds well for the main relaxation in the neat components (*cf.* Figure 24).

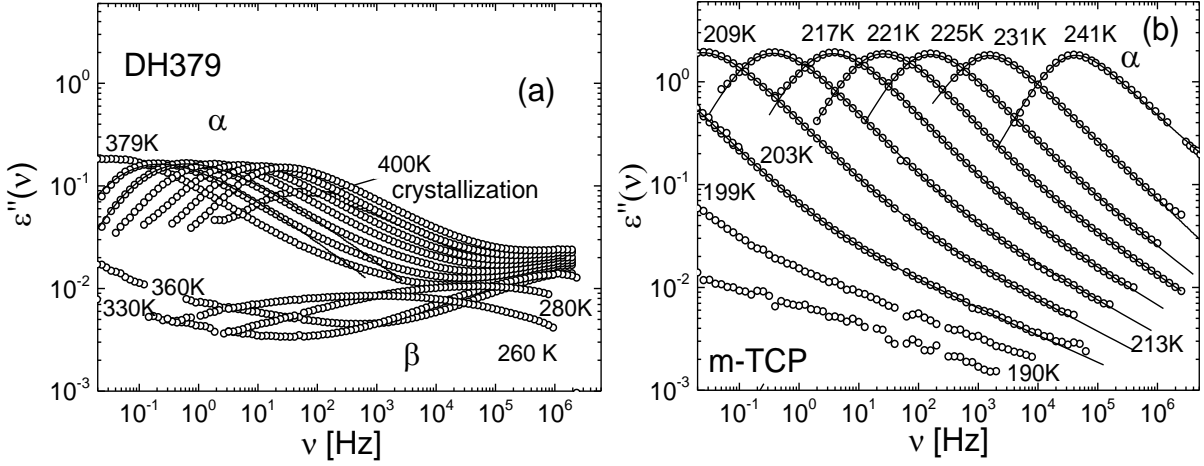


Figure 18: Dielectric spectra of the neat components of the mixture *I*: (a) High- T_g component DH379 measured in a temperature range of $T = 379$ K to 400 K in 3K steps, for which the α -relaxation is covered. For lower temperatures selected spectra of β - relaxation is shown. (b) Low- T_g component m-TCP in a temperature range of $T = 190$ K to 241 K [Reprinted with permission from *J Chem. Phys.* 2006, 124, 134503. Copyright (2006) AIP Publishing]. Solid lines: interpolating α -relaxation using a Kohlrausch fit with an additional power law exponent interpolating the excess wing contribution is used.

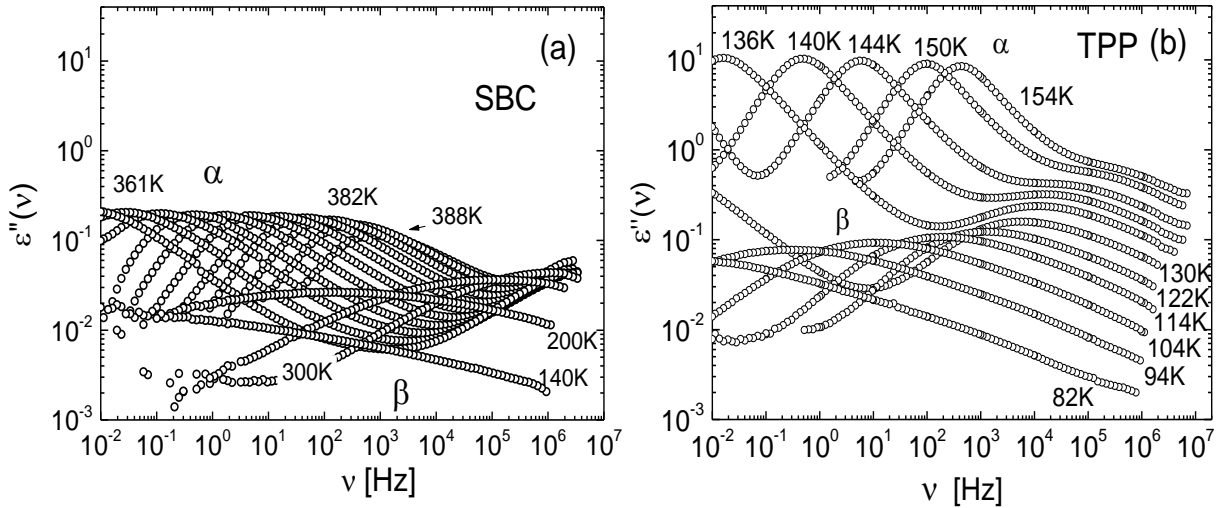


Figure 19: Dielectric spectra of the neat components of mixture *II*: (a) High- T_g component SBC measured in the temperature range of $T = 361$ K to 391 K in 3 K steps and selected spectra at lower temperatures down to 140 K are shown. (b) The low- T_g component TPP in the temperature range of $T = 82$ K to 154 K [Reprinted with permission from *J Chem. Phys.* 2014, 140, 044509. Copyright (2014) AIP Publishing].

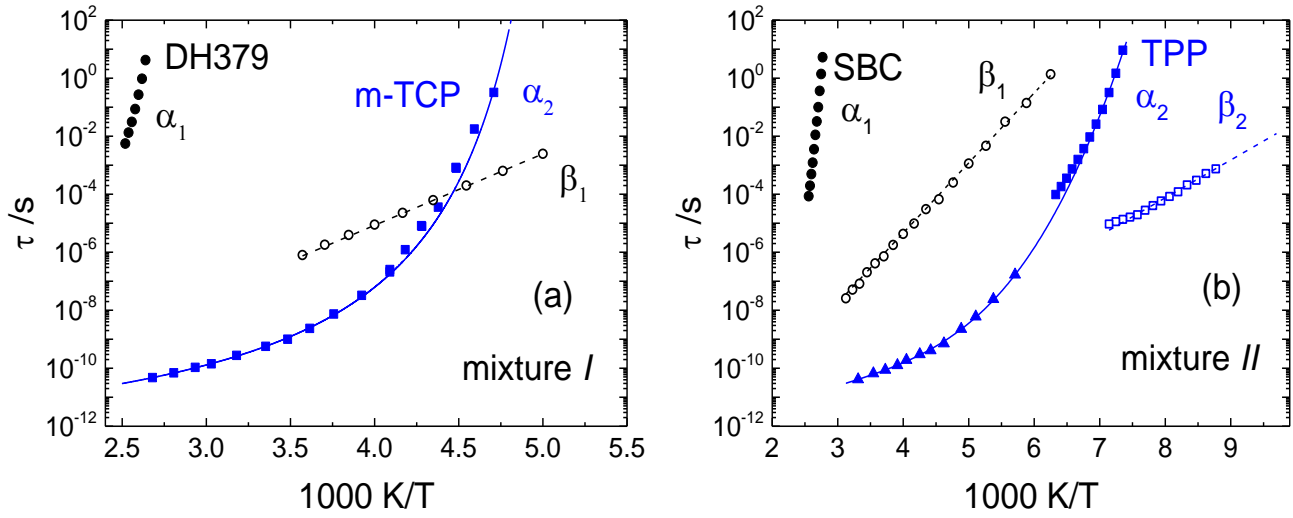


Figure 20: Time constants $\tau_\alpha(T)$ (filled symbols) and $\tau_\beta(T)$ (open symbols) of the neat components for (a) mixture *I* (DH379/m-TCP), and (b) mixture *II* (TPP/SBC) obtained from DS (circles and squares) and NMR (triangles). Data for m-TCP is taken from ref. [108] and NMR data for TPP is taken from ref. [109]. Solid lines: VFT fits and dashed lines: Arrhenius law.

Inspecting the DS spectra of the components one sees that the low- T_g components (m-TCP or TPP) display a dielectric signal much stronger than that of the high- T_g components (DH379 or SBC), i.e. the low- T_g additive is much more polar. Consequently, DS probes predominantly the dynamics of the low- T_g component in the mixtures.

4.2.2.2. Mixtures

Figure 21a shows the DS spectra of the mixture *I* (m-TCP/DH379) for $c_{\text{m-TCP}} = 80\%$, as an example for a high additive concentration. Although the original data displays only a single relaxation peak, by subtracting the dc conductivity contribution (dashed lines) a weak shoulder on the low-frequency side of the main relaxation process is recognized. For comparison a spectrum of neat m-TCP is included (filled squares). As expected, the signal in the mixture is lower than that of the neat component. Moreover, the main relaxation peak is significantly broader, in particular on the low-frequency side ($\chi''(\omega) \propto \omega^a$ with $a < 1$). This deviates from the behavior of neat glass formers for which $\chi''(\omega) \propto \omega^1$ at $\omega\tau_\alpha < 1$. The shoulder on the low-frequency side is assigned to the contribution of the high- T_g component and hereafter called α_1 -relaxation, while the faster and stronger relaxation is attributed to the

low- T_g component and called α_2 -relaxation. This assignment will be further substantiated below.

Figure 21b displays an example of the DS spectra for the mixture *II* (TPP/SBC) with $c_{\text{TPP}} = 70\%$. As expected the relaxation peak of the low- T_g component is somewhat lower than in the case presented in Figure 19b. Upon subtracting the conductivity contribution, again a well-defined shoulder is recognized on the low-frequency side of the main relaxation peak. In addition a secondary β -relaxation is seen at high-frequencies, which will be discussed in detail in section 4.3.

As the α_2 -relaxation shows an atypical main relaxation, a *HN* (Eq. (20)) function is chosen for fitting the spectra. For the α_1 -relaxation which shows a spectral shape as in neat glass formers, the Fourier transform of a *Kohlrausch* function (Eq. (19)) was taken. Additive superposition of both functions was assumed to interpolate the full spectra (cf. Figure 21). The fit provides the time constants $\tau_{\alpha 1}(T)$ and $\tau_{\alpha 2}(T)$ which are collected in Figure 26.

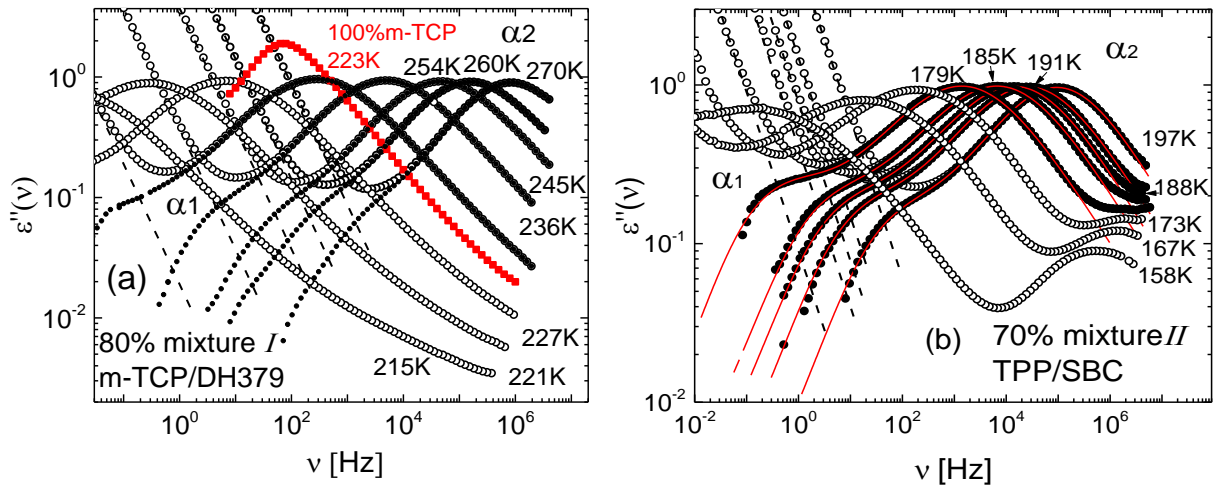


Figure 21: DS spectra of (a) the mixture *I* with $c_{\text{m-TCP}} = 80\%$ [Reprinted with permission from *J. Chem. Phys.*, 2015, 143, 154506, copyright (2015) AIP Publishing] and (b) mixture *II* with $c_{\text{TPP}} = 70\%$; open circles: the original data, filled circles: data after subtracting the conductivity contributions (dashed lines) [Reprinted with permission from *J. Chem. Phys.*, 2017, 146, 164503, copyright (2017) AIP Publishing]. Solid lines: interpolation of the data (see text).

For a low concentration, $c_{\text{m-TCP}} = 34\%$, the DS spectra are shown in Figure 22a. Clearly, at high temperatures two strong relaxations are now distinguishable, yet the slower one is partly covered by the dc conductivity. Upon subtracting the latter, two well-resolved relaxations are

observed (closed symbols). Again, the relaxation at high frequencies is assigned to the m-TCP component (α_2 -relaxation), while the slower one to the DH379 component (α_1 -relaxation). Obviously, the amplitude of the α_2 -relaxation increases with temperature while it decreases in the case of the α_1 -relaxation. Moreover, the amplitude of the α_1 -relaxation is larger than that of neat DH379 (compare to Figure 18a) although only 66% of DH379 are present. To record the enhancement factor, the signal of the $c_{\text{m-TCP}} = 20\%$ sample at $T = 320\text{K}$ is compared to that of the neat DH379 at $T = 385\text{K}$ multiplied by factor $0.8 \cdot 385\text{K}/320\text{K}$ (the factor assumes a linear concentration dependence and a Curie law), cf. Figure 22b. An enhancement factor of 1.8 is found. This suggests that the low- T_g component m-TCP is participating in the α_1 -relaxation [95].

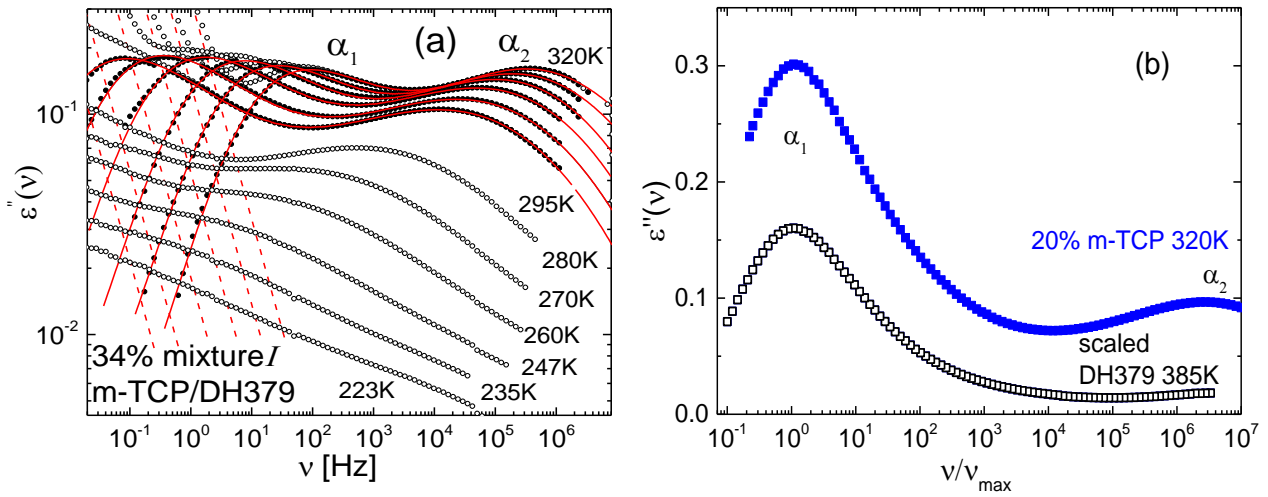


Figure 22: (a) DS spectra of the mixture *I* with $c_{\text{m-TCP}} = 34\%$; open circles: the original data, filled circles: data after subtracting the conductivity contributions along dashed lines. Solid lines: fits (see text). (b) DS data at $T = 320\text{ K}$ for the $c_{\text{m-TCP}} = 20\%$ (blue squares), frequency axis scaled to the peak position). For comparison, the spectrum of neat DH379 at $T = 385\text{ K}$ multiplied by 0.8 and $385\text{K}/320\text{K}$ (Curie correction) (open squares) is shown. Reprinted with permission from *J. Chem. Phys.*, 2015, 143, 154506, Copyright (2015) AIP Publishing.

The dielectric strength of the α_1 -relaxation with respect to that of α_2 -relaxation, $(\Delta\epsilon_{\alpha 1}/\Delta\epsilon_{\alpha 2})$, for different concentrations and temperatures is shown in Figure 23. The ratio decreases with increasing temperature, in particular, for $c_{\text{m-TCP}} \leq 45\%$. By assuming a Curie law and ideal mixing, the expected dielectric relaxation strengths can be estimated along $(\Delta\epsilon_{\alpha 1}/\Delta\epsilon_{\alpha 2})_{\text{calc}} = \frac{(1-c_{\text{low-Tg}}) \cdot \Delta\epsilon_{1n} \cdot T_1}{c_{\text{low-Tg}} \cdot \Delta\epsilon_{2n} \cdot T_2}$, where $\Delta\epsilon_{1n}$ denotes the relaxation strength of the neat components and $T_{1\text{or}2}$ is the temperature at which it was measured. The calculated ratio is also included in Figure 23

(open symbols). For all concentrations the measured ratio is larger than the calculated value. These findings give further indications that a sub-ensemble of the low- T_g component participates in the α_1 -process. The temperature dependence of the strength ratio may suggest that above a certain temperature this sub-ensemble disappears, i.e. the low- T_g component only participates in the α_2 -process. This is in accordance with the results for TPP/PS [95].

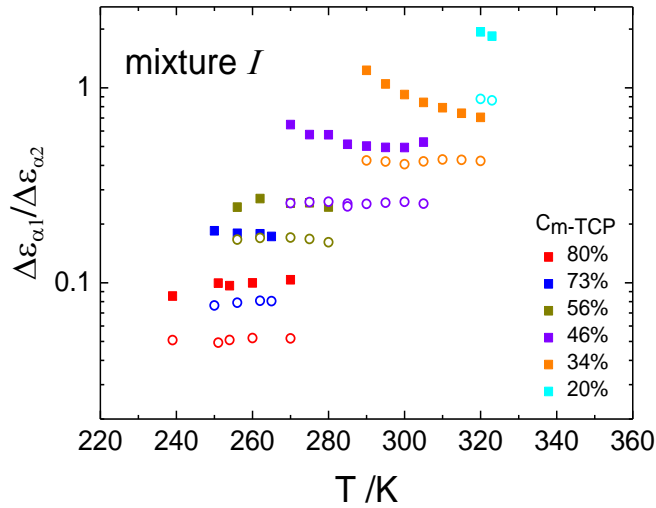


Figure 23: The dielectric strength ratio $\Delta\epsilon_{\alpha 1}/\Delta\epsilon_{\alpha 2}$ (filled squares) for different concentrations as function of temperature obtained from the spectral fit and compared to the expected ratio (open circles) assuming a Curie law (see text).

Inspecting the spectral shape of the α_2 -relaxation, Figure 24a shows the spectra for $c_{m-TCP} \geq 46\%$ scaled to the height of the α_2 -relaxation and shifted horizontally to collapse along the conductivity contribution. Clearly, FTS holds well for the neat m-TCP ($c_{m-TCP} = 100\%$) and the α_2 -relaxation is coupled to the dc conductivity, while FTS fails in the mixtures, especially on the low-frequency flank of $\epsilon''(\nu)$. In Figure 25, the dielectric spectra of the α_2 -relaxation are compared for different concentrations at the same temperature $T = 247$ K. One can recognize that the α_2 -relaxation first slows down at high concentrations and accelerates again at low concentrations; the amplitude decrease as expected due to the dilution of m-TCP. For low concentrations, $c_{m-TCP} < 46\%$, the spectral shape strongly depends on the temperature as it significantly broadens upon cooling (*cf.* Figure 24b). By contrast, FTS holds well for the α_1 -process in the mixture, yet the high-frequency flank is broader compared to that of neat DH379 (*cf.* Figure 24c). For the mixture II (TPP/SBC), similar observations were found.

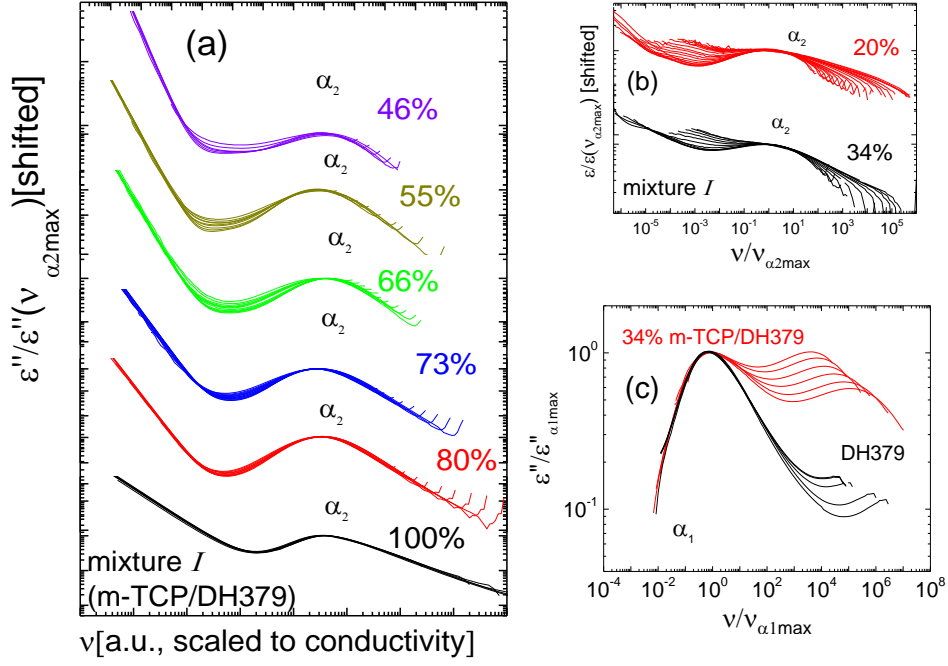


Figure 24: (a) Rescaled spectra displaying the α_2 -relaxation for the mixtures *I* with $c_{m-TCP} \geq 46\%$ to the maximum height and shifted to achieve coincidence with the conductivity contribution. (b) Rescaled data of the α_2 -relaxation for $c_{m-TCP} \leq 34\%$ samples. (c) Rescaled spectra of the α_1 -relaxation of $c_{m-TCP} = 34\%$ and pure DH379 to the height and position of α_1 -process.

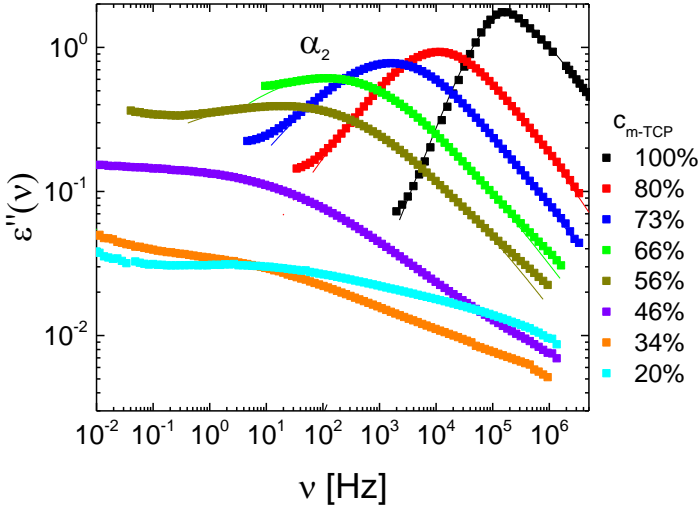


Figure 25: Dielectric spectra of m-TCP/DH379 mixtures for different concentrations at $T = 247$ K showing the α_2 -relaxation. Solid lines: fits by a HN function for $c_{m-TCP} < 100\%$, for neat m-TCP a Kohlrausch function was used. Reprinted with permission from *J. Chem. Phys.*, 2015, 143, 154506, copyright (2015) AIP Publishing.

Figure 26 (a) and (b) compile the relaxation times for both α_1 - and α_2 -process for mixture *I* and *II*, respectively as obtained by DS as well as by NMR [110,111]. The corresponding time constants show good agreement. The relaxation times of the α_1 -process, reflecting the

dynamics of the high- T_g component (DH379 or SBC filled circles), display a non-Arrhenius temperature dependence and shift to lower temperatures with increasing the concentration of the low- T_g component (m-TCP or TPP). This represents the plasticizer effect.

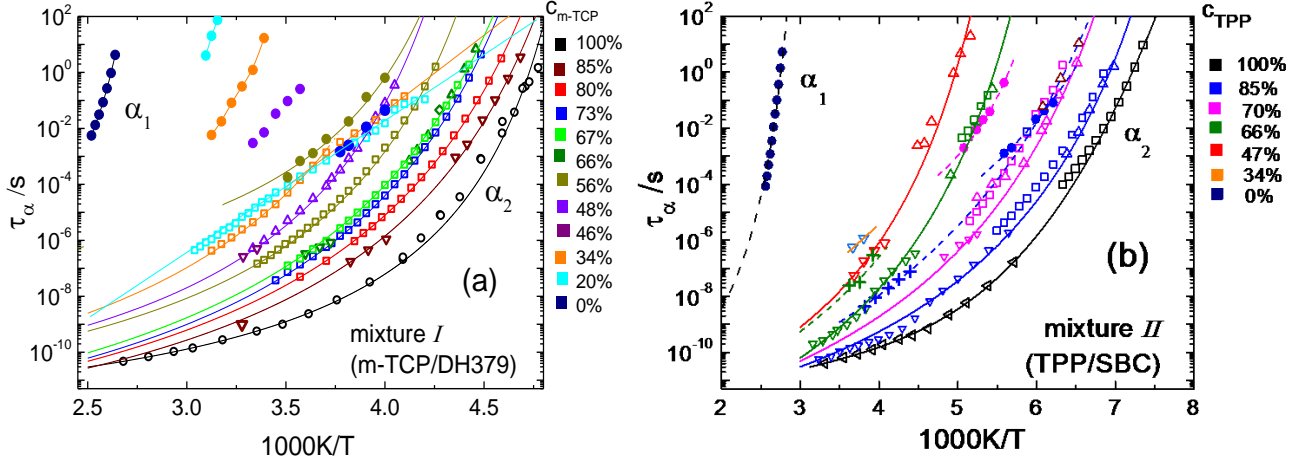


Figure 26: Time constants $\tau_{\alpha_1}(T)$ (DS : filled circles, and NMR : crosses) and $\tau_{\alpha_2}(T)$ (DS: open squares, and NMR : open triangles) for (a) mixture I (DH 379/m-TCP) [Reprinted with permission from *J. Chem. Phys.*, 2015, 143, 154506, copyright (2015) AIP Publishing] (b) mixture II (TPP/SBC) [Reprinted with permission from *J. Chem. Phys.* 2017, 146, 164503, copyright (2017) AIP Publishing] in the whole concentration range (color code defines the concentration).

The relaxation times of the α_2 -process reflecting the dynamics of the low- T_g component (m-TCP or TPP) shift to higher temperatures with decreasing the concentration. This indicates the antiplasticizer effect. Again a non-Arrhenius temperature dependence is observed. However, with further decrease of the concentration of the low- T_g component, say $c_{m-TCP} \leq 34\%$, the temperature dependence of the time constants changes from non-Arrhenius at high temperature to Arrhenius at low temperature (fragile-to-strong transition). The temperature dependence of the $\tau_{\alpha_2}(T)$ resembles that of a thermally activated process like a β -process. The phenomenon is not seen in mixture II due to lack of the data at low concentrations (*cf.* Figure 26b).

Figure 27a focuses on this fragile-to-strong transition found for $c_{m-TCP} = 34\%$ and 20% . Interestingly, this crossover happens close to T_{g1} . The same phenomenon was previously found in the case of TPP/PS mixtures [95,98] which are shown in Figure 27b for comparison.

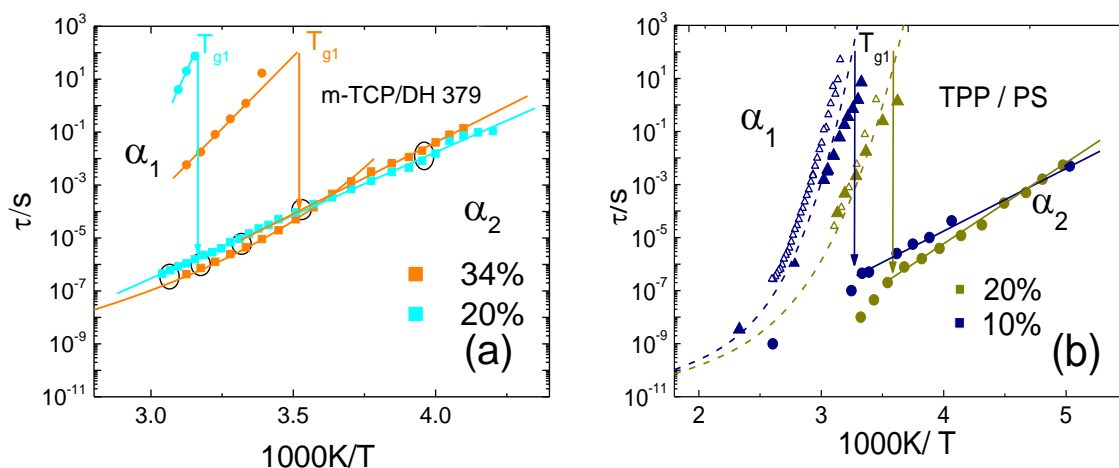


Figure 27: The relaxation times $\tau_{\alpha 1}(T)$ and $\tau_{\alpha 2}(T)$ (a) for the $c_{m\text{-TCP}} = 20\%$ and 34% mixture *I* [Reprinted with permission from *J. Chem. Phys.* 2015, 143, 154506, copyright (2015) AIP Publishing] compared to the behavior found in the polymer-additive system TPP/PS (b) [Reprinted with permission from *J. Chem. Phys.* 2014, 140, 094505, copyright (2014) AIP Publishing]. Black open circles refer to selected temperatures for which NMR experiments were performed.

As said, the temperature dependence of the relaxation time $\tau_{\alpha 2}(T)$ at low concentrations resembles that of a thermally activated process as typically observed for the β -process. However, the 1D NMR spectra shown in Figure 28 at some selected temperatures as well as 2D NMR spectra not shown [110] (marked by black circles in Figure 27a) prove that the low- T_g component ($c_{m\text{-TCP}} = 20\%$) performs an isotropic liquid-like motion. Thus, the low- T_g component displays isotropic liquid-like motion even in the frozen matrix of the high- T_g component ($T < T_{g1}$).

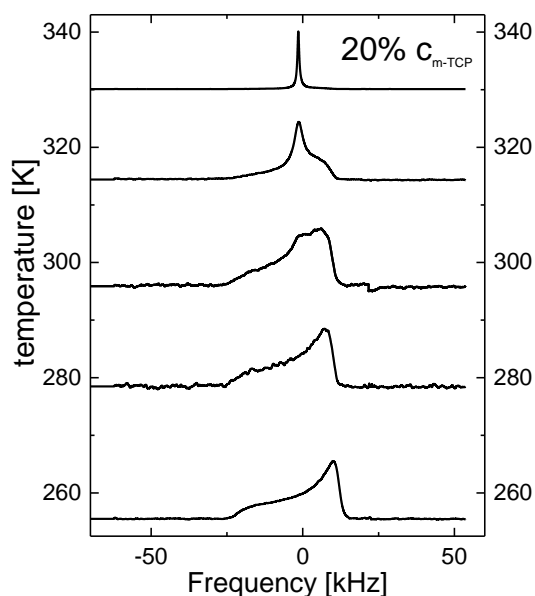


Figure 28: ^{31}P NMR spectra of m-TCP for the mass concentration $c_{m\text{-TCP}} = 20\%$, the baseline of the spectra corresponds to the temperature at which they were measured; the central Lorentzian line represents liquid-like reorientations of m-TCP molecules. Adapted with permission from *J. Chem. Phys.* 2015, 143, 154506, copyright (2015) AIP Publishing.

From Figure 26, two T_g values are extracted (T_{g1} and T_{g2}) by choosing $\tau_\alpha(T_g) = 100$ s. They are presented as function of additive concentration in Figure 29. In the case of mixture *I*, T_{g1} (c_{m-TCP}), continuously decreases upon increasing c_{m-TCP} . In contrast, T_{g2} (c_{m-TCP}) first increases upon decreasing c_{m-TCP} , shows a maximum around $c_{m-TCP} = 50\%$, and then decreases again. This is due to the fragile-to-strong transition which leads to a decrease of $T_{g2}(c)$ at low additive concentrations (*cf.* Figure 26). Three dynamical regimes can be distinguished (*cf.* Figure 29): at $T > T_{g1}$ the dynamics corresponds to that of a binary liquid, at $T_{g2} < T < T_{g1}$ a liquid-like motion of the low- T_g additive arrested in a frozen matrix of the high- T_g component is found. At lowest temperatures ($T < T_{g2}$), both components are arrested. All the features found here are in good agreement with those found by Kahlau et al. [95] for TPP/PS mixtures, shown again in Figure 29c. Due to the lack of the data in the case of mixture *II*, no information at low concentrations can be given (*cf.* Figure 29b).

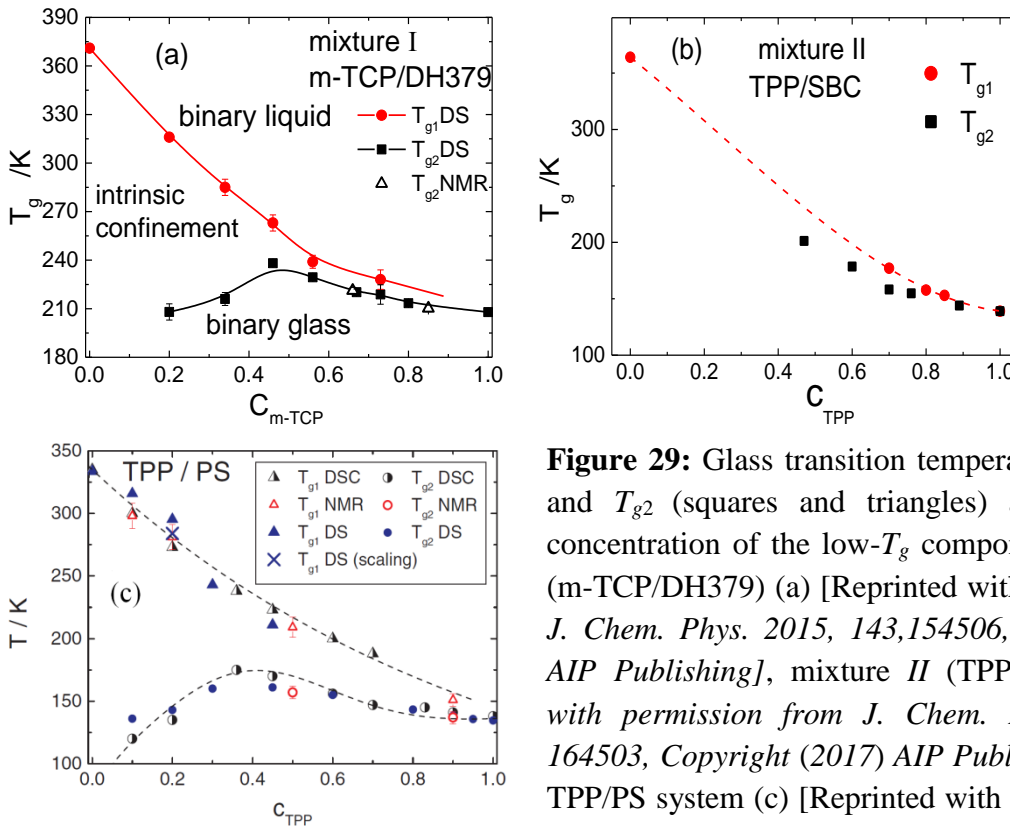


Figure 29: Glass transition temperatures T_{g1} (circles) and T_{g2} (squares and triangles) as a function of concentration of the low- T_g component for mixture *I* (m-TCP/DH379) (a) [Reprinted with permission from *J. Chem. Phys.* 2015, 143,154506, copyright (2015) AIP Publishing], mixture *II* (TPP/SBC) [Reprinted with permission from *J. Chem. Phys.* 2017, 146, 164503, Copyright (2017) AIP Publishing] (b), and in TPP/PS system (c) [Reprinted with permission from *J Chem. Phys.* 2014, 140, 044509. Copyright (2014) AIP Publishing]. Lines are guides for the eye.

4.2.3 Discussion

The results presented here provide a complex scenario for the dynamics of the two asymmetric non-polymeric mixtures with a large T_g contrast of $\Delta T_g = 179\text{K}$ and 222K . Two separate (α_1 and α_2) processes were found even at very low concentrations of the high- T_g component. They were assigned to the dynamics of each component. This situation was not found in some mixtures with small T_g contrast [90-92]; there only one main relaxation process was observed. Yet, two relaxation processes were also observed in polymer-additive mixtures [95-98]. Although a merging of the two processes was suggested at high additive concentrations by Blochowicz et al. [96,97], two separate processes are found in the non-polymeric mixtures even at high concentrations. The process reflecting the dynamics of the low- T_g component (α_2 -process) broadens and shows the anti-plasticizer effect. The broadening depends on temperature, i.e. FTS is violated for the α_2 -process in contrast to the neat component. The transition from a non-Arrhenius to an Arrhenius temperature dependence (fragile-to-strong transition) of $\tau_{\alpha_2}(T)$ is found at T_{g1} . These features remind of the motion of glass formers observed in porous systems where the α -relaxation of the neat glass formers was flattened [112] or governed by broad heterogeneous distribution of correlation times [113,114].

While the α_1 -process is akin to that of the neat high- T_g component, it shows the plasticizer effect. Yet, an indication that a (small) fraction of the low- T_g component participates on the α_1 -process is found which is in accordance with previous results for other asymmetric binary systems [95, 96]. Thus, a scenario of two different sub-ensembles of the low- T_g component, in accordance with Blochowicz et al. [96,97] and Kahlau et al. [95], is found. The participation in the α_1 -process is more pronounced at low concentrations of the low- T_g component, which means that for $c_{low-T_g} \rightarrow 0$ one expects that the α_2 -process disappears and the low- T_g component probes the dynamics of the high T_g component. Further experiments are needed to test this hypothesis. In accordance with Kahlau et al. [95], a maximum is found in $T_{g2}(c)$ at much lower additive concentrations.

Finally, all the dynamical features which were observed in polymer additive [93-99] systems are rediscovered in the present non-polymeric mixtures. Also these qualitative features are in accordance with those revealed by MD simulations [104-107] (*cf.* Figure 17). The dynamic heterogeneities in binary glass formers are usually explained in terms of local concentration fluctuations [115-118] leading to a local distribution of glass transition temperatures in the

mixture. These are either attributed to thermally driven concentration fluctuations or self-concentration effects [119,120]. Yet; for highly asymmetric binary mixtures, an additional effect emerges, specifically; the low- T_g component is confined by essentially rigid matrix of the high- T_g component.

The question arises how large the T_g -contrast is needed to yield asymmetric binary glasses, i.e. systems displaying two T_g values. Mixtures of toluene ($T_g = 117$ K) with quinaldine ($T_g = 180$ K), are currently investigated in our group [121]. Some preliminary results are presented in Figure 30. The spectra of different concentrations and different temperatures are compared to these of neat toluene; all at the peak position of $\nu \cong 10$ Hz. The main relaxation shifts to lower temperatures and becomes broader upon decreasing the concentration of quinaldine. At $c_{\text{quinaldine}} = 20\%$, a shoulder on the low frequency side of the main relaxation appears which indicates the presence of a second process. It appears that even a T_g -contrast of 63 K is sufficient to observe two main relaxations in the mixtures.

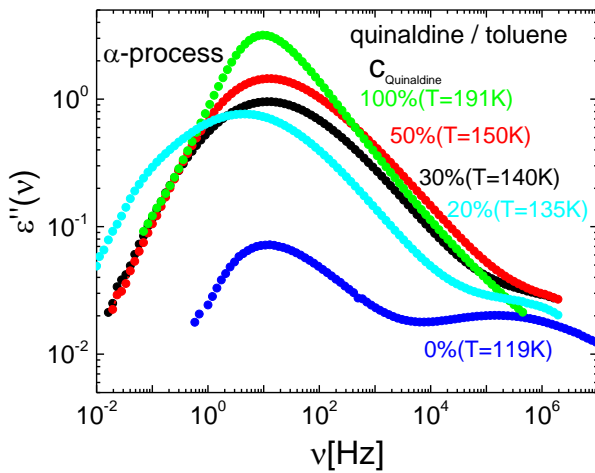


Figure 30: Dielectric data for quinaldine/toluene mixtures of different concentrations compared at $\nu \sim 10$ Hz.

4.3 Secondary process in binary glass formers

In mixtures consisting of type A (no β -process) and type B glass formers (β -process), a secondary (β -) relaxation is observed dielectrically. In some cases, the process shows of a gradual transition to an excess wing with increasing type A concentrations [91,92]. In other mixtures, the process is resolved even at low concentration of the type B glass formers [122,123]. For example, in TPP/PS mixtures, although the neat PS is type A glass former and TPP is a type B glass former, the β -process is observed at low TPP concentration ($c_{\text{TPP}} = 20\%$). The process resembles that of TPP and does not show any concentration dependence. The authors suggested with the help of $^2\text{HNMR}$ that the TPP molecules “enslave” the PS molecules to participate in the process [122]. Moreover, β -relaxation was observed in mixtures containing both components are of type A glass formers [96,124].

In this section, the secondary (β -) process in the binary mixtures (mixture *I* and *II*) is addressed.

4.3.1 Results

Concerning the mixture *II* (SBC and TPP), it has been mentioned in section 4.2.2.1 that the neat components show a well-resolved β -processes, called β_1 -process and β_2 , respectively (*cf.* Figure 19). In the mixtures, the β_2 -process introduced by TPP molecules is rediscovered for all investigated concentrations, i.e. for $c_{\text{TPP}} \geq 60\%$. Figure 31 shows the DS spectra at $T = 105$ K, $T = 115$ K and $T = 125$ K compared to that of neat TPP at the same temperatures. Obviously, position and spectral shape do not alter upon mixing. Yet, the amplitude decreases due to dipole dilution.

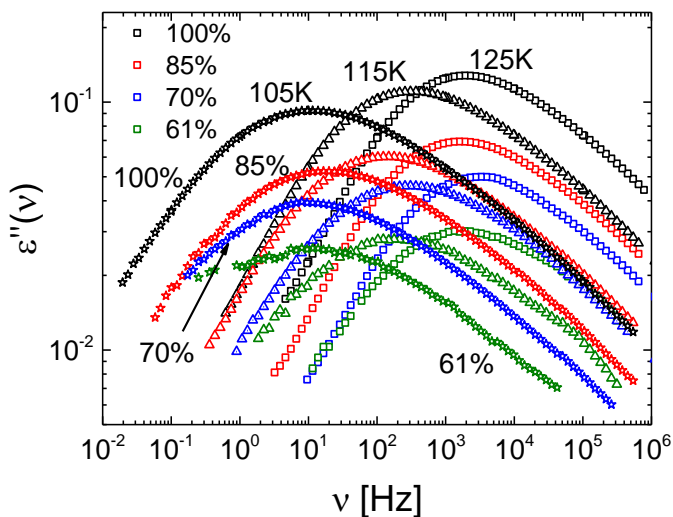


Figure 31: Dielectric spectra of the mixture *II* (TPP/SBC) showing the β -process at $T = 105$ K, 115 K and 125 K for the concentrations as indicated. The amplitudes of the spectra of $c_{\text{TPP}} = 61\%$ are adapted for better comparison. [Reprinted with permission from *J. Chem. Phys.* 2017, 46, 164504, copyright (2017) AIP Publishing].

The relaxation times $\tau_\beta(T)$ are collected along $\omega_{\max}\tau_{\beta 2} = 1$, and are presented in Figure 32 as well as those of the (α_1 -), (α_2 -) and (β_1 -) process of the neat component. The $\tau_{\beta 2}(T)$ data (including data collected by NMR at even lower concentrations from ref. [123]) does not show any concentration dependency; they are the same within experimental uncertainty compared to that of the neat low- T_g component (TPP).

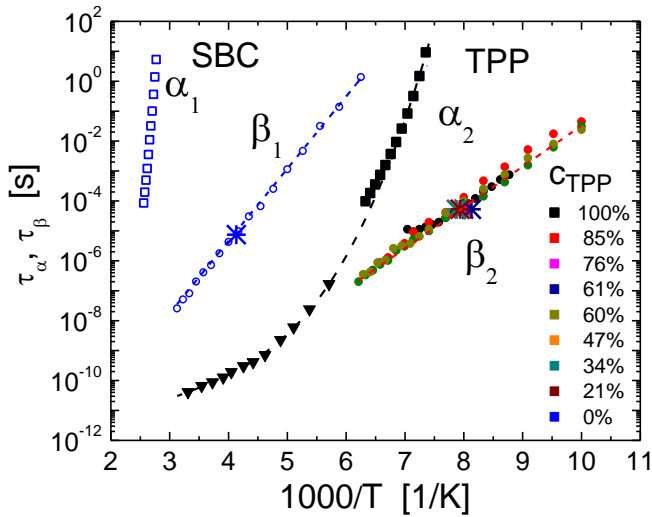


Figure 32: The relaxation times $\tau_{\beta 2}(T)$ (circles: DS for $c_{\text{TPP}} \geq 60\%$; stars: NMR) obtained for different concentrations of the mixture *II* (TPP/SBC). The $\tau_{\alpha 1,2}(T)$ $\tau_{\beta 1,2}(T)$ of the neat components (triangles: NMR; squares: DS) are also displayed. [Reprinted with permission from *J. Chem. Phys.* 2017, 46, 164504, copyright (2017) AIP Publishing]

Regarding the mixture *I* (m-TCP/DH379), it has been mentioned in section 4.2.2 that the neat (m-TCP) component shows an excess wing, while the high- T_g (DH379) component shows a β -relaxation (cf. Figure 18). In the mixture the dielectric loss of different concentrations of m-TCP at the same temperature $T = 180$ K ($T < T_{g2}$) is shown in Figure 33 and for comparison a spectrum of DH379 at the same temperature is included. In the mixture at $c_{\text{m-TCP}} \leq 34\%$, the excess wing develops to a clear relaxation peak which resembles the β -relaxation of the neat DH379.

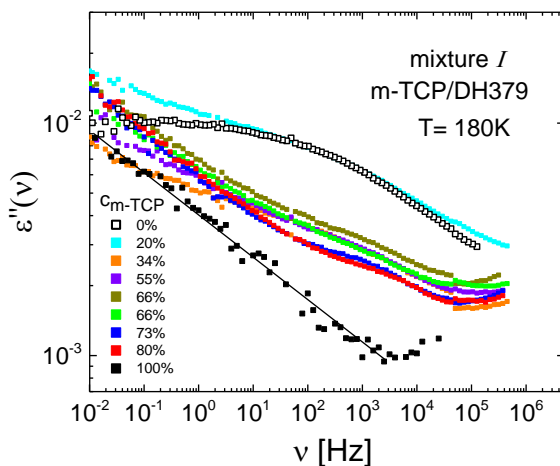


Figure 33: The dielectric loss data for different concentrations of m-TCP in the DH379 mixture at $T = 180$ K.

4.3.3 Discussion

The secondary β -relaxation is examined in binary mixtures. In the mixture *II* (TPP/SBC), both neat components exhibit a well resolved β -process at $T < T_g$; yet with different activation energy. In the mixture, the β_1 -process introduced by SBC interferes with the α_2 -process, while the β_2 -process introduced by TPP molecules is well observable at $T < T_{g2}$, and shows no concentration dependence. Such observations were previously found in other binary mixtures, e.g., THF/PS [96], TPP/PS [122], toluene/picoline [123], and toluene/polychlorinated biphenyl PCB54 [125]. However, a concentration dependence of the time constant was revealed in water/propylene glycol mixtures; an acceleration with decreasing concentration of propylene glycol was reported [126].

Pötzschner et al. [127] applied $^{31}\text{P}/^2\text{H}$ NMR in the mixture *II* (TPP/SBC) which selectively probes TPP or SBC, respectively. They confirmed that the dynamics of the β_2 -process is concentration independent. Further, they claimed that the TPP molecules enslave the large SBC molecules to perform a similar hindered motion which is taken as a strong hint that the secondary process is of cooperative nature [127]. Yet, at lower concentrations, a disintegration of the β_2 -process and so called “islands of rigidity” were proposed [54]. Similar features were found by Bock et al. [122] and Micko et al. [123] where the participation of the type-A component in the β -process of the type-B component was also proposed. Also, there a disintegration of β -process was observed below a certain threshold concentration.

The idea of enslavement could not be forwarded from the presented DS results due to the low dipole moment contribution of the high- T_g molecule. Thus, instead a decrease in the DS signal is observed with increasing the SBC concentration. In the mixture *I* (m-TCP/DH379), the β -process introduced by the large molecule (DH397) is rediscovered in the mixtures of $c_{\text{m-TCP}} \leq 34\%$ and is much akin to that of pure DH379.

5. Dynamics of linear polymers

5.1 State-of-the-art

As said in section 2.3, dynamically, polymers are similar to simple glass formers on short time scales, while they exhibit specific features on long time scales: reptation ($M > M_c$) or Rouse ($M < M_c$) dynamics are observable [128]. As mentioned in section 3.3, in the TR approach a polymer chain “reptates” in a virtual tube exerted by its neighbors [75, 76]. The model predicts for the msd $\langle r^2(t) \rangle$ four characteristic times delimiting the relaxation regimes: $\tau_s \cong \tau_\alpha$ (the segmental or structural relaxation time), τ_e (the entanglement time which defines the onset of entanglement effects), τ_R (the Rouse time), and $\tau_d = \tau_l$ (the disengagement or terminal relaxation time). The scenario was verified by NMR spin echo and NS techniques [129-132]. An example for msd master curve combining those techniques is shown In Figure 34; three different power law regimes are revealed [132]: regime *I* (Rouse) with $\langle r^2(t) \rangle \propto t^{0.5}$, regime *II* with $\langle r^2(t) \rangle \propto t^{0.2}$ (incoherent reptation), and regime *III* with $\langle r^2(t) \rangle \propto t^{0.51}$ (reptation). Also, τ_e can be easily identified by those techniques as well as by FC NMR [133-135] (*cf.* Figure 34). The latter was also applied recently to reveal the msd and agreement with that from NS technique was recorded [136].

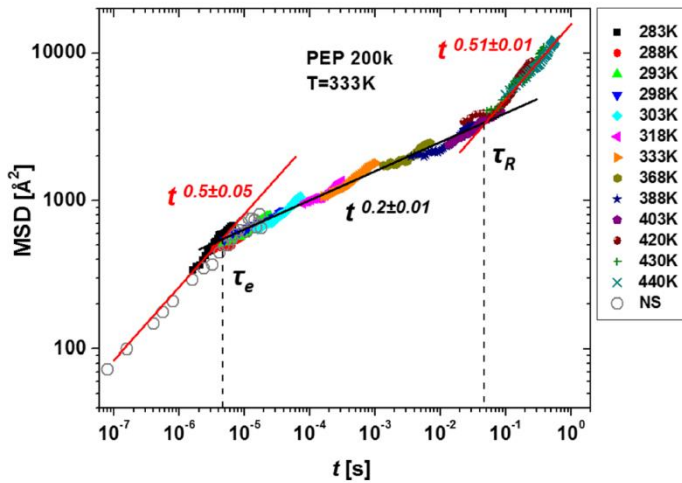


Figure 34: The master curve of the mean square displacement $\langle r^2(t) \rangle$ for PEP measured by the NMR spin echo (filled symbols) and extended with those from NS (open symbols). [Adapted with permission from *J. Chem. Phys.*, 2017, 89, 224901, copyright (2017) AIP Publishing].

Also, measuring the complex shear response $\hat{G}(\omega)$ is most important method to disclose the different relaxation regimes; an example of $\hat{G}(\omega)$ in the case of PB was displayed in section 2.3 (*cf.* Figure 8). From such an experiment, the plateau modulus G_N^0 or $M_e \propto 1/G_N^0$ as well as $\tau_l = \tau_d$ are well defined, while identifying τ_e remains ambiguous. Liu et al. proposed a possible experimental definition for τ_e using the crossover frequency of the loss modulus with the storage modulus in the transition frequency region [137], while Park et al. extracted τ_e value

by isolating the Rouse regime upon subtracting glassy relaxation [138]. Also, it is well-established that the TR model is not sufficient to reproduce details of the $\hat{G}(\omega)$ of entangled polymer melts, additional relaxation mechanisms have to be taken into account, most prominently CLF and constraint release CR according to LM theory [77]. In addition to predicting certain relaxation regimes in terms of characteristic power laws, in particular in the loss $G''(\omega)$, the exact values of the exponents have to be determined and understood. For example, it is well-established for several polymers that in the Rouse relaxation regime $G''(\omega) \propto \omega^{0.7}$ holds [138], i.e. the forecast of the classical Rouse model of $G''(\omega) \propto \omega^{0.5}$ fails [76]. This experimental fact is not taken into account by most polymer theories. Moreover, all polymer theories ignore the crossover to glassy relaxation which is observed at highest frequencies (transition zone) and may impede the appearance of pure Rouse relaxation [138]. Also, several rheological experiments omitted the glass transition regime and focused only on the polymer-specific relaxation [80,137-142].

All these problems will be considered in the present section, as the complex shear modulus $G^*(\omega)$ will be measured for a large temperature range including low temperatures down to the glass transition temperature T_g , i.e., polymer-specific as well as glassy relaxations are covered for linear poly(isoprene) (PI), and poly(butadiene) (PB). Due to the limited frequency window in rheological experiments, τ_α is only available at low temperatures close to T_g . Polymer melts like PI, poly(ethylene-alt-propylene) (PEP), and poly(propylene sulfide) (PPS) will be investigated first by dielectric spectroscopy, which will be taken as a reference data for the rheological measurements. While the dielectric response of PI as a type A polymer has been widely studied, it will be recapitulated and compared to some published data. These data on PI will be further taken as reference for those of complex topology “PI-nanocomposites” which will be discussed in chapter 6.

5.2 Results

The present section is organized as follows. Dielectric results on linear polymers: PI, PEP and PPS are characterized in section 5.2.1. In section 5.3, the viscoelastic response of polymer melts will be investigated.

5.2.1 Polymers studied

Three different molecular weights of polyisoprene (PI) ($M = 4.5, 15.7$ and 58 kg/mol) were synthesized via the standard living anionic polymerization method (provided by *AG Förster, Universität Bayreuth.*). They are produced with a polydispersity D better than 1.04. Poly (ethylene-alt-propylene) (PEP) samples with $M = 3k, 50k$, and $200k$ were provided by the *Richter* group (*Forschungszentrum Jülich, Germany*). Poly (propylene sulfide) (PPS) of $M = 44k$ was provided by *Holger Pletsch Universität Bayreuth.*

For the rheological measurements, eight PI samples were purchased from *PSS Mainz* (Germany) with $M = 4.47k, 10.9k, 23k, 47.3k, 157k, 436k$ and $1090k$. The D was better than 1.04, and in the case of $M = 1090k$ D was better than 1.08. The 1,4-polybutadiene of $M = 119k$ and $441k$ was purchased from *PSS Mainz* (Germany) with a D better than 1.04.

5.2.2 Polymer dynamics studied by dielectric spectroscopy

As said in section 2.3, DS spectra of PI as a type A polymer at $T > T_g$ show two relaxations: a slower normal mode (n) relaxation which probes the fluctuations of the dipole moment along the chain contour (end-to-end fluctuations) and a faster segmental (α) relaxation. Typical DS spectra of PI-5k, PI-16k and PI-58k (studied in this work) are shown in Figure 35. As it is expected, the n-mode slows down with increasing M as it becomes more separated from the α -relaxation. Also, the high-frequency flank of the n-mode exhibits a power law $\varepsilon''(\nu) \propto \nu^{-\gamma}$ with γ decreasing with M : $\gamma \approx 0.8$ in the case of unentangled ($M < M_c \cong 10k$) PI-5k and $\gamma \approx 0.4$ in the case of entangled PI-16k [74]. In the case of PI-58k, highly entangled, the high-frequency flank of the n-mode can be described by two different power laws, the one next to the peak with $\varepsilon''(\nu) \propto \nu^{-\beta}$ and the other further away from the peak $\varepsilon''(\nu) \propto \nu^{-\gamma}$ with $0 < \gamma < 1$, and $\gamma < \beta$ (dashed lines in Figure 35c). The γ value was found to be 0.26 ± 0.01 , which is close to the expected value of $\gamma = 0.25$ from LM model reflecting mainly CLF [77,143].

The relaxation times were extracted via $\tau_i = 1/2\pi\nu_{i\max}$ and compared to those from Abou Elfadl et al. [74] (*cf.* Figure 36). Clearly, the relaxation time of the n-mode $\tau_n(T)$ increases with increasing M [69-74], while $\tau_\alpha(T)$ shows only a weak M dependence. The absolute values of the relaxation times are comparable with those from ref. [74], except in the case of PI-16k; they are smaller than those of the reference sample (PI-14.9, *cf.* Figure 36). For a series of different M , Abou Elfadl et al. [74] demonstrated that $\tau_\alpha(M)$ of PI increases with M and then

saturates at higher M . From which, the $T_g(M)$ was extracted and found to follow the Fox-Flory equation [144].

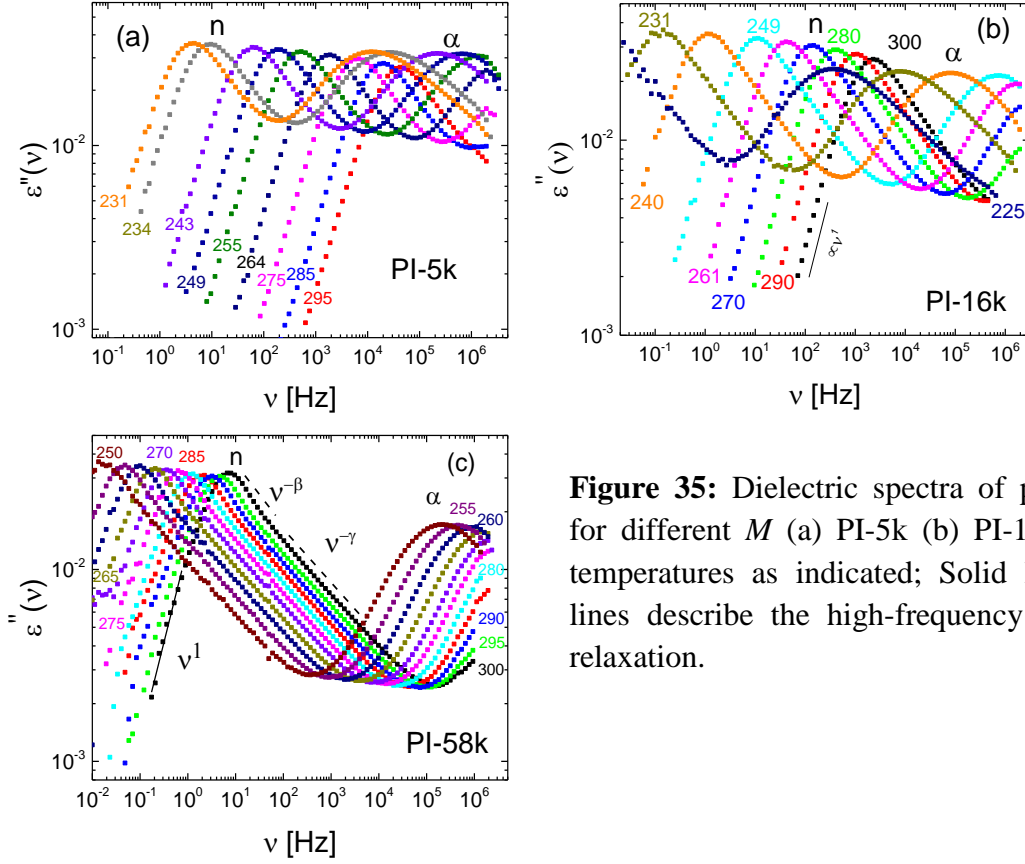


Figure 35: Dielectric spectra of polyisoprene (PI) for different M (a) PI-5k (b) PI-16k (c) PI-58k at temperatures as indicated; Solid lines: ν^I , dashed lines describe the high-frequency flank of the n -relaxation.

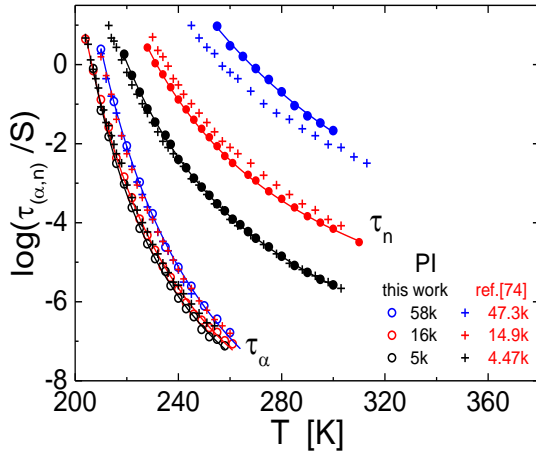


Figure 36: The relaxation times $\tau_\alpha(T)$ (open circles) and $\tau_n(T)$ (filled circles) for PI samples studied in this work and compared to those from ref. [74] (crosses). Solid lines: fits by the VFT equation.

On a reduced frequency scale ($\epsilon''/\epsilon''_{\alpha\max}$ vs. $\nu/\nu_{\alpha\max}$), the spectra are compared to those from ref. [74] in Figure 37a. Clearly, the amplitude of the α -relaxation becomes closer to that of the n -mode with decreasing M in contrast to the published data (the n -mode is always higher than α -relaxation). The separation in frequency between the n -mode and the α -relaxation is in

good agreement with the finding in the reference samples. This is reflected in the $\tau_n/\tau_\alpha(M)$ (cf. Figure 37b). Three different power law regimes are disclosed: $\tau_n/\tau_\alpha \propto M^{2.6}$ for $M < M_c$; $\tau_n/\tau_\alpha \propto M^4$ for $M_c < M < M_{\text{rep}}$, and $\tau_n/\tau_\alpha \propto M^3$ for $M > M_{\text{rep}}$ (cf. section 2.3).

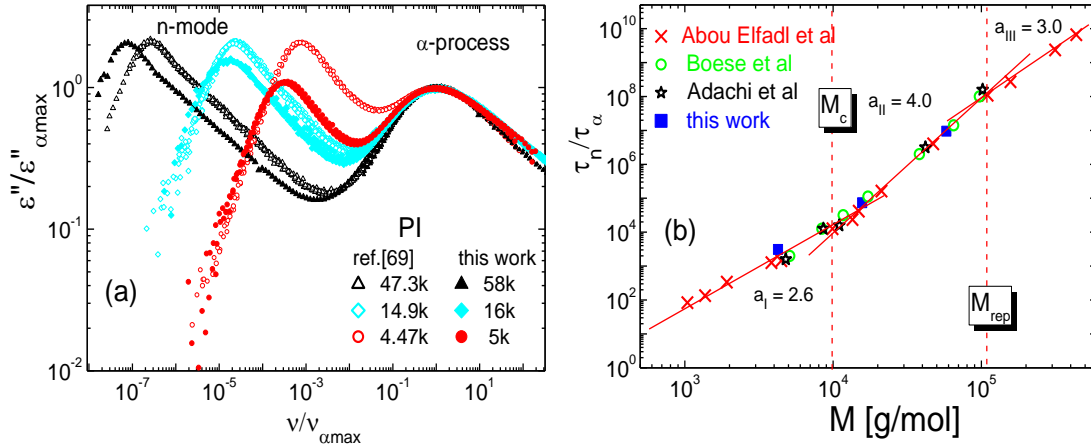


Figure 37: (a) Dielectric spectra scaled to the maximum height and position of the α -process for PI of different M measured in this study (filled symbols) compared to those reproduced from ref. [74] (open symbols). (b) The τ_n/τ_α ratio as function of M obtained from (a) and compared to those from refs. [69,70,74].

In Figure 38 DS spectra above as well as below T_g of PEP with $M = 3k$, and $50k$, and PPS with $M = 44k$ as type B polymers are shown. Also, DS spectra of PI-58k (type A polymer) at $T \leq T_g$ are shown in Figure 38d. In all the cases, the α -relaxation is recognized at high temperatures. Upon cooling, a β -relaxation is distinguished which is well described by a distribution of correlation times $G_\beta(\ln \tau)$, given by Eq. (21) (solid lines in Figure 38). The relaxation times $\tau_\alpha(T)$ and $\tau_\beta(T)$ are collected along $\tau_i(T) = 1/(2\pi \nu_{i\text{max}})$ and presented in Figure 39a. The relaxation times $\tau_\alpha(T)$ obtained from FC ^1H NMR at higher temperatures (PEP [133], PI [74], PPS [147]) as well as from ^2H NMR in the case of (deuterated) PEP-50k [147] are also included. The data obtained from different techniques matches well. A non-Arrhenius temperature dependence is found for $\tau_\alpha(T)$, while $\tau_\beta(T)$ follows an Arrhenius law. In contrast to PI ($\tau_\alpha(T)$ increases with M : cf. above), no M dependency of $\tau_\alpha(T)$ as well as of $\tau_\beta(T)$ is found in the case of PEP (cf. Figure 39a). In all cases the glass transition temperatures T_g were defined along $\tau_\alpha(T_g) = 100\text{s}$ and are listed in Table 2.

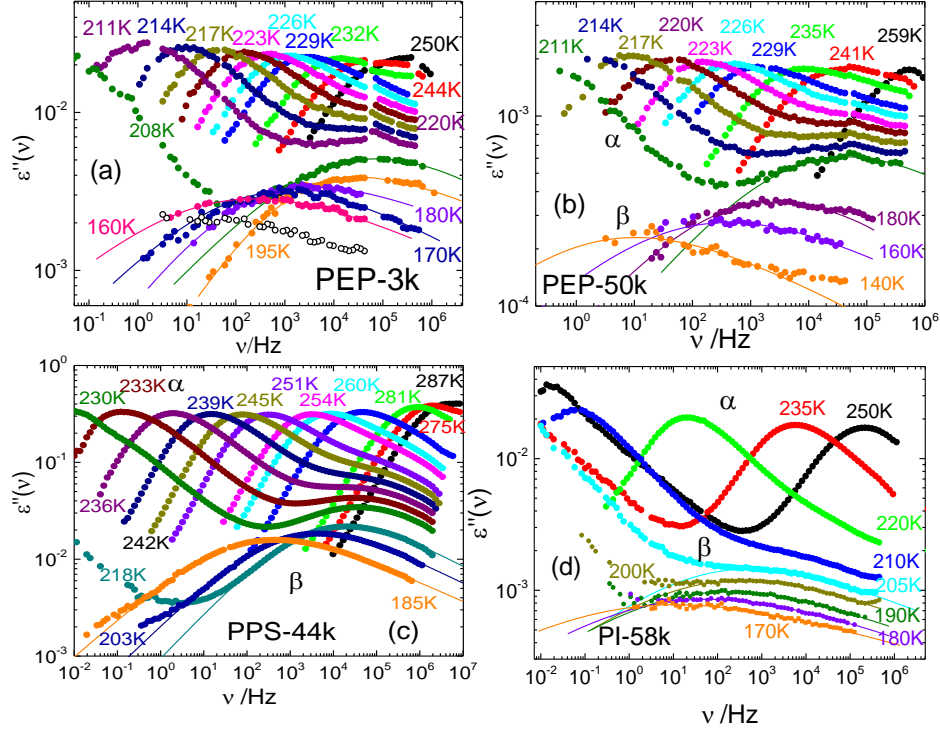


Figure 38: Dielectric spectra of (a) PEP-3k, (b) PEP-50k, (c) PI-58k (normal mode relaxation is not shown) and (d) PPS-44k measured at different temperatures; below T_g selected spectra are shown; solid lines: fits for the β -relaxation using a distribution of correlation times Eq. (21).

In Figure 39b the relaxation times $\tau_\alpha(T_g/T)$ and $\tau_\beta(T_g/T)$ for different polymer melts are compared. Literature data of poly(butadiene) (PB) [148], poly(methyl methacrylate) (PMMA) [149], poly(propylene glycol) (PPG) [134] as well as toluene [150] are also included. Regarding the α -relaxation, $\tau_\alpha(T_g/T)$ for different polymers do not virtually differ, except in the case of PMMA [149]. Assuming the same Arrhenius dependence at $T > T_g$, a merging of the α and β processes around $\tau_\beta = 10^{-6}$ s may be suggested. Again PMMA is an exception. Among polymers, activation energies in the range of $E/R = 17\text{--}26 T_g$ and an attempt time of $\tau_0 = 10^{-18}\text{--}10^{-15}$ s are found (*cf.* Table 2), which are typical of glass formers [23,60].

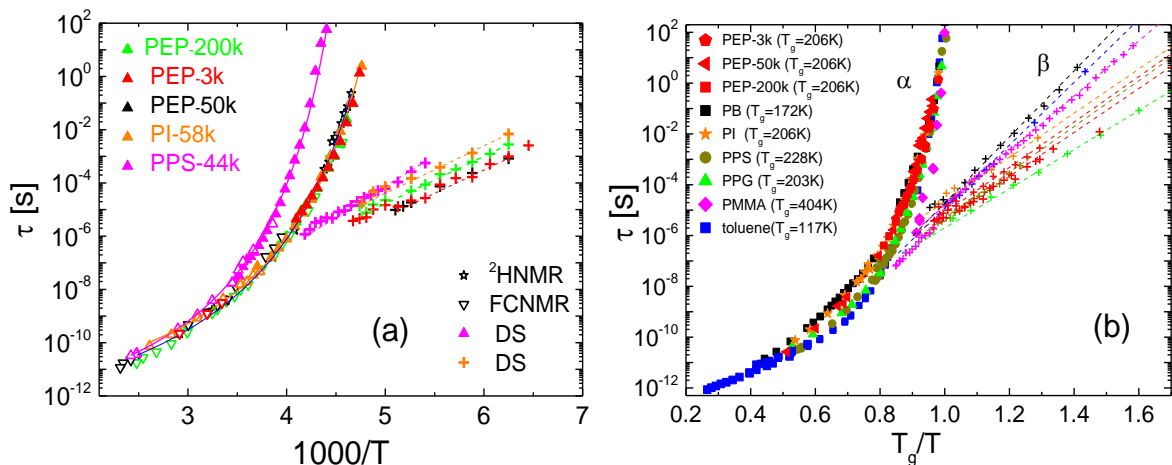


Figure 39: (a) Time constants $\tau_\alpha(T)$ (DS: closed symbols, FC NMR: open symbols, and $^2\text{HNMR}$: stars) and $\tau_\beta(T)$ (crosses) as a function of temperature for different polymers. (b) Time constants $\tau_\alpha(T_g/T)$ (closed symbols) and $\tau_\beta(T_g/T)$ (crosses) for different polymers as well as for toluene for the α -process, Solid lines: VFT fits; dashed lines: Arrhenius fit. [Reprinted with permission from (Koerber, T.; Mohamed, F.; Hofmann, M., Lichtinger, A.; Willner, L.; Rössler, E.A. *Macromolecules* 2017, 50, 1554-1568.) Copyright (2017) American Chemical Society].

system	M [g/mol]	T_g [K]	τ_0 [s]	E/R [K]	E/T_g
PEP	3000	205	9×10^{-15}	4100	20
PEP	50000	205	8.6×10^{-15}	4100	20
PEP	200000	205	8.6×10^{-15}	4243	20.7
PB	87000	172	1.8×10^{-18}	5160	30
PI	58000	206	4.4×10^{-14}	4124	20.0
PPS	44000	228	4.7×10^{-15}	4731	20.8
PPG	18000	203	3.9×10^{-14}	3603	17.8
PMMA	50000	404	2.34×10^{-16}	10051	24.88
toluene	92	117	5×10^{-18}	3240	27.7

Table 2 Different parameters characterizing different polymers and toluene; molecular mass M , glass transition temperature T_g , attempt time τ_0 , and most probable E/R activation energy.

5.2.3 Discussion

Comparing the dielectric results of PI samples used in the present work revealed that the amplitude of the α -process is getting closer to that of the n-mode although the relaxation time ratio $\tau_n/\tau_\alpha(M)$ is in good agreements with those collected by Boese et al.[69], Adachi et al [70,71], and Abou Elfadl et al. [74] (as depicted in Figure 37b). Inspecting the literature results about PI, differences in the height of the α -process are also found [cf. refs. 69-74]. However, Abou Elfadl et al. [74] got the PI samples from the same supplier (*PSS Mainz*); they reported that two PI samples did not follow the overall trend of the strength ratio $\Delta\epsilon_n/\Delta\epsilon_\alpha(M)$ (cf. Figure 40 data shown in brackets). Qualitatively, the $\Delta\epsilon_n/\Delta\epsilon_\alpha(M)$ from the present results shows similar trend, but quantitatively it deviates from the previous results especially at lower M as they show a smaller value (red squares in Figure 40). Thus, one may attribute the difference recorded here to the difference in the preparation method of polyisoprene. Yet, the polymer characteristics like $\tau_n/\tau_\alpha(M)$ or the power exponents are not altered.

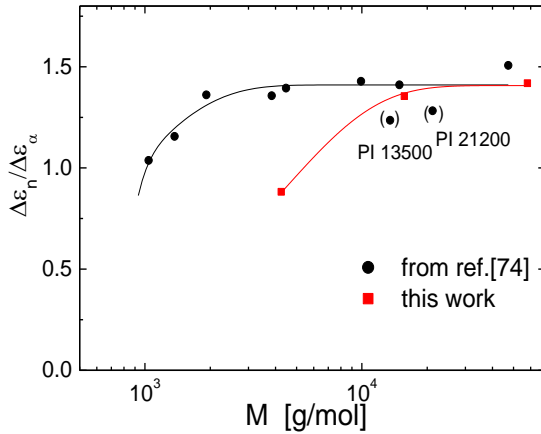


Figure 40: Molecular weight dependence of the ratio $\Delta\epsilon_n/\Delta\epsilon_\alpha$ of PI used in this work (squares) compared to that reproduced from ref. [74] (circles). Solid lines are guide for the eye.

5.3 Viscoelastic properties of PI and PB

The complex shear modulus $\hat{G}(\omega)$ for the polymers PI and PB with M up to 1000k was measured in a temperature range $200\text{K} < T < 373\text{K}$, in order to cover the terminal as well as the glassy dynamics close to T_g (cf. the submitted publication [89]). The measurements were achieved in plate-plate geometry and in a frequency window of $0.003\text{ Hz} \leq \omega/2\pi \leq 30\text{ Hz}$ on an Anton Paar *MCR-500* rheometer (*AG Prof. Aksel, Universität Bayreuth.*). The gap between the plates was $d = 1\text{ mm}$ and plates of $d = 8\text{ mm}$ and $d = 25\text{ mm}$ diameters were used. To reduce the influence of the machine compliance, a plate of 4 mm diameter was also used

when the glass state was accessed [151]. All measurements were done in the linear response regime which was tested by amplitude sweeps carried out at every temperature.

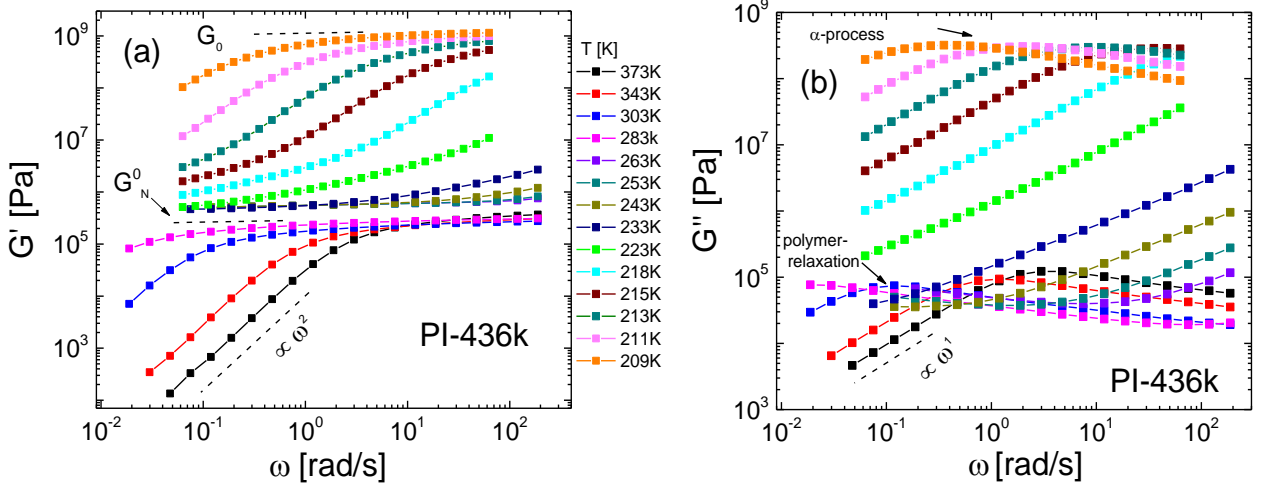


Figure 41: (a) Real $G'(\omega)$ and (b) imaginary part $G''(\omega)$ of the complex shear modulus for PI-436k at temperatures as indicated. Symbols: data as measured; see text.

Figure 41 a and b show storage $G'(\omega)$ and loss $G''(\omega)$ modulus for PI-436k. The data is collected in a temperature range from $T = 209\text{K}$ to $T = 373\text{K}$ covering all relaxation processes. At highest temperature and lowest frequencies, the terminal behavior of a liquid is resolved, i.e. $G'(\omega) \propto \omega^2$ and $G''(\omega) \propto \omega^1$, as illustrated by dashed lines. At lowest temperature, the high-frequency plateau ($G_0 = 1.05 \times 10^9 \text{ Pa}$) is recognized in $G'(\omega)$, while the α -relaxation is observed in $G''(\omega)$. The G_0 value is in accordance with that reported by Santangelo et al. [152] and by Inoue et al. [153] for PI. In between, the polymer relaxation process is observed in $G''(\omega)$, while the rubber plateau modulus G_N^0 is recognized in $G'(\omega)$, which is the characteristic of the entanglement dynamics [142].

The relaxation times obtained via $\tau_i = 1/\omega_{\text{peak}}$ with ω_{peak} denoting the peak position of the polymer or glassy relaxation are shown in Figure 42a and compared to those from DS [74]. For small M , $\tau_{\text{(DS)}} / \tau_{\text{(rheo)}} \cong 3\text{-}5$ is found, while this factor declines for higher M . Glomann et al. reported a similar $\tau_{\text{(DS)}} / \tau_{\text{(rheo)}}$ ratio in the case of PI [143]. Regarding the glassy relaxation time, $\tau_{\alpha(\text{DS})} / \tau_{\alpha(\text{rheo})} = 6$ is found.

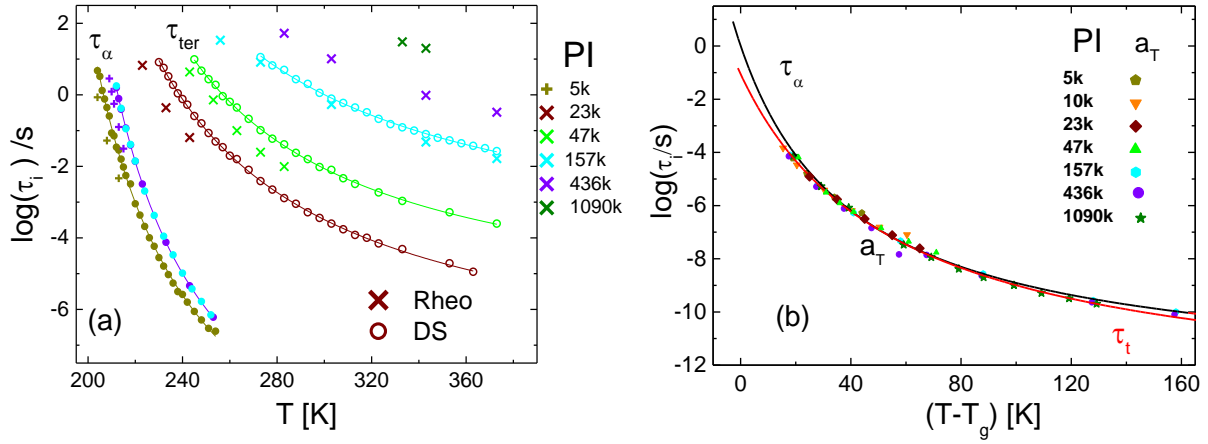


Figure 42: (a) Relaxation times $\tau_{\text{ter}}(T)$ and $\tau_{\alpha}(T)$ of the polymer and α - relaxation as obtained by rheology and by DS [74], respectively. (b) $\tau_{\alpha}(T - T_g)$ from DS (black line). Filled symbols: shift factor $a_T(T - T_g)$ in comparison to $\tau_t(T - T_g)$ (red line); both are scaled vertically to coincide with $\tau_{\alpha}(T - T_g)$. Note the different temperature dependence at lowest temperatures.

5.3.1 Testing FTS

In order to test the applicability of FTS in building master curves, the loss tangent $\tan \delta(\omega) = G''(\omega)/G'(\omega)$ is considered first. In contrast to the modulus it is insensitive to density changing with temperature or to the filling factor. A reference temperature (T_{ref}) is selected much higher than T_g with a shifting factor $a_T(T_{\text{ref}}) = 1$. The data at other temperatures is shifted by applying $a_T(T) \neq 1$ to observe best overlap [142]. Thereby, a master curve $\tan \delta(\omega a_T)$ is obtained as is shown for PI-436k and PB-441k in Figure 43 assuming that FTS holds for all temperatures. This was easily possible until some temperature, in the case of PI till $T = 233\text{K}$ and in the case of PB till $T = 188\text{K}$. Below these temperatures, $\tan \delta$ gradually deviates (*cf.* Figure 43). Colby et al. [78] accepted the failure in the case of PB-130k as they showed a master curve covering terminal relaxation down to glassy dynamics (*cf.* Figure 8).

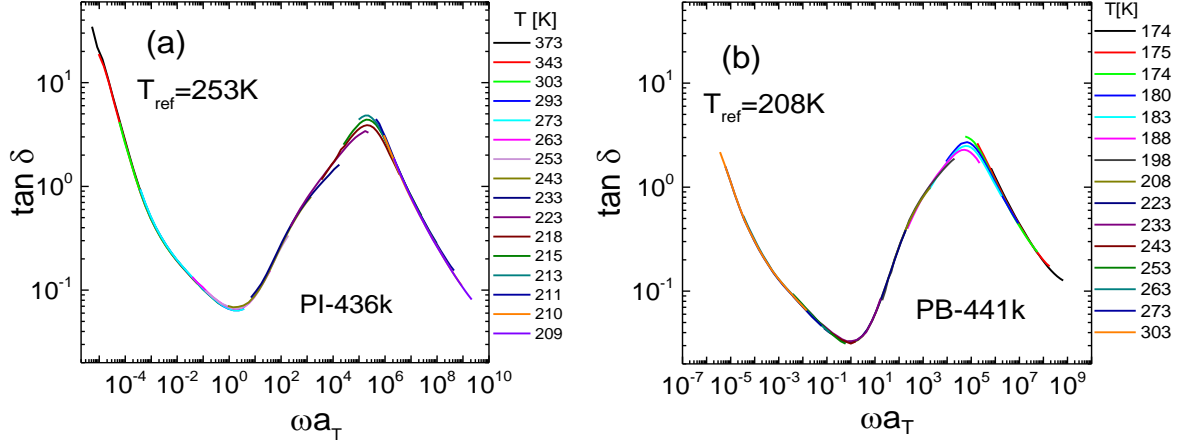


Figure 43: Loss angle $\tan\delta(\omega a_T) = G''(\omega)/G'(\omega)$ for (a) PI-436k and (b) PB-441k, master curves are built assuming that FTS holds.

In terms of DS as a technique with a wider frequency window, in particular in the case of PI (type A polymer, as discussed above), the failure of FTS was also revealed [74]. In Figure 42b, the relaxation time $\tau_{\alpha(DS)}(T-T_g)$ and those of the n-mode $\tau_n(T-T_g)$ are shown; the latter scaled vertically to collapse with $\tau_{\alpha(DS)}(T-T_g)$. The $a_T(T-T_g)$ used in the case of PI are also included in Figure 42b and scaled vertically to collapse with those from DS. Clearly, close to T_g , the temperature dependence of the $\tau_n(T)$ (red) or of $a_T(T-T_g)$ and that of $\tau_{\alpha}(T)$ (black) are decoupled, i.e. $\tau_{\alpha}(T)$ grows faster upon cooling. The phenomenon is known as “rheological complex” [153-161]. Accordingly, the part where $\tan\delta(\omega a_T)$ did not reveal any systematic deviation (FTS works) is converted to $\tan\delta(\omega \tau_{\alpha(DS)})$ by introducing $\tau_{\alpha}(T_{ref})$ from DS (*cf.* above) [74,147,148], as shown in Figure 44 for PI of different M . This part displays the polymer specific relaxation.

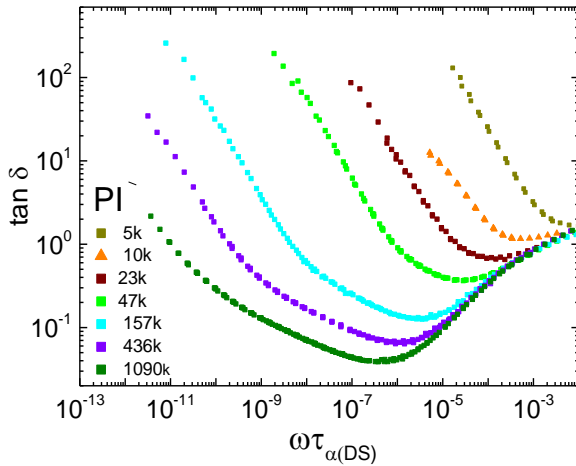


Figure 44: Loss tangent $\tan\delta(\omega \tau_{\alpha})$ displays the polymer specific relaxation for PI of different M .

5.3.2 Master curves $G'(\omega\tau_a)$ and $G''(\omega\tau_a)$

Next, the moduli $G'(\omega\tau_a)$ and $G''(\omega\tau_a)$ were obtained. A vertical shift factor b_T is used in order to remedy some weak changes of the density with temperature. In such a way, the master curves for PI of different M are obtained and are presented in Figure 45. As said, for the polymer relaxation part are displayed on the left side of Figure 45, while a single spectrum at $T = 215$ K for the case of PI-436k is displayed on the right side and scaled using $\tau_{a(\text{theo})}$. The latter shows the glassy relaxation. Thus, all relaxation regimes are covered avoiding FTS problems.

Regarding the polymer relaxation (left side of Figure 45(a) and 45(b)), satisfactory master curves are obtained until $\omega\tau_a = 10^{-2}$. Effectively, almost 10 decades in frequency are covered. At $3 \times 10^{-3} < \omega\tau_a < 1 \times 10^{-2}$, $G'(\omega\tau_a)$ and $G''(\omega\tau_a)$ are essentially M -independent. At such high (reduced) frequencies a power law response close to $G'(\omega\tau_a) \propto G''(\omega\tau_a) \propto (\omega\tau_a)^{0.7}$ is seen for highest M (dashed line in Figure 45(b)) which discloses Rouse relaxation. The exponent, yet, does not agree with that expected for Rouse dynamics of $G''(\omega\tau_a) \propto (\omega\tau_a)^{0.5}$ [67]. At lower frequencies, $G'(\omega\tau_a)$ develops the rubber plateau. It extends toward lower frequencies with increasing M [78,79,142]. There, $G''(\omega\tau_a)$ develops a minimum which weakly shifts toward lower frequencies upon increasing M . At lowest frequencies, while G' decays, the terminal relaxation peak in G'' is observed at $\omega \cong \tau_a^{-1}$, which again depends strongly on M . The terminal power laws $G'(\omega) \propto \omega^2$ and $G''(\omega) \propto \omega^1$ typical of liquid flow are found for all M .

Regarding the data on right side (glassy relaxation), for comparison the results for PG as a simple liquid is also included [162]. While the data of PI incidentally agrees with that of PG at high frequencies, it deviates below frequencies of $\omega\tau_a \cong 10^{-1}$. This is expected due to the crossover to polymer (Rouse) relaxation which impedes full establishment of glassy relaxation.

To identify different relaxation regimes in terms of their power laws exponents, a derivate method is proposed. The method provides the power law exponent ε as a function of (reduced) frequency, along $\varepsilon'(\omega\tau_a) = d \log G' / d \log(\omega\tau_a)$. The exponents ε' and ε'' are shown in Figure 45(c) as a function of $\omega\tau_{a(\text{DS})}$ (left) and $\omega\tau_{a(\text{theo})}$ (right). Regarding the polymer relaxation (left side), at highest frequencies an apparent exponent of about $\varepsilon'' \cong 0.7$ is observed. Within about one decade lower, the exponent settles to a plateau value $\varepsilon'' \cong 0.6$ at

$\omega\tau_\alpha \cong 3 \times 10^{-3}$, which extends down to $\omega\tau_\alpha \cong 5 \times 10^{-5}$ for the highest M . The extension of the Rouse regime at low frequencies appears to grow with M . Yet, the Rouse regime is expected to be terminated by the entanglement time τ_e which is independent of M . Here, $G'(\omega\tau_\alpha)$ reaches its plateau reflected by ε' reaching zero.

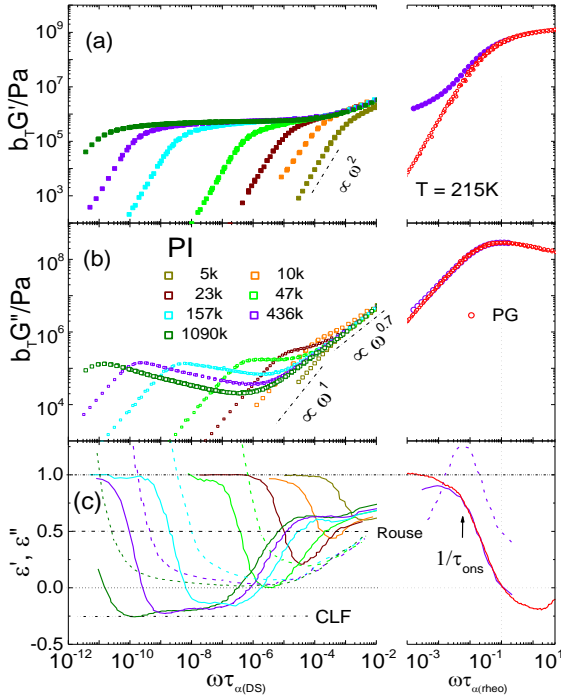


Figure 45: Master curves (a) $G'(\omega\tau_\alpha)$ and (b) $G''(\omega\tau_\alpha)$ of PI; different M values as indicated. Left: polymer specific ($T \geq 233$ K) and right: a single glassy relaxation spectrum at $T = 215$ K scaled by $\tau_{\alpha(\text{rheo})}$. Note interruption of the frequency axis. Data of the propylene glycol (PG) is included [162]. (c) Power law exponents $\varepsilon'(\omega\tau_\alpha)$ and $\varepsilon''(\omega\tau_\alpha)$ of $G'(\omega\tau_\alpha)$ (dashed lines) and $G''(\omega\tau_\alpha)$ (solid lines), respectively. Terminal power laws ω^1 and ω^2 as well as Rouse and CLF behavior are indicated (dashed dotted lines). Onset frequencies of polymer relaxation are marked (see text).

Regarding the low-frequencies, the exponent ε'' crosses over from the Rouse plateau to surpass zero, which reflects the minimum in $G''(\omega)$. At even lower frequencies, the high-frequency flank of the terminal peak shows up characterized by again a plateau value of $\varepsilon'' = -0.20 \pm 0.01$ at highest M . Indeed, a power law behavior of $G''(\omega) \propto \omega^{-0.25}$ is expected for the tube-survival function at highest frequencies reflecting the effect of CLF (incoherent reptation) (*cf.* section 3.2) (“CLF” in Figure 45c). The expected $G''(\omega) \propto \omega^{0.5}$ for pure reptation is not observed. Remarkably, there is a further “step-wise” decrease of the exponent ε'' at lowest frequencies of the high-frequency flank of the terminal peak. On the other hand, the rubber plateau is signaled by ε' reaching almost zero, yet there is some weak (linear) increase with decreasing $\omega\tau_\alpha$.

In the case of the glassy relaxation, the exponents $\varepsilon'(\omega\tau_{\alpha(\text{rheo})})$ and $\varepsilon''(\omega\tau_{\alpha(\text{rheo})})$ as well as those of the simple liquid (PG) are shown in Figure 45c (right). While in the case of PG the terminal relaxation involving a low-frequency exponent $\varepsilon'' = 1.0$ is immediately reached, as expected

for a simple liquid, a maximal exponent of $\varepsilon'' \cong 0.7 - 0.8$ is found for PI. The difference between the exponent of PG and that of PI sets in at frequencies for which $\varepsilon'(\omega\tau_\alpha)$ exhibits a maximum. The crossover from glassy to Rouse relaxation at $\omega_{\text{ons}}\tau_\alpha \cong 6 \cdot 10^{-2}$ may be identified as the onset frequency, i.e., at $\omega < 1/\tau_{\text{ons}}$ polymer-specific relaxations become dominant (“ $1/\tau_{\text{ons}}$ ” in Figure 45c).

Analogous to the case of PI, the analysis is also performed in the case of PB of $M = 119\text{k}$ and 441k (cf. $\tan\delta(\omega a_T)$ in Figure 43b). The relaxation time $\tau_{\alpha(\text{DS})}(T_{\text{ref}})$ was taken from ref.[148] (using the high- M limit of $\tau_{\alpha(\text{DS})}(T, M)$). Again, Figure 46 shows the polymer relaxation on the left side and single spectrum of glassy relaxation on the right side. The latter is extended in $G''(\omega\tau_\alpha)$ to higher frequencies with a fit of the α -process at lower temperature using a generalized Cole-Davidson function (with $\beta = 0.27$ and $\alpha = 0.5$) [84]. An onset frequency $\omega_{\text{ons}}\tau_\alpha \cong 6 \cdot 10^{-2}$ is extracted being the same as in PI within the experimental error. The Rouse regime which is clearly identified in the left part of Figure 46 exhibits a power law exponent of $\varepsilon'' \cong 0.7$. Its low-frequency end shows for the higher M , a weak overshoot as in the case of PEP. The exponent in the CLF regime is again close to $\varepsilon = -0.20$. As for PI and PEP, a further small step-wise decrease is observable at lower frequencies.

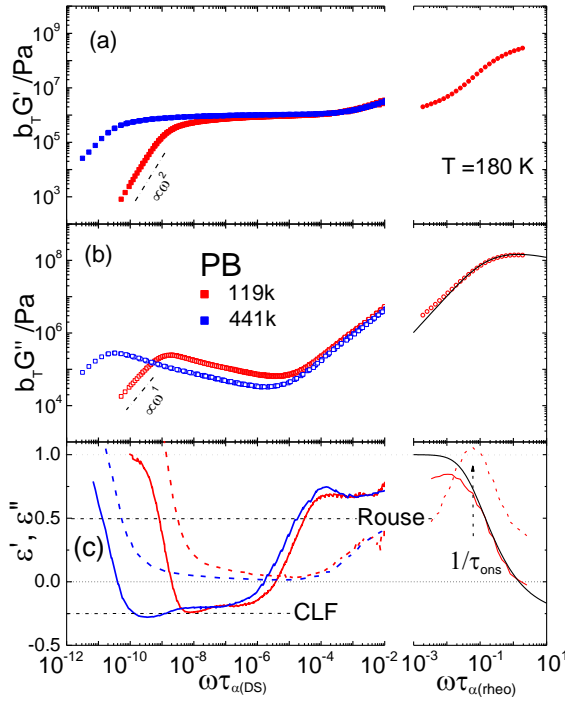


Figure 46: Master curves (a) $G'(\omega\tau_\alpha)$ and (b) $G''(\omega\tau_\alpha)$ of PB, different M values as indicated. Left: polymer specific ($T \geq 233\text{K}$); right: single spectrum glassy relaxation at $T = 180\text{ K}$. A generalized Cole-Davidson function [84] (with $\beta = 0.27$ and $\alpha = 0.5$) interpolating the α -relaxation is included. Note the interruption of the frequency axis. (c) Power law exponent $\varepsilon''(\omega\tau_\alpha)$ and $\varepsilon'(\omega\tau_\alpha)$ of $G'(\omega\tau_\alpha)$ (solid lines) and $G''(\omega\tau_\alpha)$ (dashed lines), respectively. Terminal power laws ω^1 and ω^2 as well as Rouse and CLF behavior are indicated (dashed dotted lines). Onset frequencies of polymer relaxation are marked (see text).

5.3.2 Scaling analysis

Regarding the polymer relaxation of PI and PB, for high M the apparent exponent passes through zero twice, at the minimum of $G''(\omega\tau_\alpha)$ and at maximum of the terminal relaxation peak. From these points, $(\tau/\tau_\alpha)^{-1}(M)$ and $(\tau_{\min}/\tau_\alpha)^{-1}(M)$ can be obtained. In the case of the terminal relaxation, for lower M values, $\varepsilon''(\omega\tau_\alpha)$ not any longer passing through zero, the spectra still can be included when best overlap at lowest frequencies is achieved. In other words, one constructs master curves for the exponent scaled along $\varepsilon''(\omega\tau_i)$ and $\varepsilon''(\omega\tau_{\min})$, respectively. Curves rescaled in this way are displayed in Figure 47 for PI; very similar results are found for PEP from ref. [89,164]. As expected, the $\varepsilon(\omega\tau_i)$ curve of the highest M provides the low-frequency envelope of all the other curves with lower M values. Analogously, an envelope is found for $\varepsilon''(\omega\tau_{\min})$ around $\omega\tau_{\min} \cong 0.5 - 10$, yet only for the highest M values. Further, as the minimum of $G''(\omega\tau_\alpha)$ can be described by a sum of two power laws with exponent $\varepsilon' = \varepsilon_{eCLF}$ ($\omega < \omega_{\min}$) and ε_a ($\omega > \omega_{\min}$)[1]

$$G''(\omega\tau) = G_{\min} \frac{1}{\varepsilon_{eCLF} + \varepsilon_a} \left[\varepsilon_a (\omega/\omega_{\min})^{-\varepsilon_{eCLF}} + \varepsilon_{eCLF} (\omega/\omega_{\min})^{\varepsilon_a} \right] \quad (39)$$

this leads to an interpolation formula of the power law exponent

$$\varepsilon''(\omega/\omega_{\min}) = \varepsilon_{CLF} \varepsilon_e \frac{(\omega/\omega_{\min})^{\varepsilon_a} - (\omega/\omega_{\min})^{-\varepsilon_{eCLF}}}{\varepsilon_a (\omega/\omega_{\min})^{-\varepsilon_{eCLF}} + \varepsilon_{eCLF} (\omega/\omega_{\min})^{\varepsilon_a}} \quad (40)$$

A satisfying interpolation of the universal part of $G''(\omega\tau_{\min})$ is revealed in Figure 47b (dotted lines) using $\varepsilon_a = 0.75$. In the scaling analysis $\varepsilon_a = 1$ is expected (*cf.* Figure 12), however, we note that in the quantitative LM approach $\varepsilon_a < 1$ is observed, too [77].

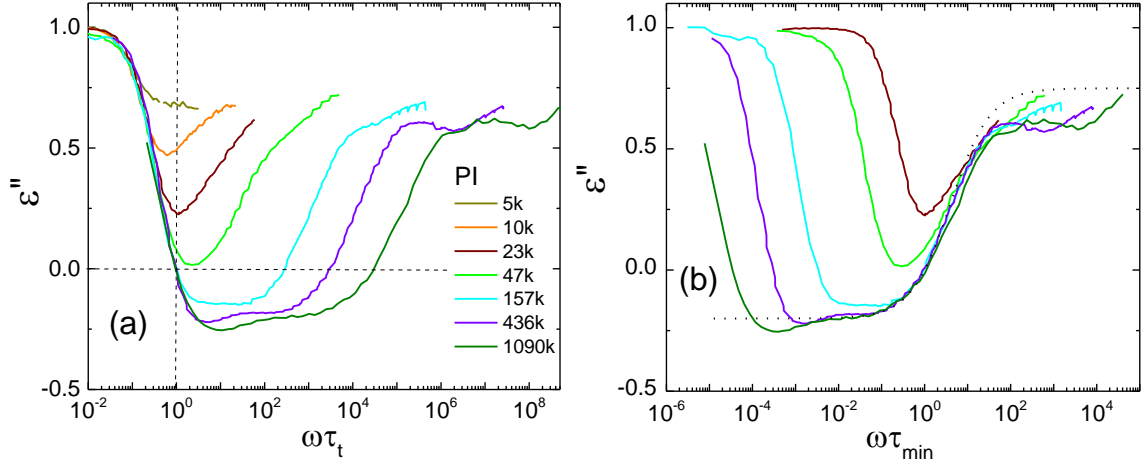


Figure 47: (a) Power law exponent ε'' of PI as a function of frequency scaled by the terminal relaxation time τ_t , and (b) scaled by the relaxation time τ_{\min} of the minimum in $G''(\omega\tau_\alpha)$; molar masses are indicated. Dotted lines: interpolation applying Eq. (40) with $\varepsilon_a \approx 0.75$ and $\varepsilon_{\text{CLF}} = 0.2$.

From the scaling in terms of $\varepsilon''(\omega\tau_t)$ and $\varepsilon''(\omega\tau_{\min})$, the M dependence of τ_t/τ_α and τ_{\min}/τ_α for PI and PB can be extracted; as displayed in Figure 48. The $\tau_t/\tau_\alpha(M)$ and $\tau_{\min}/\tau_\alpha(M)$ for PEP from refs. [89,164] are also included in Figure 48. At intermediate M values, the terminal relaxation scales along $\tau_t/\tau_\alpha \propto M^{\alpha_t}$ with $\alpha_t = 4.0 \pm 0.1$ (PI) and 3.9 ± 0.1 (PEP). In the former case we omitted the two data points at highest M values which disclose a lower exponent $\alpha_t = 3.1 \pm 0.1$ at $M > 157$ k. An exponent of 3.0 is characteristic of pure reptation, while the influence of CLF leads to an exponent larger than 3.0. Richter and coworkers [80] reported for PI a crossover to $\alpha_t = 3.0$ above $M_r \cong 150$ k and $\alpha_t = 3.9$ below. In a dielectric study on PI, an exponent of $\alpha_t = 4.0 \pm 0.2$ below $M \cong 100$ k and $\alpha_t = 3.0$ for higher M was found [74]. Thus, our rheological data do agree with previous findings. In the case of PB the two data point and that obtained by analyzing the data of Colby et al. [78] (*cf.* Figure 8) belong to the pure reptation regime as an exponent $\alpha_t = 3.0 \pm 0.2$ is found. Here, Unidad et al. reported $\alpha_t = 3.0 \pm 0.2$ [81]. As the crossover molar mass M_c of PI is significantly different from that of PEP and PB the individual data are shifted on the M axis.

Regarding the second generic relaxation regime, $\tau_{\min}(M)$ approximately scales with $M^{1.0 \pm 0.1}$ and the amplitude G''_{\min} value shows $M^{0.7}$ dependence. Both exponents are close to the predictions of the scaling approach yielding $\tau_{\min} \propto M^{4/5}$ and $G''_{\min} \propto M^{4/5}$ (*cf.* section 3.3). From the experimental finding $(\omega\tau_\alpha)_{\min} \propto M^1$, one can estimate a corrected exponent $a_e = 3/4$

which leads to $G''_{\min} \propto M^{-3/4}$ which is close to empirical exponent 0.75. This value $a_e = 0.75$ was also chosen to interpolate the master curve in Figure 47b.

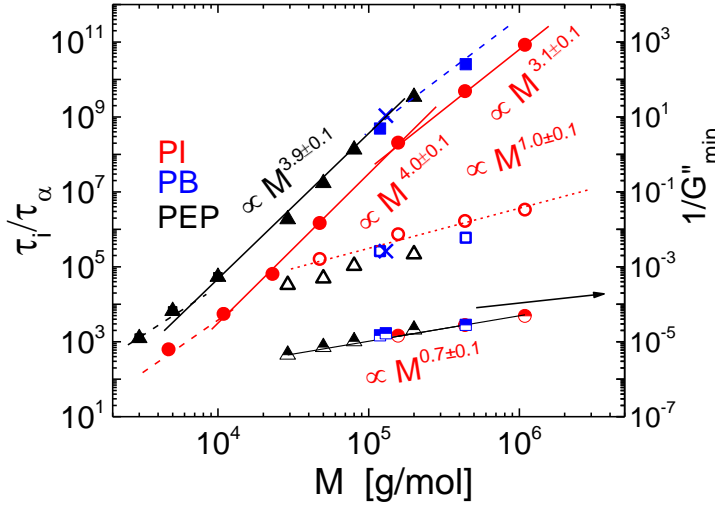


Figure 48: The ratios τ_i/τ_α (closed symbols) and τ_{\min}/τ_α (open symbols) as a function of the molar mass M , the right hand axes refers to the amplitude of the local minimum found in G'' . Crosses: data obtained from ref. [78]. Solid and dotted lines: power exponent for different regimes. Dashed lines: guide for the eyes.

5.3.3 Discussion

Measuring the rheological response of PI and PB over a large M and temperature range, master curves $G'(\omega\tau_\alpha)$ and $G''(\omega\tau_\alpha)$ were constructed containing solely polymer relaxation and covering over 10 decades in frequency. Data down to lowest temperatures is included for which the master curve $\tan\delta(\omega\tau_T)$ does not reveal any systematic deviations. A single relaxation spectra in the transition zone including the glassy (α) relaxation peak is presented to cover the response over the full frequency range. Such broad “iso-frictional” spectra were only reported in a few cases, yet, assuming FTS to hold over the whole temperature range [78,152,160]. In the present case, the discussion of iso-frictional spectra was achieved by taking recourse to previously published data of $\tau_\alpha(T)$ [69,147,148], and thereby direct comparison among different polymers becomes possible.

Before discussing the experimental results on the exponent $\varepsilon''(\omega\tau_\alpha)$, a scheme showing the expected exponent $\varepsilon''(\omega)$ of a simple scaling approach given in section 3.3 is presented in Figure 49a including a calculated $\varepsilon''(\omega)$ curve within the full LM approach (dashed line) by applying the “REPTATES” program available in the web [89,165]. The crossover times/frequencies are indicated and are expected to be easily identified experimentally in $\varepsilon''(\omega\tau_\alpha)$, including the entanglement frequency τ_e^{-1} . Also, all power law regimes expected

from the scaling approach given in section 3.3 are re-discovered in the so-calculated LM curves, yet the absolute values of the exponent may be somewhat different (see discussion below). In Figure 49b the experimental $\varepsilon''(\omega)$ for rather high M of PI, PB and those for PEP from ref. [164], is compared. Qualitatively, high similarity is recognized among the polymers. All subtle features to be discussed subsequently show up in all the three polymers.

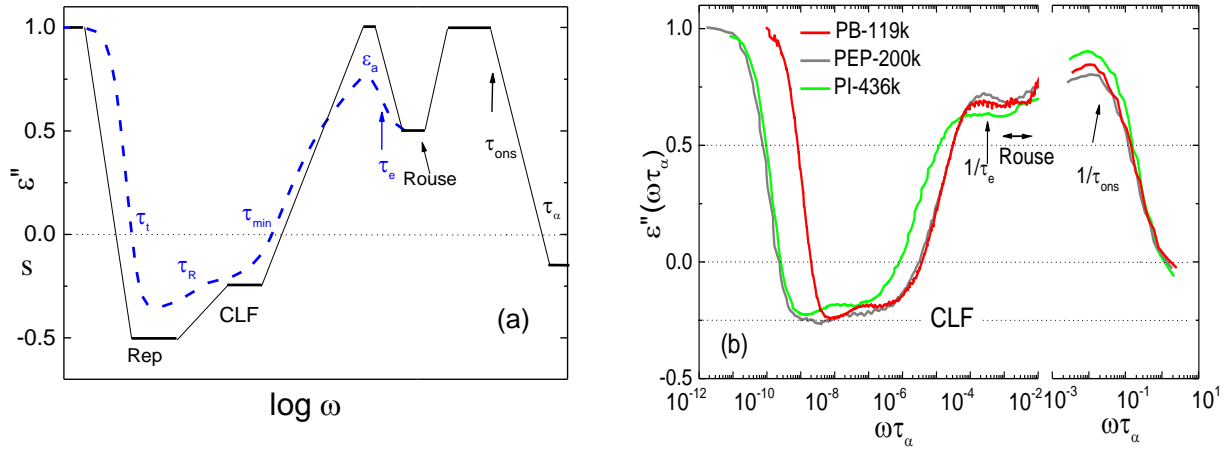


Figure 49: (a) Schematic behavior of $\varepsilon''(\omega)$ expected in the frame of the TR model including CLF (black lines) (*cf.* Figure 12); $\varepsilon''(\omega)$ curve calculated from to the full LM approach are included (dashed lines); crossover frequencies/times are indicated. (b) Power law exponent ε'' as a function of the (reduced) frequency for PB, PEP, and PI with higher M ; Dotted lines represent ideal Rouse and CLF behavior.

From Figure 49a, at frequencies below those of the minimum in $G''(\omega)$ ($1/\tau_{\text{R}} \ll \omega \ll 1/\tau_{\min}$) which reflect the high-frequency flank of the terminal relaxation peak, one first expects an exponent $\varepsilon''_{\text{CLF}} = -0.25$ (CLF and incoherent reptation) and $\varepsilon''_{\text{rept}} = -0.5$ (pure or coherent reptation) at lower frequencies. Indeed, indications of two separate regimes are found in Figure 49b with an effective exponent $\varepsilon''_{\text{eCLF}}$ (at high frequencies) and $\varepsilon''_{\text{emin}}$ (at lower frequencies) (*cf.* Table 3). Within the experimental error $\varepsilon''_{\text{eCLF}}$ of PI, PEP, and PB is identical, which is close but slightly above the expected value of $\varepsilon''_{\text{CLF}} = -0.25$ [77]. In contrast to $\varepsilon''_{\text{eCLF}}$, $\varepsilon''_{\text{emin}}$ slightly decreases with M , which may be taken as a reminiscent of the crossover to pure reptation at lower frequencies. Inspecting the calculated curves of the LM approach, such an undershoot of ε'' is seen too. Richter and coworkers, measuring PI up to extremely high $M = 3600\text{k}$, did not find indications of a behavior approaching $G''(\omega) \propto \omega^{-0.5}$, either [80]. The authors interpolated their relaxation spectrum by the mode spectrum proposed by Winter et al. (BSW spectrum) [166] and found an average exponent of -0.19 ± 0.02 which is

very close to the ε''_{eCLF} . Yet, using the BSW spectrum one is not able to extract the subtle changes revealed when analyzing the exponent $\varepsilon''(\omega\tau_\alpha)$, in particular, the slight further decrease of ε'' signals the onset of coherent reptation at lower frequencies.

System	ε''_{eCLF}	ε''_{\min}	ε''_{eRouse}	M_0 [g/mol]	M_e [kg/mol]
PI-1090k	-0.20±0.01	-0.25	0.62±0.02	120 [79]	4.8 [139,140]
PEP-200k	-0.23±0.02	-0.25	0.68±0.02	113	2.25 [81]
PB-441k	-0.19±0.02	-0.27	0.67±0.01	113 [79]	2.2 [81]

Table 3: Parameters obtained or used: experimental exponents ε''_{eCLF} , ε''_{\min} , and ε''_{eRouse} found for the different polymer (see text).

Regarding the relaxation regime around the minimum in $G''(\omega)$, in $1/\tau_{\min} \ll \omega \ll 1/\tau_e$, a M dependence of the minimum frequency $\tau_{\min} \propto M^{1.0 \pm 0.1}$ is found which is not far off from the prediction of $\tau_{\min} \propto M^{0.8}$ (*cf.* Eq. (38) and Figure 12). In this regime, a modified power law exponent $G''(\omega) \propto G_N^0(\omega\tau_e)^{\varepsilon_a}$ can be derived which is experimentally found $\varepsilon_a \approx 0.75$ (*cf.* Figure 47). This value is virtually identical with that of the full LM theory (dashed lines in Figure 49a).

Considering high frequencies well above the minimum in $G''(\omega\tau_\alpha)$ ($\omega \gg \omega_{\min}$), one expects two power law regimes, namely the Rouse regime with an exponent of 0.5 and the low-frequency flank of glassy regime with $\varepsilon_{\text{glassy}} = 1$ (*cf.* Figure 49a). In the case of PI a clear-cut Rouse regime with a constant exponent $\varepsilon''_{eRouse} = 0.62 \pm 0.01$ is recognized. At highest frequencies the exponent increases indicating the crossover to glassy relaxation. In the case of PEP and PB actually two weak maxima at the high- and low-frequency end of the Rouse regime and a shallow minimum in between are recognized in Figure 49b. We tentatively attribute the minimum value to an effective Rouse exponent ε''_{eRouse} . It only slightly varies among the different polymers –see Table 3, yet it is off the prediction of $\varepsilon''_{Rouse} = 0.5$. The weak maximum foreshadowed at lowest frequencies before $\varepsilon''(\omega\tau_\alpha)$ passes through zero may be a reminiscence of the behavior expected at $\omega < 1/\tau_e$ (*cf.* below). However, as the actual

exponent $\varepsilon_a = 0.75$ is very close to that of the Rouse regime, it is difficult for the present polymers to clearly discriminate it from that of the Rouse regime.

Finally, the onset frequency $\tau_\alpha/\tau_{\text{ons}} = 6 \times 10^{-2}$ specifying the crossover from Rouse to glassy dynamics is indicated in Figure 49b by operationally taking the maximum in $\varepsilon'(\omega\tau_\alpha)$ (cf. Figures 45 and 46). It essentially agrees among the polymers.

Taking a closer look to Figure 49b one finds that $\varepsilon''(\omega\tau_\alpha)$ of PB and of PEP coincide at $\omega \geq 1/\tau_{\text{min}}$. Thereby, one expects that they have quite a similar τ_e/τ_α , or M_e . Unidad et al. [81] reported the same values of PB and PEP (cf. Table 3). In contrast, their $\varepsilon''(\omega\tau_\alpha)$ curves differ in the terminal regime due to different $Z = M/M_e$. On the other hand, $\varepsilon''(\omega\tau_\alpha)$ curves of PI-436k and of PEP-200k coincide revealing that they have a similar Z , while they deviate at $\omega \geq 1/\tau_{\text{min}}$. Reducing the x axes of Figure 49b to $\omega\tau_e$ by using $\tau_e/\tau_\alpha = N_e^2 = (M_e/M_0)^2$ with M_0 being the molar mass of Kuhn monomer (cf. Table 3), one expects that $\varepsilon''(\omega\tau_e)$ for the different polymers coincides at $\omega\tau_e \geq 1$. This is the case in Figure 50 except for some slightly different Rouse exponent and M_e matches with those in literature [81,139]. Yet, the M_e of PI is adjusted to get good collapse of $\varepsilon''(\omega\tau_e)$ with those of PB and PEP. A value of $M_e = 4.8\text{k}$ is found which is identical with that reported in refs. [139,140], yet, somewhat smaller than the value 6.2k listed by Unidad et al. [81]. Besides this coincidence at $\omega\tau_\alpha > \omega_{\text{min}}\tau_\alpha$, the position of the terminal relaxation does not comply with the order of Z . It appears that there is no unique function $f(Z)$ describing the M dependence of τ/τ_e (cf. below).

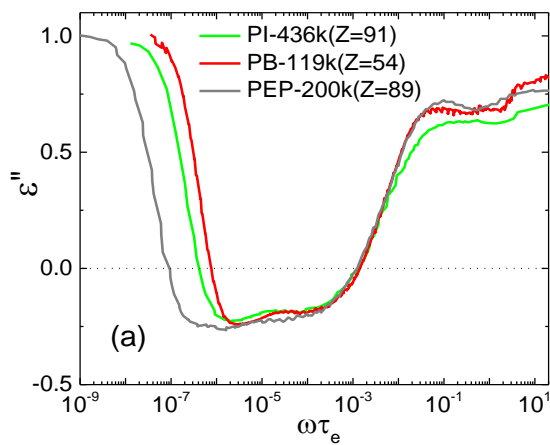


Figure 50: Data of Figure 49b plotted versus $\omega\tau_e$; Z values are indicated (cf. Table 3).

From the $\varepsilon''(\omega\tau_t)$, $\tau_t/\tau_\alpha(M)$ is reported for the three polymers (*cf.* Figure 48). Considering the M dependence of the extracted τ_t/τ_α , different power law regimes are described which are in good agreement with literature revealed by different methods [74,78,81,141]. Depending on the particular polymer, the M dependence crosses over from an exponent significantly larger than 3.0 at intermediate M values to an exponent approaching 3.0 at highest M indicative of a diminishing influence of CLF and the dominance of pure reptation.

All in all, the suggested derivative approach is well suited to reveal subtle effects in all kinds of viscoelastic as well as dielectric relaxation spectra and allows a direct comparison with the prediction of current polymer theories. For example, polymers of different topologies may be compared. Differences in amplitudes, specifically in the rubber plateau modulus, caused by sample-to-sample variation of the microstructure do not spoil such comparisons.

6. Dynamics of polymer nanocomposites

6.1 State-of-the-art

Adding nanoparticles to polymers enhances their mechanical, optical and thermal properties. Therefore, such polymer-nanoparticle composites (PNCs) are used in wide technological fields, e.g. biomedical applications [167,168], water purification or treatments [169,170], and photovoltaic devices [171,172]. Dynamically, PNCs usually show a higher rubber plateau modulus G_N^0 compared to that of neat polymers, from which a reinforcement factor can be defined. At longest times, the rheological response for PNCs may show a change from a “liquid-like” to a “solid-like” behavior with a high viscosity, i.e. a non-vanishing shear modulus is observed [173-177]. In spite of these observations, an anomalous decrease of the viscosity was also recorded in some PNCs [178-180].

Just adding nanoparticles in a host polymer does not necessarily lead to a stable and homogeneous mixing needed for controlling material properties. Particles agglomerations need to be avoided. In one route, the particles may be coated by a low molecular mass ligand. For example, SiO₂ nanoparticles are hydrophobically modified to get a homogeneous mixture of SiO₂ nanoparticles in PEP [173,174]. The rheological spectra of such system show an enhancement in the G_N^0 modulus, and a gradual disappearance of liquid-like behavior at lowest frequencies with increasing SiO₂ fractions (cf. Figure 51) [174]. The authors attributed these findings to some gel-like contributions [174].

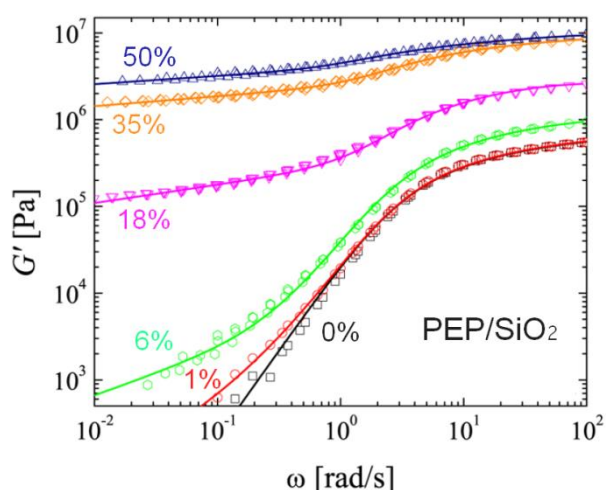


Figure 51: Storage modulus $G'(\omega)$ for PEP-50k/SiO₂ nanocomposites with different particle concentrations as indicated. [Reprinted with permission from (Nusser, K.; Schneider, G. J.; Richter, D. *Macromolecules* 2013, 46, 6263-6272). Copyright (2013) American Chemical Society].

Regarding the entanglement dynamics, CR and CLF effects (cf. section 5) were reported to disappear in PNCs [173,174]. The investigations point towards a significant disentanglement when particle concentration increases above a certain threshold value [173,174]. These ideas

were also forwarded by MD simulations [181, 182]. Moreover, different regimes were suggested when the polymer and particle size ratio $\Psi = R_{g\text{-poly}}/R_{\text{par}}$ ($R_{g\text{-poly}}$ and R_{par} representing polymer gyration radius and particle size, respectively) is considered: for $\Psi < 1$, the chains are hardly affected by the presence of nanoparticles; for $\Psi \approx 1$, a slight decrease in the gyration radius R_g is recorded [183-186].

By considering strong polymer-particle interactions, a layer of adsorbed polymers on the particle surface was assumed and more or less dynamic heterogeneities were discussed as a consequence of mobility gradients [187-190]. Experimentally, segments in the layer were concluded to be less mobile or dynamically rigid than the bulk chains [191-193].

In another route to prevent particles agglomeration, they are coated with a polymeric ligand which is usually of the same type as the matrix polymer. In other words, the polymer chains are attached to the particle surface (grafted particles) [193]. In this case, densely grafted particles are produced and characterized by a grafting density Σ (units of chains/nm²). Theoretically, the attached chains may display different conformations: a crossover from a mushroom-like structure (the chains do not overlap) at low Σ to a highly stretched structure at high Σ is discussed [195-198]. From NS experiments on poly(ethylene glycol) PEG grafted SiO₂, Glomann et al. concluded that the chains are assembled into a micelle-like corona around the particle and the mobility of the chains resembles that of the bulk [199, 200]. Such findings were also reported by MD simulations [201].

In the present section, polymer as well segmental dynamics of PNCs consisting of PI coated (attached) PbS nanoparticles which are dispersed presumably homogeneously will be investigated by means of DS and rheology.

6.2 Results

The present section is organized as follows. The DS results for PI coated particles and their mixtures with PI will be presented in section 6.2.2. In section 6.3, the same samples will be studied rheologically and the results will be compared to those from DS.

6.2.1 Systems investigated

Polyisoprene, PI-58k, PI-16k and PI-5k, were attached to PbS nanoparticles of 7.5 nm diameter by using the ligand–ligand exchange method (provided by *AG Förster, Universität Bayreuth*) [202]. The coated PI@PbS particles were produced with different characteristic grafting densities Σ as obtained from thermogravimetric analysis (TGA) and an inter-particles

distance d as measured by SAXS [203]. The smaller M , the more densely coated particles are produced (PI-5k@PbS) (*cf.* Table 4) [202]. From these parameters, one can assume that N number of chains of contour length R is located in a layer of thickness L around the PbS nanoparticles of radius r (*cf.* sketch in Figure 52); all parameters are listed in Table 4.

Further, PNCs consisting of different concentrations of theses coated particles (PI@PbS) in PI of the same M (PI@PbS/PI) are prepared. The pure PI is dissolved in THF with the desired amount of the PI@PbS. Then, THF is removed under vacuum. The dynamics of neat PI has been discussed in section 5.1 and are taken here as reference. For PNCs, the concentration is defined by the mass percentage w of the PI@PbS coated particles.

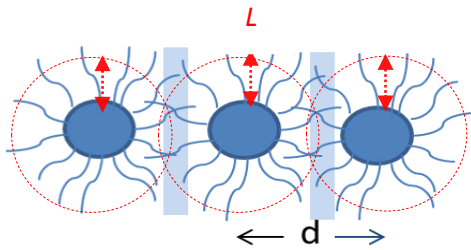


Figure 52: Sketch displays the coated particles with inter-particle distance d . Chains of length R are located in a layer of thickness L .

Linear PI		PbS	PI@PbS coated particle					
M (g/mol)	$R^{(*)}$ (nm)	$2r$ (nm)		ϕ	Σ (chains/nm ²)	$N^{(**)}$	d (nm)	$L^{(***)}$ (nm)
58000	406	7.5	PI-58k@ PbS	0.94	0.98	173	42	17.2
15700	110	7.5	PI-16k@ PbS	1.2	2.86	504	12	2.25
4505	31	7.5	PI-5k@ PbS	2.45	4.9	866	10	1.25

Table 4: Chemical properties of linear PI and PI@PbS coated particles: R is the calculated contour length, r is the radius of PbS nanoparticles, ϕ denotes the PbS core particle volume fraction, Σ is the grafting density, N is number of the chains per particle, d is the mean inter-particles distance of the particles and L is the thickness of the layer filled with PI chains (*cf.* Figure 52).

(*): calculated using $R = (M/M_0) \times b$, with $M_0 = 120$ g/mol being the mass of the Kuhn monomer and b is the Kuhn length 0.84nm [79].

(**): calculated using $N = \Sigma \times 4\pi r^2$.

(***): calculated along $L = (d/2) - r$.

6.2.2 Dielectric spectroscopy

The DS spectra of the neat PI-58k@PbS coated particle containing PI-58k ($M > M_c = 10k$) and produced with $\Sigma = 0.98$ chains/nm² is displayed in Figure 53b. For comparison, the DS spectra of pure PI-58k are shown in Figure 53a. The relaxation peaks observed for pure PI-58k, i.e. the normal mode (n) relaxation at low frequencies and the α -process (α) at high frequencies are also found in the case of PI-58k@PbS particles. The n-mode broadens on its high-frequency flank $\varepsilon \propto \nu^{-\gamma}$, reflected in a smaller value of the exponent γ with respect to that of neat PI-58k. Moreover, the amplitude of the segmental mode is close to that of the n-mode which is not the case in pure PI. Upon subtracting dc conductivity (*cf.* Appendix Figure 1A), indications of an additional slow relaxation are observed which is hereafter called “composite mode”.

Figure 53c shows the DS spectra of PNCs of PbS@PI-58k/PI-58k with $w = 40\%$. Clearly, the spectra are similar to that of the pure PI-58k but again the high-frequency flank of the n-mode is broader. Yet, it is sharper than in the case of pure PI-58k@PbS particle (*cf.* Figure 53b). Traces of a slow “composite mode” are found, too.

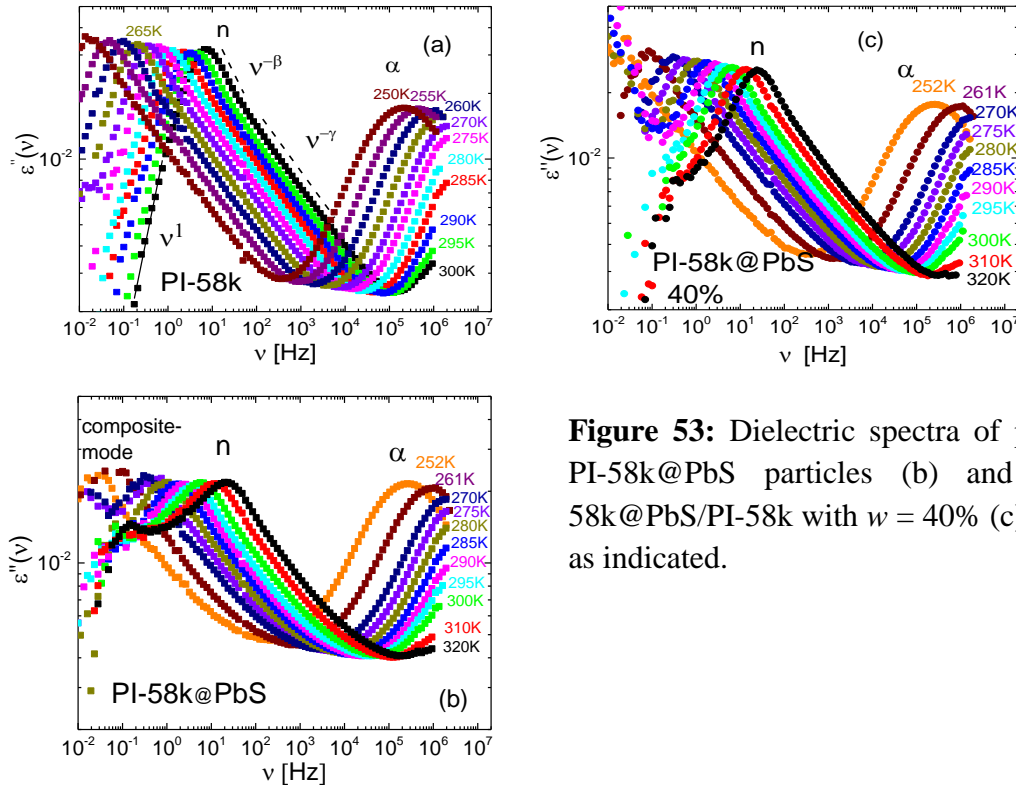


Figure 53: Dielectric spectra of pure PI-58k (a), PI-58k@PbS particles (b) and PNCs of PI-58k@PbS/PI-58k with $w = 40\%$ (c) at temperatures as indicated.

In order to illustrate the changes of the spectral shape of the n-mode relaxation as well as that of the α -relaxation, master curves for different concentrations of PI-58k@PbS/PI-58k defined by w are compared in Figure 54. They reveal that FTS works well for each w . Regarding the n-mode, master curves in a temperature range of $T = 290 \text{ K} - 320 \text{ K}$ are constructed by rescaling to the maximum and the frequency position (*cf.* Figure 54a). Clearly, the n-mode broadens, in particular at its high-frequency flank, and the strength of the slow composite mode increases with increasing w . Regarding the α -process, the spectral shape is significantly independent on w (*cf.* Figure 54b).

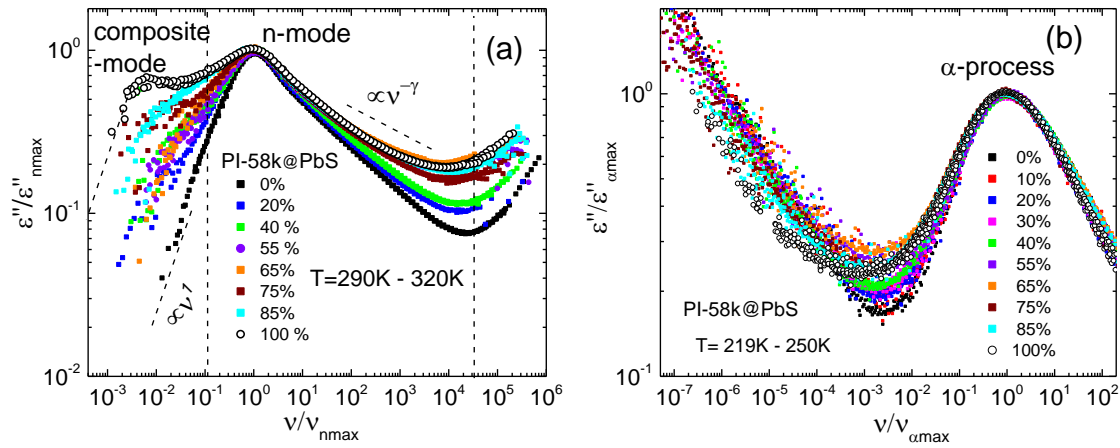


Figure 54: Dielectric master curves for PNCs of PI-58k@PbS/PI-58k with different w in the temperature range (a) $T = 290 \text{ K} - 320 \text{ K}$ rescaled to the height and the position of the n-mode peak and (b) $T = 219 \text{ K} - 250 \text{ K}$ rescaled to the height and the position of the α -process.

In the case of PI-16k ($M > M_c$) [74], the PI-16k@PbS particles are produced with $\Sigma = 2.6$ chains/nm², i.e. with a higher Σ compared to that of PI-58k@PbS particles. As in the case of the PI-58k@PbS/PI-58k composites (*cf.* above), the master curves obtained for each w are rescaled to frequency position and height of the n-mode or the α -process, respectively (*cf.* Figure 55). Again, FTS holds well for each w . Clearly, the higher w is, the broader is the n-mode compared to neat PI-16k. The composite mode is again observed upon subtracting the conductivity (*cf.* Appendix Figure 1A), which shows an increasing amplitude with increasing w . Here, the composite mode is more pronounced compared to the case of PI-58k@PbS/PI-58k. Again, no significant change in the spectral shape parameters of the α -relaxation is recognized.

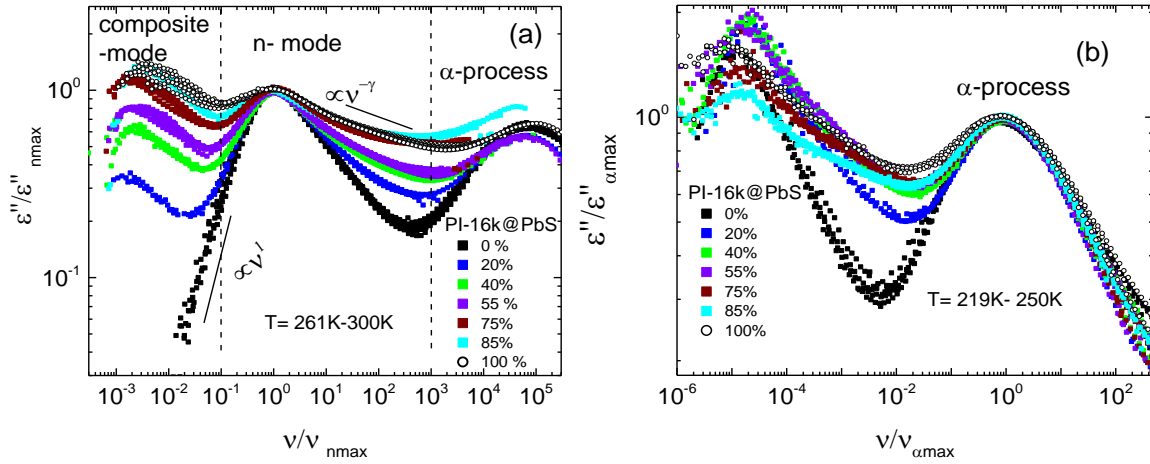


Figure 55: Dielectric master curves for PNCs of PI-16k@PbS/PI-16k with different w in the temperature range (a) $T = 261\text{ K}-300\text{ K}$ rescaled to the height and the position of the n-mode and (b) $T = 219\text{ K} - 250\text{ K}$ rescaled to height and position of the α -process.

In the case of shortest chains PI-5k ($M < M_c$), PI-5k@PbS particles with $\Sigma = 4.9$ chains/nm² were produced, i.e. the number of the chains per nm² is nearly five times higher than that in the case of PI-58k@PbS (*cf.* Table 4)]. Figure 56 a and b display the DS spectra of neat PI-5k and PI-5k@PbS coated particles, respectively. Again, three relaxations are observed (α , n-mode and composite mode). The n-mode relaxation is much broader compared to that of neat PI-5k, and the composite mode is well separated from the conductivity contribution in contrast to PI-58k@PbS and PI-16k@PbS; and its signal is larger than that of the n-mode relaxation.

The DS spectra of a PI-5k@PbS/PI-5k composite with $w = 80\%$ are shown in Figure 56c. Again three relaxations can be identified. Yet, the n-mode relaxation is narrower than in the case of the PI-5k@PbS particles (*cf.* Figure 60b).

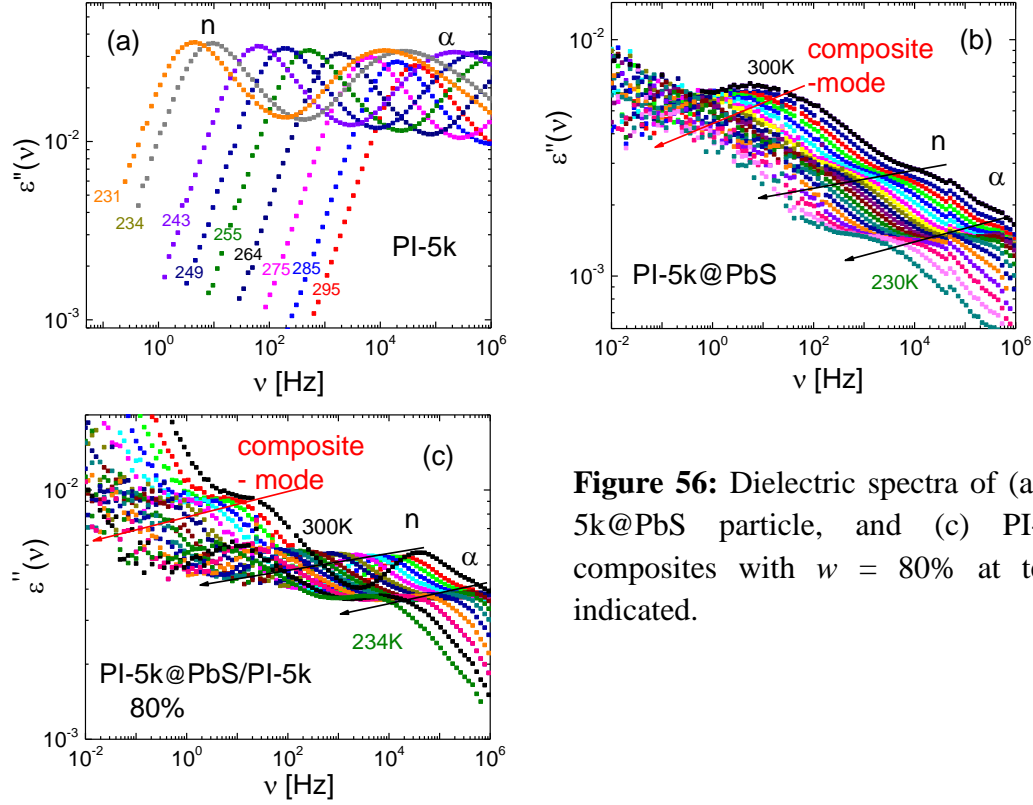


Figure 56: Dielectric spectra of (a) PI-5k, (b) PI-5k@PbS particle, and (c) PI-5k@PbS/PI-5k composites with $w = 80\%$ at temperatures as indicated.

Similar to Figures 54 and 55, DS master curves of PNCs of PI-5k@PbS/PI-5k with different w are compared in Figure 57. Obviously, the n-mode broadens with increasing w , and the composite mode increases in the amplitude. The latter is more pronounced than in the cases of PI-16k@PbS and PI-58k@PbS.

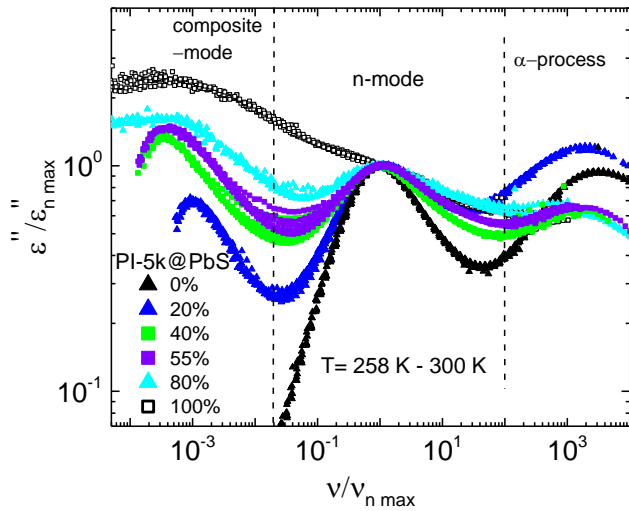


Figure 57: Dielectric master curves for PNCs of PI-5k@PbS/PI-5k with different w in the temperature range $T = 258 \text{ K} - 300 \text{ K}$.

The relaxation times

The relaxation times of the n-mode $\tau_n(T)$, the segmental relaxation $\tau_\alpha(T)$, and of the composite mode $\tau_{\text{comp}}(T)$ for all PNCs are extracted via $\tau_i = 1/2\pi\nu_{\text{imax}}$ and presented in Figure 58. In the case of PI-58k@PbS/PI-58k, the $\tau_n(T)$ and the $\tau_\alpha(T)$ are not changing with w compared to those of neat PI-58k (*cf.* Figure 58a). Thus, no change in T_g is found in accordance with those reported in the literatures [204-207]. In the case of neat PI-16k@PbS particles, the $\tau_n(T)$ weakly increases by a factor of about 3 with respect to those of neat PI-16k (*cf.* Figure 58b open squares and open circles) while they decrease again upon mixing with PI-16k. Regarding the relaxation time of PI-5k@PbS particles, an increase by a factor of 5-7 for both τ_n and τ_α is found (*cf.* Figure 58c). This enhancement of the relaxation time almost vanishes in the mixtures, while the relaxation time τ_{comp} does not depend on w .

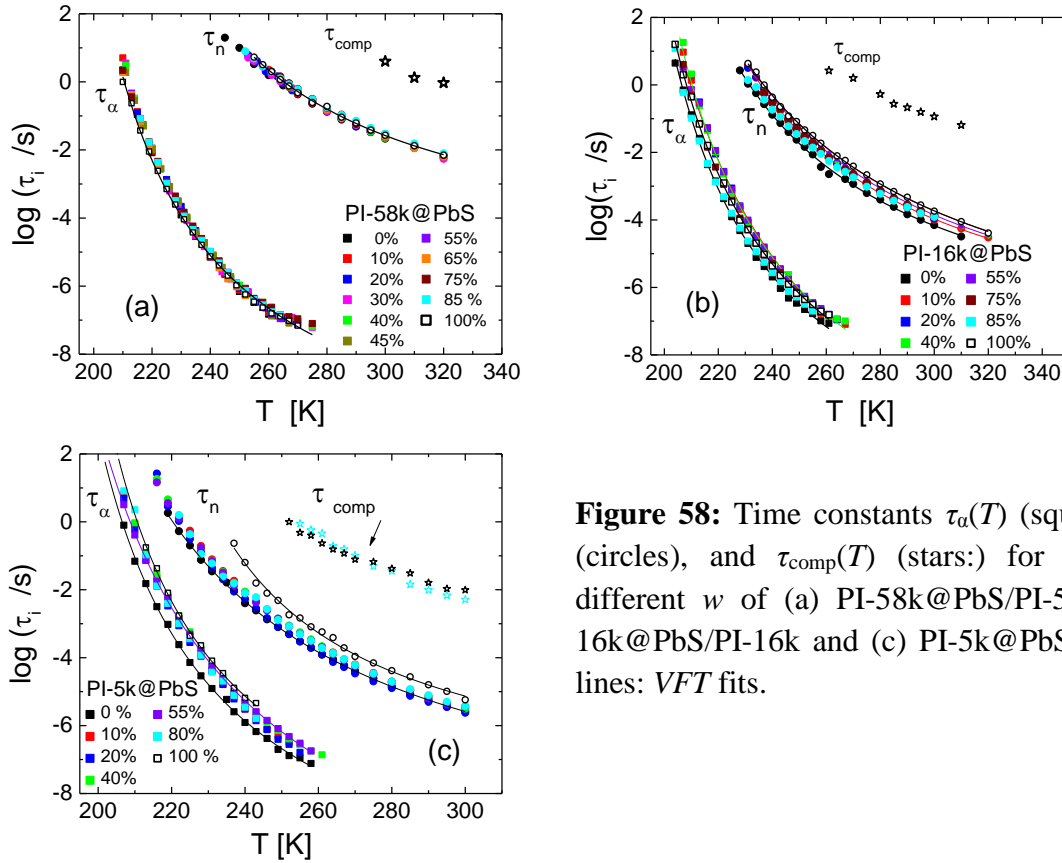


Figure 58: Time constants $\tau_\alpha(T)$ (squares), $\tau_n(T)$ (circles), and $\tau_{\text{comp}}(T)$ (stars:) for PNCs with different w of (a) PI-58k@PbS/PI-58k, (b) PI-16k@PbS/PI-16k and (c) PI-5k@PbS/PI-5k. Solid lines: VFT fits.

Spectral shape of the n-mode

As said, the high-frequency flank $\varepsilon \propto \nu^{-\gamma}$ of the n-mode broadens with increasing w . In order to extract the exponent γ , the n-mode relaxation is isolated by subtracting the contribution of the α -process. The master curves of the latter were interpolated by a HN function to obtain the spectral shape parameter used for subtracting. The isolated spectrum at $T = 260$ K is scaled to the position and maximum of the n-mode for each w of PI-58k@PbS/PI-58k, PI-16k@PbS/PI-16k or PI-5k@PbS/PI-5k at $T = 240$ K. In the case of PI-5k@PbS/PI-5k, the isolation is accepted with some errors (*cf.* Figure 59). Clearly, γ changes systematically.

Following Watanaba et al. [208], the n-mode relaxation was interpolated using a distribution of $G(\ln \tau)$ along Eq.(43) which is similar to the BSW model [166]. In the distributions three parameters are assumed; τ_R denotes the long-time limit, τ_s short-time limit and τ_l is the crossover between the two limits (*cf.* scheme in Figure 59a).

$$G(\ln \tau) = \begin{cases} \frac{1}{A} \left(\frac{\tau}{\tau_n} \right)^\beta & \text{for } \tau_l < \tau < \tau_R \\ \frac{1}{B} \left(\frac{\tau}{\tau_n} \right)^\gamma & \text{for } \tau_s < \tau < \tau_l \end{cases} \quad (43)$$

with A and B being weighting factors. Satisfying fits are presented as solid lines in Figure 59(b-d). The β value is independent on w , while γ is.

The exponent γ as a function of w is presented in Figure 60. In all PNCs, the exponent γ drops below the value of the neat PI. For both PI-58k@PbS/PI-58k and PI-16k@PbS/PI-16k, the γ value reaches a minimum value of $\gamma_{\min} \approx 0.15$ which is significantly below the CLF limit determined for entangled polymers [77]. This indicates that the mode distribution of the entanglement dynamics changes, in particular, in the regime which is attributed to CLF dynamics. Also, it reaches $\gamma_{\min} \approx 0.25$ in the case of PI-5k@PbS/ PI-5k, which is below the value determined for unentangled polymers ($\gamma = 0.5$) [67].

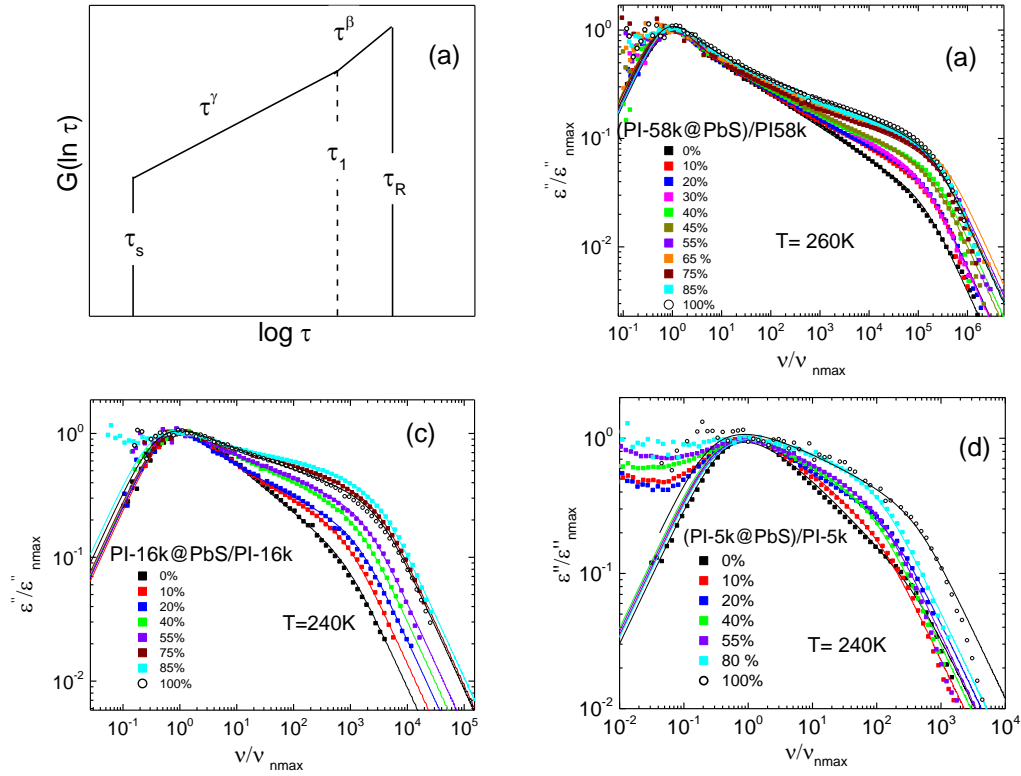


Figure 59: (a) Schematic representation of the distribution defined in Eq.(43). (b) The isolated n-mode normalized by its height and position for mixtures of different w for PI-58k@PbS at $T = 260$ K, (b) the same plot for PI-16k@PbS at $T = 240$ K and (c) PI-5k@PbS. Solid lines: fits (see text).

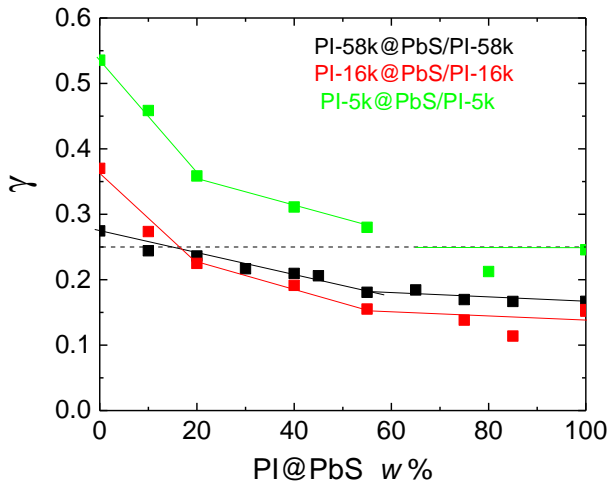


Figure 60: The exponent γ as a function of the particle concentration w for PI-58k@PbS/PI-58k, PI-16k@PbS/PI-16k and PI-5k@PbS/PI-5k composites. Dashed line: expected exponent considering CLF effect. Solid lines are guides for eye.

6.3 Rheology

In addition to DS, the viscoelastic behavior of the PI@PbS/PI nanocomposites was investigated using a plate of 8 mm diameter in the linear response regime. The results are compared to those of the pure polymers.

Figure 61 displays the $G'(\omega)$ and $G''(\omega)$ for neat PI-5k@PbS particles. The data was collected in a temperature range from $T = 223\text{K}$ to $T = 300\text{K}$. At the highest temperature ($T = 300\text{K}$) and low frequencies, a power law behavior of $G''(\omega) \propto \omega^1$ and $G'(\omega) \propto \omega^{-2}$ is found (dashed lines), which indicates flowing of PI-5k@PbS particles. Upon cooling, two relaxations appear (see the data at $T = 243\text{K}$). In between a plateau regime is recognized in $G'(\omega)$. The behavior at the lowest temperature ($T = 223\text{K}$) indicates that the glassy relaxation is not reached yet.

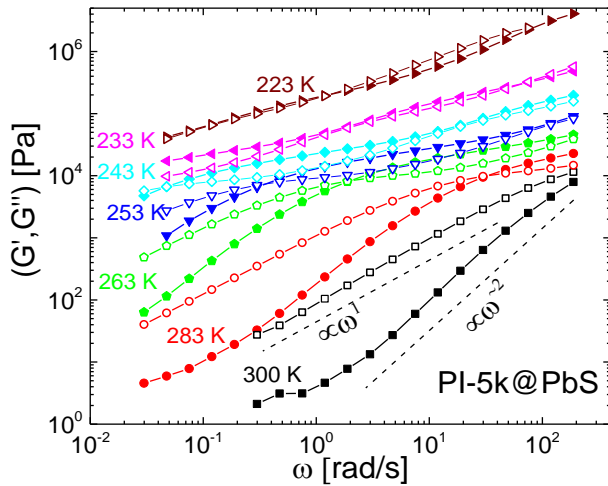


Figure 61: Complex shear modulus (filled symbols: $G'(\omega)$ and open symbols: $G''(\omega)$) for neat PI-5k@PbS coated particles at temperatures as indicated. Dashed lines display the power law behavior.

In Figure 62, the shear modulus of the PI-5k@PbS particles (red symbols) is compared to that of pure PI-5k (black symbols) at the same temperature ($T = 243\text{K}$). At this temperature, pure PI-5k shows a liquid-like behavior of $G''(\omega) \propto \omega^1$ and $G'(\omega) \propto \omega^2$, while in the case of PI-5k@PbS particles, as said, two relaxations appear. The relaxation at high frequencies can be assigned to the reminiscence of the polymer relaxation process as in the case of PI-5k, and only at much lower frequencies a terminal relaxation of highly viscous liquid is recognized. The latter resembles a slow composite mode observed by DS (see below). In the case of the PNCs of PI-5k@PbS /PI-5k with $w = 40\%$, the moduli are much smaller compared to those of pure PI-5k. These features in the case of PI-5k@PbS/PI-5k as well as in the other cases (PI-58k@PbS /PI-58k and PI-16k@PbS /PI-16k) are better seen in the master curves, see below.

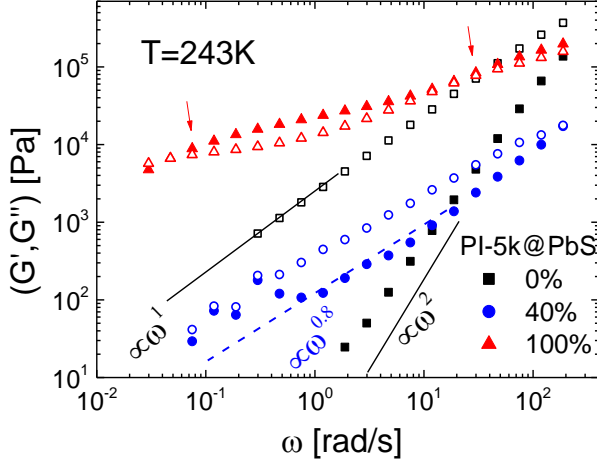


Figure 62: The storage $G'(\omega)$ (filled symbol) and loss $G''(\omega)$ (open symbol) modulus for PI-5k@PbS at $T = 243\text{K}$ compared to those of the pure PI-5k and those of PI-5k@PbS/PI-5k with $w = 40\%$.

6.3.1 Comparison of the rheological and dielectric Master curves

Master curves, $G'(\omega\tau_a)$ and $G''(\omega\tau_a)$ are constructed including data from a wide temperature range ($233\text{ K} < T < 353\text{ K}$) as it is described in section 5. Briefly, the curves are shifted first with respect to a reference temperature T_{ref} using a shift factor $a_T(T)$ yielding $G'(\omega a_T)$ and $G''(\omega a_T)$. Then, they are converted to $G'(\omega\tau_a)$ or $G''(\omega\tau_a)$ by using $\tau_a(T_{\text{ref}})$ from DS results (*cf.* section 6.2.2). They are compared to the DS master curves $\epsilon''(\omega\tau_a) / \epsilon''_{\text{amax}}$.

Master curves, $G'(\omega\tau_a)$ or $G''(\omega\tau_a)$ and those from DS ($\epsilon''(\omega\tau_a) / \epsilon''_{\text{amax}}$), for PNCs of PI-5k@PbS/PI-5k are shown in Figure 63. In order to get better comparison, the data was rescaled by the height of the polymer relaxation (*cf.* the appendix Figure 2A for unscaled data). Some major points can be stated:

- i.) In addition to α -relaxation at highest frequencies (not measured by $G''(\omega\tau_a)$, yet by DS), two relaxations (normal or polymer and composite mode) are resolved, in particular in the case PI-5k@PbS coated particles, by both methods.
- ii.) At the lowest frequencies, the rheological response reveals that the samples are flowing as the terminal power laws of $G''(\omega) \propto \omega^1$ and $G'(\omega) \propto \omega^2$ are found, yet with an increasing viscosity.
- iii.) In PNCs of PI-5k@PbS/PI-5k with $w = 40\%$, the composite process is barely recognized in rheology in contrast to DS.

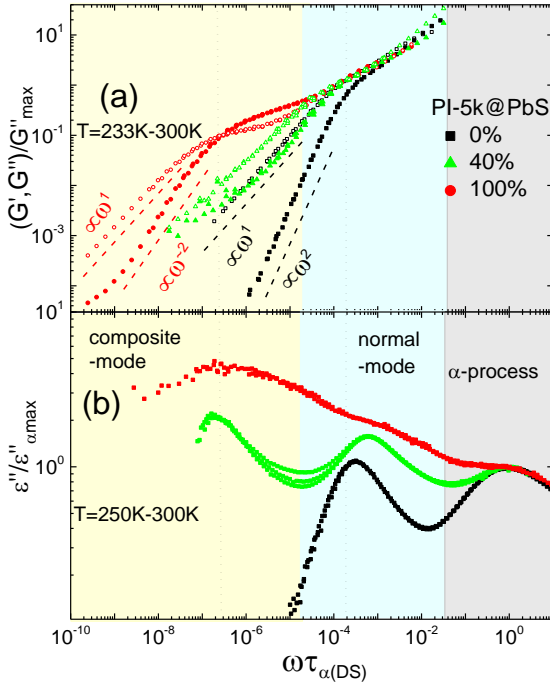


Figure 63: (a) Master curves of G' ($\omega\tau_{\alpha(\text{DS})}/G''_{\max}$) (filled symbols) and $G''(\omega\tau_{\alpha(\text{DS})})/G''_{\max}$ (open symbols) for neat PI-5k@PbS particles, a PNCs of PI-5k@PbS/PI-5k with $w = 40\%$ and pure PI-5k in a temperature range $T = 233\text{ K} - 300\text{ K}$. (b) DS master curves of the same samples in a temperature range $T = 250\text{ K} - 300\text{ K}$.

For the other PNCs containing long PI chains ($M > M_c$), PI-16k@PbS/PI-16k and PI-58k@PbS/PI-58k, the master curves are compared to those from DS in Figure 64. The observables may be stated as follows:

- i.) In rheology, the characteristic rubber plateau modulus is enhanced in case of PI-16k@PbS coated particles by a factor of two with respect to that of neat PI-16k (left panel of Figure 64a), while it is not altered in the case of PI-58k@PbS coated particles (right panel of Figure 64a).
- ii.) In both PNCs, the polymer relaxation observed in $G''(\omega)$ slightly broadens and slightly slows down compared to that of neat polymer. The findings agree with that found by DS (*cf.* Figure 64b)
- iii.) In contrast to DS and the case of PI-5k@PbS (*cf.* above), the composite mode cannot be easily resolved at the low-frequency range. Instead, a comparable shoulder with $G'(\omega) \neq G''(\omega)$ is recognized in the PI-16k@PbS coated particles (*cf.* left panel Figure 64a) and power laws of $G''(\omega) \propto \omega^{0.8}$ and $G'(\omega) \propto \omega^{0.8}$ are found in the case of PI-58k@PbS coated particles.
- iv.) At lowest frequencies, a liquid-like behavior $G''(\omega) \propto \omega^1$ and $G'(\omega) \propto \omega^2$ is observed in the case of coated PI-16k@PbS particles (left panel, dashed lines) or only traces of these power laws in the case of PI-58k@PbS coated particles, i.e. the coated particles flow like the pure PI, but about 3 decades slower.

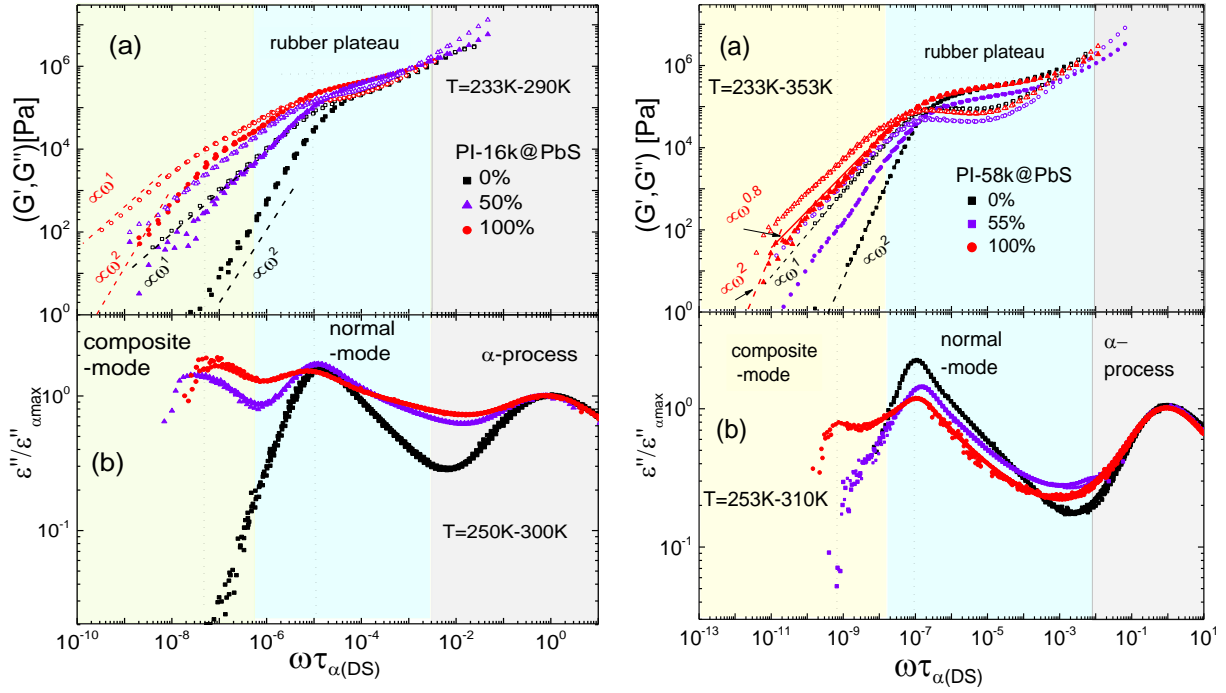


Figure 64: Master curves of $G'(\omega\tau_{\alpha(DS)})$ (filled symbols) and $G''(\omega\tau_{\alpha(DS)})$ (open symbols) compared to those of DS for PI-16k@PbS/PI-16k (left panel) and PI-58k@PbS/PI-58k (right panel) composites.

Thus, the composited mode is resolved by rheology as well as by DS and is more pronounced in the case of PI-5k@PbS. The presented PNCs flow in contrast to other PNCs where a gel-like contribution was discussed.

6.3.2 Discussion

The dielectric and viscoelastic response of PI@PbS particles containing long (PI-58k@PbS and PI-16k@PbS) and short (PI-5k@PbS) PI chains and PNCs of PI@PbS/PI are presented. Generally, in the dielectric and rheological spectra three relaxations are found: α , normal mode or polymer relaxation and composite mode (*cf.* Figures 63 and 64).

Polymer/normal mode and α -relaxations. Dielectrically, the relaxation times $\tau_{\alpha}(T)$ and $\tau_n(T)$ virtually do not alter in the case of the neat PI-58k@PbS coated particles compared to those of the corresponding neat PI, while they slightly increase in the case of PI-16k@PbS or PI-5k@PbS particles (*cf.* Figure 65). Similar results were reported in PNCs of PI/clay [204] or in PI/C₆₀ [205], as well as in PI@SiO₂ coated particles containing long PI [206,207]. The spectral shape of the α -relaxation does not alter, while the normal mode broadens, in particular, on its high-frequency flank. The corresponding power law exponent γ describing

this flank significantly drops below the value typical of that of neat polymer ($\gamma = 0.25$ or 0.5) [67,77], reaching $\gamma_{\min} = 0.15$ in the case of PI-58K@PbS and PI-16K@PbS and $\gamma_{\min} \approx 0.25$ in the case of PI-5K@PbS. Rheologically, such broadening in the spectral shape of the polymer relaxation is observed, in particular, in the case of PI-5k@PbS (*cf.* Figures 63 and 64) either. Archer and coworkers [206, 207] reported two (normal mode and segmental) relaxations in PI@SiO₂ coated particles in contrast to the three relaxations found here. They also reported a broadening in the high-frequency flank of the normal mode relaxation [206,207]. In contrast, Richter and coworkers [173] found an increase in the exponent γ in the case of PEP/SiO₂ (non-coated) system. They speculated that CLF and CR effects are less important. It is noted that the dielectric spectra of PI@PbS samples are similar to those of PI star polymers [208,209]. There, the normal mode relaxation broadens compared to that of linear polymers. In this sense, the PI chains in the PI@PbS assemble in a corona (or arms) and may perform some kind of arm retraction dynamics [208].

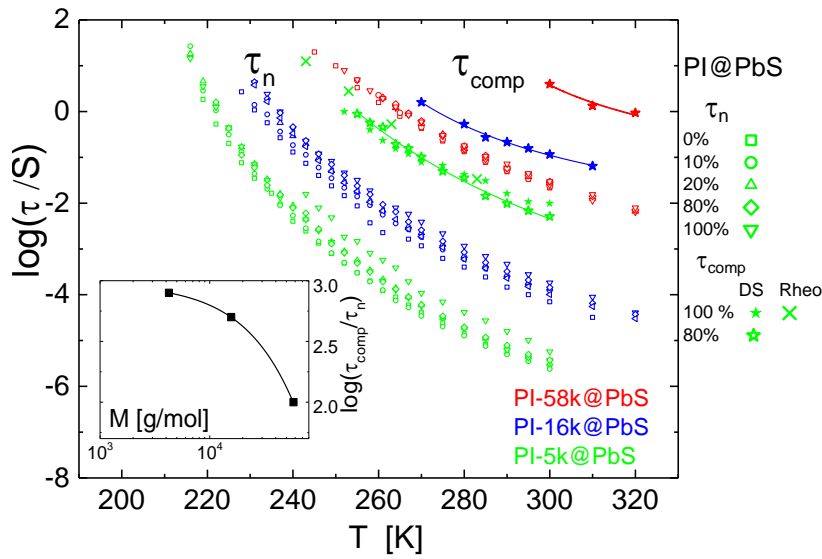


Figure 65: Time constants of the n-mode $\tau_n(T)$ (open symbols) and the composite mode $\tau_{\text{comp}}(T)$ (stars) for PbS@PI-58k, PbS@PI-16k, PbS@PI-5k particles as well as mixtures with different particle concentration w , as indicated. Crosses: τ_{comp} from rheology. Lines are guide for eyes. Inset: $\tau_{\text{comp}}/\tau_n$ as a function M ; the solid line is a guide for eye.

In the PNCs, a systematic increase of $\tau_a(T)$ or $\tau_n(T)$ (*cf.* Figure 65) with increasing the particle concentration w is observed. Also, the exponent γ systematically decreases with increasing the particle concentration w (*cf.* Figure 60).

The composite mode. At frequencies 2-3 orders lower than those of the normal mode relaxation, a composite mode is observed in both dielectric and rheological spectra. Dielectrically: *i.*) The composite mode is more decoupled from the normal mode for PI@PbS systems containing smaller M than for those containing higher M , as it is revealed by plotting $\tau_{\text{comp}}/\tau_n$ as function of M (*cf.* inset of Figure 65), *ii.*) The strength of the composite mode increases with decreasing M compared to that of the normal mode; it is more pronounced in the case of PI-5k@PbS than in the other cases PI-16k@PbS or PI-58k@PbS. Archer et al. [206,207] showed in the case of PI@SiO₂ with short PI chains that the normal mode slowed down by 3–4 orders of magnitude with respect to that of neat PI. This is similar to the behavior of the composite mode observed in PI-5k@PbS, i.e., the composite mode is also observed in the case of PI@SiO₂ [206, 207]. In the PNCs, $\tau_{\text{comp}}(T)$ does not depend on w (*cf.* Figure 65 in the case of $w = 80\%$) while the strength of the composite mode decreases with decreasing w .

Similar findings are observed by rheology: the composite mode is more pronounced in the case of PI-5k@PbS than in the other cases (compare Figures 63 and 64) and $\tau_{\text{comp}}(T)$ virtually agrees with those from DS (crosses in Figure 65). Moreover, this mode yields a much higher viscosity in PI@PbS compared to pure PI and discloses a liquid-like behavior. This is in contrast to the gelation effect (solid-like response) discussed in other PNCs [174-177,210] (*cf.* Figure 51).

The composite mode, especially in the case of PI-5k@PbS, reminds of a general shear response expected for a colloidal suspension undergoing a glass transition as it develops a plateau-like elastic modulus in G' and a relaxation peak in G'' . In other words, it may be associated with the structural relaxation of a “colloidal glass” [211, 212].

By considering the structural parameters of the PI@PbS systems listed in Table 4, one can propose an explanation of the increasing of the ratio $\tau_{\text{comp}}/\tau_n$ and of the more pronounced composite mode in the case of PI-5k@PbS. In the case of PI-5k@PbS particles, a higher number N of PI-5k chains is located in a layer of smaller thickness L , compared to the other cases. This may lead to less probable chains interpenetration (shaded area in Figure 52). Thereby, the response of PI-5k@PbS may be influenced by “hard” spheres undergoing glass transition. In contrast, in the other cases (PI-16k@PbS and PI-58k@PbS) the penetration is probably higher; together with entanglement effect may yield a “softer” (polymer) response [176,211,212].

Regarding star polymers, an additional slow process was observed in those of multiarms. The process shows a dependence of the number of arms; the higher number the arms the more pronounced and decoupled slow process [213]. Thus, for the present PI@PbS particles, the polymer or normal mode relaxation, as said, depends on M (arm molecular weight), while the composite mode depends on N (number of the grafted chains).

7. Dynamics of Dendrimers

7.1 State-of-the-art

Dendrimers are a special type of hyperbranched polymers. They are repetitively branched. From a central core, the segments with functionality f are regularly added giving “shells”. Each shell defines the generation number G , starting from $G = 0$ for the functional core. Dendrimers are perfectly monodisperse. Their volume increases cubically with G while the mass depends exponentially on G . Thus, dendrimers can be obtained only for a limited number of generations [214,215]. The molecules are used in a wide range of applications e.g., drug delivery [216,217], catalyst [218] or as a carrier for MRI contrast agent [219]. They are synthesized either in a core first [214] (divergent method) or core last (convergent method) manner by using cycles of preparations [215]. MD simulations revealed that dendrimers become compact and spherical in shape as the generation increases. Their density decreases gradually from the center to the surface [220].

Due to the unique structure of dendrimers they show physical properties which differ from those of linear polymers. Regarding the melt viscosity, the M dependence of the zero shear viscosity (η) in linear polymers changes from a power law behavior of M^1 described by Rouse dynamics to $M^{3.4-3.7}$ in the entanglement regime. In contrast, in polyamidoamine PAMAM dendrimers, no rubber plateau was distinguished in the shear modulus and thus no entanglement regime could be defined [221-222], revealing that some reminiscence of unentangled polymer dynamics is present in dendrimers. In addition, segmental dynamics and secondary relaxation processes known from molecular glass formers were discussed in PAMAM dendrimers [223].

According to MD simulations, the orientational mobility of the segment of a dendrimer in solution is governed by three main relaxation processes: (i) the local mobility which weakly depends on the position of the segment in the shell, (ii) the mobility of the branch, and (iii) the rotation of the dendrimers as a whole [224,225].

Several experimental works addressed the dynamics of dendrimers in solutions, but dendrimers in the melt state are rarely addressed. In the present section the dynamics of a series of pure dendrimers in the melt state is studied. The question arises whether some reminiscence of polymer dynamics can be resolved in dendrimers dielectrically or whether

they are similar to type B polymers (Stockmayer notation). Beyond that, the question arises whether the dynamical features show generation dependence?

7.2 Results

7.2.1 Systems measured

In the present chapter, the dynamics of poly(propyleneimine) (PPI) melt dendrimers of generations (G) 2–5 is investigated by DSC, DS, and with the help of FC ^1H NMR in a wide temperature range (120 K – 400 K). PPI dendrimers were purchased from *SyMO-Chem BV* (*University of Eindhoven*). PPI dendrimers consist of a di-aminobutane core with functionality $f = 3$. The chemical structure of G2 is shown in Figure 66. Some chemical properties are listed in Table 5 along with the T_g values obtained from DSC and DS (see below).

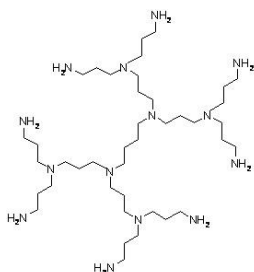


Figure 66: Chemical structure of PPI dendrimer of G2.

Generation	Molecular formula	Molar mass (g/mol)	Number of amino end groups	T_g (K) (DSC)	T_g (K) (DS)	E_A/R (β) (K)	τ_∞ (β) (s)
2	$\text{C}_{40}\text{N}_{14}\text{H}_{96}$	773.3	8	195	196	3522	5×10^{-15}
3	$\text{C}_{88}\text{N}_{30}\text{H}_{208}$	1686.8	16	198	200	3914	2×10^{-14}
4	$\text{C}_{184}\text{N}_{62}\text{H}_{432}$	3513.9	32	204	204	4282	5.2×10^{-15}
5	$\text{C}_{372}\text{N}_{126}\text{H}_{880}$	7198.1	64	200	200	3868	5.5×10^{-16}

Table 5: Properties of the investigated PPI dendrimers: Molecular formula, molar mass, number of amino groups, glass transition temperature (T_g) as obtained within this work from DSC and DS, activation energy of β -process (in terms of E_A/R) and the corresponding attempt time τ_∞ .

7.2.2 DS results in PPI dendrimers

Typical DS spectra of the G2 PPI dendrimers are shown in Figure 67a. Three broad relaxations are clearly observed. The slowest relaxation is partly covered by the dc conductivity in the cases of higher G; see for example the DS spectra of G3 in Figure 67b. Upon subtracting the dc conductivity contribution using $\varepsilon''_{dc}(\nu) = \frac{\sigma_{dc}}{2\pi\varepsilon_0\nu}$, the slower relaxation is resolved as it is shown in Figure 68 for G4 and G5. This relaxation leaves the frequency window upon cooling, and the other two relaxations persist at lower temperatures. Apparently, their amplitudes decrease and their widths broaden. Inspecting the DS spectra for different G, one can conclude that the relaxation patterns are rather similar for all generations. So PPI dendrimers show three relaxation processes which we call, for reasons becoming clear below, α , d, and β according to the order of their appearance in the DS spectra. At lowest temperatures only the β -relaxation can be probed in the given frequency window.

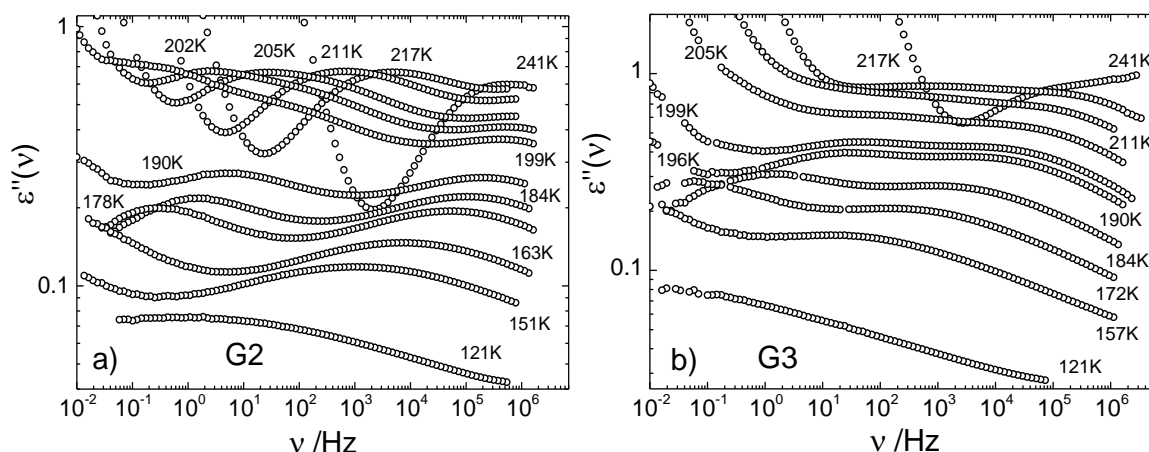


Figure 67: (a) Dielectric spectra of PPI dendrimer G2 measured for temperatures 121 K to 241 K as indicated. (b) Analogous spectra of PPI dendrimer G3 from 121 K to 241 K. [Reprinted with permission from (Mohamed, F.; Hofmann, M.; Pötzschner, B.; Fatkullin, N.; Rössler, E.A. *Macromolecules* 2015, 48, 3294). Copyright (2015) American Chemical Society].

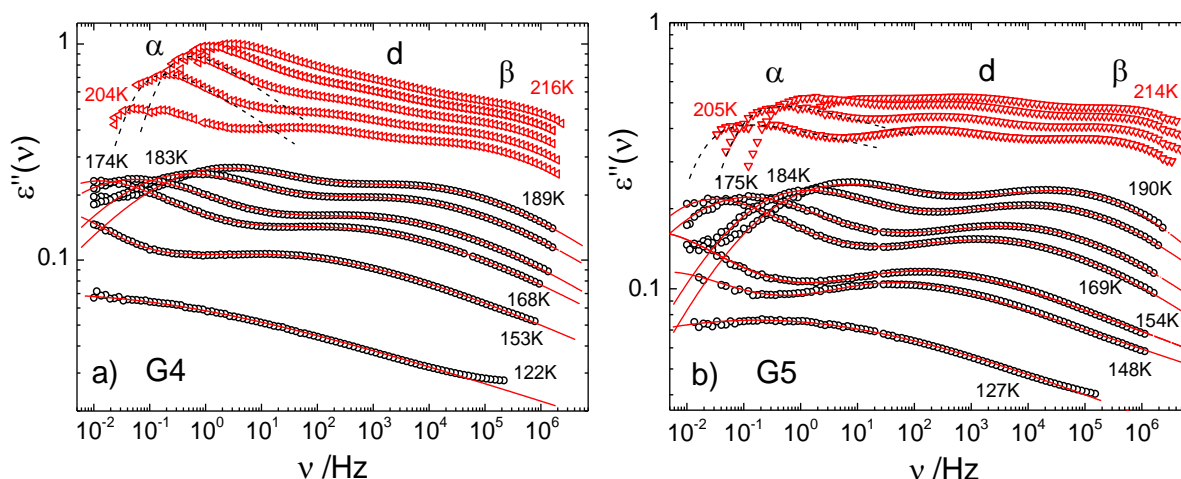


Figure 68: Dielectric loss of PPI dendrimer G4 (a) and G5 (b) after subtracting the conductivity contribution; red triangles: $T > T_g$ in 3 K steps; black circles: $T < T_g$ (selected data). Solid lines: fits by a superposition of two sub-spectra along Eq. (21) corresponding to d- and β -processes. Dashed lines: CD fits of the α -relaxation. [Reprinted with permission from Mohamed, F.; Hofmann, M.; Pötzschner, B.; Fatkullin, N.; Rössler, E.A *Macromolecules* 2015, 48, 3294. Copyright (2015) American Chemical Society].

The time constants are extracted along $\tau_i = 1/(2\pi\nu_{i\max})$, with i referring to the corresponding relaxation; all are presented in Figure 69a. For high temperatures NMR (^2H NMR and ^1H FC NMR) data for $\tau_\alpha(T)$ are added. Altogether, $\tau_\alpha(T)$ shows a super-Arrhenius temperature dependence as it is well described by a VFT equation, and weakly depends on G. They almost coincide around 200 K, revealing quite similar T_g which is in good agreement with those from DSC (*cf.* Table 5) [226]. The relaxation times for the other two processes ($\tau_d(T)$ and $\tau_\beta(T)$) follow an Arrhenius temperature dependence. The relaxation time τ_d is virtually independent on G with an activation energy $E_A/RT_g \cong 42$, while the relaxation time τ_β depends on G with an activation energies in a range of $18 < E_A/RT_g < 21$ (*cf.* Table 5); yet not in a systematic way.

The spectral shape of the α -relaxation is well described by a CD function (dashed lines in Figure 68) with a stretching parameter $\beta_{CD} = 0.3$. Thus, this process resembles the structural process of super-cooled liquids or polymers [55,69]. Below T_g , a sum of two distributions $G(\ln\tau_{d,\beta})$ defined in Eq. (21) is used for interpolating the spectra. The fits are well reproducing the corresponding spectra (*cf.* Figure 68). Concerning the β -relaxation, the shape parameter ab obtained from the fit is displayed as a function of temperature in Figure 69b. It decreases

linearly with cooling, which is a typical trend for β -relaxation as observed in glasses [23]. The inset of Figure 69b shows the relaxation strength of the d-process with respect to that of the sum of both β and d processes. Clearly, the ratio is independent of temperature below T_g while it tends to increase around T_g . In Figure 70 parts a and b the spectra of both d- and β -processes are scaled to position and maximum of the corresponding process, respectively. This demonstrates that FTS holds in the case of the d-process while it fails in the case of the β -process. From all these findings it can be concluded that the d-process is an atypical secondary process while the β -relaxation is a typical [23].

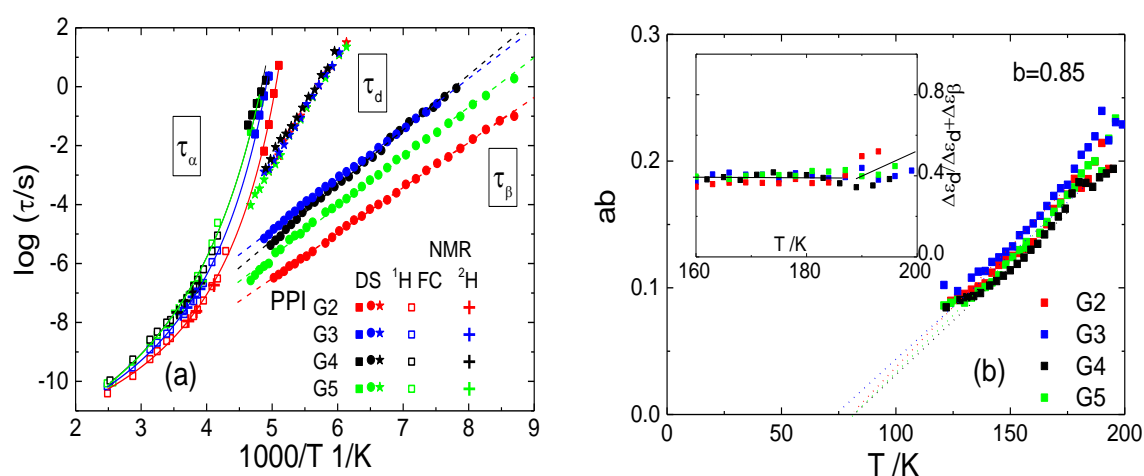


Figure 69: (a) Relaxation time map of the PPI dendrimers of G 2-5 for the (α , d and β) processes, identified by DS, FC ^1H NMR and ^2H NMR. (b) Temperature dependence of the spectral shape parameter ab (cf. Eq. 21) of the β -process, asymmetry parameter b is kept constant. Inset: Temperature dependence of the dielectric strength of the d -process with respect to that of the sum of both β - and d-processes. [Adapted with permission from (Mohamed, F.; Hofmann, M.; Pötzschner, B.; Fatkullin, N.; Rössler, E.A *Macromolecules* 2015, 48, 3294). Copyright (2015) American Chemical Society].

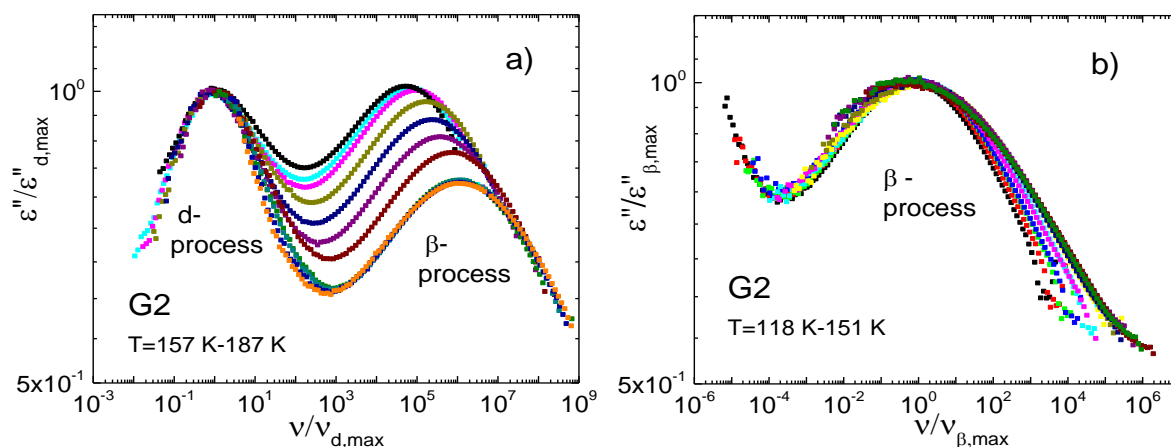


Figure 70: Dielectric spectra of PPI dendrimer G2 rescaled by the height ϵ''_{\max} and frequency position ν_{\max} for (a) the d-relaxation in the temperature range $T=157\text{ K} - 187\text{ K}$ and (b) the β -relaxation in the range $T=118\text{ K} - 151\text{ K}$. [Adapted with permission from (Mohamed, F.; Hofmann, M.; Pötzschner, B.; Fatkullin, N.; Rössler, E.A *Macromolecules* 2015,48, 3294). Copyright (2015) American Chemical Society].

7.2.3. Discussion

Four different generations of PPI dendrimers were investigated. As revealed by DS, three relaxation processes are resolved. The main (α -) process is observed at $T > T_g$ which depends weakly on G and follows a super-Arrhenius temperature dependence. Thus, T_g virtually does not depend on G which is in accordance with previous studies [223]. Its spectral shape is broader than observed for most neat glass formers, which may reflect some heterogeneous dynamics coming from different mobilities in different shells. This idea was forwarded by MD simulations [223, 225]. At $T < T_g$, the secondary relaxations (d & β) are recognized. They merge with the α -process at high temperatures. The temperature dependence of their relaxation times follows an Arrhenius law. The d-process is an atypical secondary process as FTS holds. Its time constant is virtually independent on G. Therefore, it may be speculated, whether the d-process is of cooperative nature and reflects internal motion of the dendrimers which still proceeds in the structurally frozen state, i.e., below T_g . The faster secondary (β -) process exhibits features characteristic for glasses, as it broadens upon cooling which reflects the failure of FTS. In this sense the β - process is typical [23, 46]. The relaxation patterns found for PPI dendrimers highly resemble the ones previously found studying PAMAM dendrimers [223] or hyperbranched polymers [225-229]. Yet, no indication of the collective

polymer dynamics is probed by DS, i.e. the dendrimers are of type B polymers (Stockmayer notation) [68].

The FC ^1H NMR, probing the dispersion of the spin-lattice rate R_I in the frequency range 200 Hz –30 MHz, is sensitive to the collective polymer dynamics. The rate can be transferred to susceptibility representation along $\chi''(\omega) \equiv \omega R_I(\omega)$. By applying FTS, a master curve of $\chi''(\omega\tau_\alpha)$ as function of reduced frequency in range of nine decades was obtained (cf. Figure 71). By doing so, the segmental time $\tau_\alpha(T)$ from DS are extended to higher temperatures (cf. Figure 69a). In addition to the segmental relaxation, an excess contribution at low-frequencies ($\omega\tau_\alpha < 1$) is observed in the PPI dendrimers compared to that of a liquid (very low M of PB as a reference). This contribution shows G dependence as it increases with G , reflecting the collective dynamics of the dendrimers. For comparison with the linear polymers, master curves of unentangled and highly entangled PB are included. Clearly, this contribution from dendrimers resembles that of the unentangled polymers, and no entanglement dynamics is observed. These findings are in good agreement with theories considering the dynamics of dendrimers [224,225].

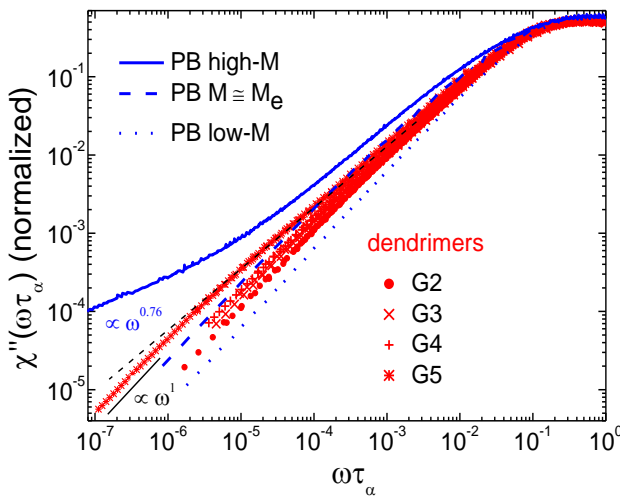


Figure 71: Normalized susceptibility master curves obtained from FC NMR of the PPI dendrimers of G2 to G5; for comparison master curves of PB for $M = 460$ g/mol (simple liquid, dotted blue line), $M = 2000$ g/mol (un-entangled, dashed blue line) and for $M = 87000$ g/mol (entangled, blue line) are included. [Reprinted with permission from (Mohamed, F.; Hofmann, M.; Pötzschner, B.; Fatkullin, N.; Rössler, E.A *Macromolecules* 2015, 48, 3294). Copyright (2015) American Chemical Society].

More Recently, Hofmann et al. [162] studied the rheological response of the PPI dendrimers of generations G2 to G5 and showed that no rubber plateau (entanglement dynamics) could be resolved in PPI dendrimers. This is in agreement was that found by FC NMR. From ^2H NMR

measurements and the line width analysis, $\tau_\alpha(T)$ has been extracted; all are included in the relaxation map drawn for the PPI dendrimers (*cf.* Figure 69a).

Finally, one can conclude that the local dynamics of PPI dendrimers is covered by DS which resembles that observed in hyperbranched polymers as well as in PAMAM dendrimers [223, 227-229]. The collective dendrimer dynamics is covered by FC NMR, which is similar to the Rouse dynamics for unentangled polymers.

References

1. Götze, W. Complex Dynamics in Glass-Forming Liquid A Mode-Coupling Theory. *Oxford University Press: New York*, **2009**.
2. Yarnell, J. L.; Katz, M.J.; Wenzel, R.G.; Koenig, S. H. Structure Factor and Radial Distribution Function for Liquid Argon at 85 °K. *Phys. Rev. A*, **1973**, 7,2130 <https://doi.org/10.1103/PhysRevA.7.2130>
3. Debenedetti, P. G.; Truskett, T. M.; Lweis, C.P.; Stillinger, F.H. Theory of supercooled liquids and glasses: energy landscape and statistical geometry perspectives. *Adv. Chem. Engin.* **2001**, 28, 21-79. <https://www.princeton.edu/~fhs/supliq/supliq>.
4. Angell, C. A. Relaxation in liquids, polymers and plastic crystals: strong/fragile patterns and problems. *J. Non-Cryst. Solids*, **1991**, 13, 131–133 [https://doi.org/10.1016/0022-3093\(91\)90266-9](https://doi.org/10.1016/0022-3093(91)90266-9).
5. Adam, G.; Gibbs, J. H., On the Temperature Dependence of Cooperative Relaxation Properties in Glass-Forming Liquids. *J. Chem. Phys.* **1965**, 43, 139. <http://dx.doi.org/10.1063/1.1696442>.
6. Lubchenko, V.I.; Wolynes, P.G. Theory of structural glasses and supercooled liquids. *Annu. Rev. Phys. Chem.* **2007**, 58, 235-266. Doi: 10.1146/annurev.physchem.58.032806.104653.
7. Kirkpatrick, T. R.; Thirumalai, D.; Wolynes, P. G. Scaling concepts for the dynamics of viscous liquids near an ideal glassy state. *Phys. Rev. A*. **1989**, 40, 1045 <https://doi.org/10.1103/PhysRevA.40.1045>.
8. Götze, W.; Sjögren, L. Relaxation processes in supercooled liquids. *Rep. Prog. Phys.* **1992**, 55, 241.
9. Richter, D.; Monkenbusch, M.; Arbe, A.; Colmenero, J. Neutron Spin Echo in Polymer Systems. *Advances in Polymer Science, Springer, Berlin*, **2005** 174, 1-221. <https://doi.org/10.1007/b106578>.
10. Bartsch, E.; Fujara, F.; Geil, B.; Kiebel, M.; Petry, W.; Schnauss, W.; Sillescu, H.; Wuttke, J. Signatures of the glass transition in a van der Waals liquid seen by neutrons and NMR. *Physica A*, **1993**, 201, 223-236. [https://doi.org/10.1016/0378-4371\(93\)90418-4](https://doi.org/10.1016/0378-4371(93)90418-4)

11. Petry, W.; Wuttke, J. Quasielastic neutron scattering in glass forming viscous liquids. *Trans. Theo. Statis. Phys.* **1995**, *24*, 1075-1095. <http://dx.doi.org/10.1080/00411459508203945>.
12. Tölle, A. Neutron scattering studies of the model glass former ortho-terphenyl. *Rep. Prog..Phys.* **2001**, *64*, 1473-1532. Doi: 10.1088/0034-4885/64/11/203
13. Berne, B. J.; Pecora, R. Dynamic Light Scattering; Wiley: New York, **1976**.
14. Li, G.; Du, W. M.; Chen, X. K.; Cummins, H. Z.; Tao, N. J. Testing mode-coupling predictions for and relaxation in $\text{Ca}_{0.4}\text{K}_{0.6}(\text{NO}_3)_{1.4}$ near the liquid-glass transition by light scattering, *Phys. Rev. A* **1992**, *45*, 3867-3879. Doi: 10.1103/PhysRevA.45.3867
15. Cummins, H.; Li, G.; Hwang, Y.; Shen, G.; Du, W.; Hernandez, J.; Tao, N.. Dynamics of supercooled liquids and glasses: comparison of experiments with theoretical predictions. *Zeitschrift für Physik B*, **1997**, *103*, 501-519
16. Adichtchev, S.; Benkhof, S.; Blochowicz, T.; Novikov, V. N.; Rössler, E.; Tschirwitz, C.; Wiedersich, Anomaly of the Nonergodicity Parameter and Crossover to White Noise in the Fast Relaxation Spectrum of a Simple Glass Former *J. Phys. Rev. Lett.* **2002**, *88*, 0557031-4. <https://link.aps.org/doi/10.1103/PhysRevLett.88.055703>
17. Petzold, N.; Rössler, E. A. Light scattering study on the glass former o-terphenyl. *J. Chem. Phys.* **2010**, *133*, 124512. <http://dx.doi.org/10.1063/1.3478533>
18. Torre, R.; Bartolini, P.; Pick, R. M. Time-resolved optical Kerr effect in a fragile glass-forming liquid, salol. *Phys.Rev. E* **1998**, *57*, 1912-1920. <https://doi.org/10.1103/PhysRevE.57.1912>
19. Hinze, G.; Brace, D. D.; Gottke, S. D.; Fayer, M. D. A detailed test of mode-coupling theory on all time scales: Time domain studies of structural relaxation in a supercooled liquid. *J. Chem. Phys.* **2000**, *113*, 3723-3733. <http://dx.doi.org/10.1063/1.1287595>
20. Cang, H.; Novikov, V. N.; Fayer, M. D. Logarithmic decay of the orientational correlation function in supercooled liquids on the Ps to Ns time scale. *J. Chem.Phys.* **2003**, *118*, 2800-2807. <http://dx.doi.org/10.1063/1.1536612>
21. Dixon, P. K.; Wu, L.; Nagel, S. R.; Williams, B. D.; Carini, J. P. Scaling in the relaxation of supercooled liquids. *Phys. Rev. Lett.* **1990**, *65*, 1108-1111. Doi: 10.1103/PhysRevLett.65.1108
22. Lunkenheimer, P.; Schneider, U.; Brand, R.; Loidl, A. Glassy dynamics. *Contemporary Physics*, **2000**, *41*, 15. <http://dx.doi.org/10.1080/001075100181259>

23. Kudlik, A.; Benkhof, S.; Blochowicz, T.; Tschirwitz, C.; Rössler, E. The dielectric response of simple organic glass formers. *J. Mol. Struct.* **1999**, *479*, 201-218.. [https://doi.org/10.1016/S0022-2860\(98\)00871-0](https://doi.org/10.1016/S0022-2860(98)00871-0)
24. Williams, G. Molecular motion in glass-forming systems. *J. Non-Crys. Sol.* **1991**, *131-133* Part 1, 1-12. [https://doi.org/10.1016/0022-3093\(91\)90265-8](https://doi.org/10.1016/0022-3093(91)90265-8)
25. Blochowicz, T.; Tschirwitz, C.; Benkhof, S.; Rössler, E. A. Susceptibility functions for slow relaxation processes in supercooled liquids and the search for universal relaxation patterns. *J. Chem. Phys.* **2003**, *118*, 7544-7555. <http://dx.doi.org/10.1063/1.1563247>
26. Schmidt-Rohr, K.; Spiess, H. W. Multidimensional Solid State NMR and Polymers; *Academic Press: London*, **1994**.
27. Böhmer, R.; Hinze, G.; Diezemann, G.; Geil, B.; Sillescu, H. Dynamic heterogeneity in supercooled ortho-terphenyl studied by multidimensional deuteron NMR. *Euro. Phys. Lett.* **1996**, *36*, 55-60. <https://doi.org/10.1209/epl/i1996-00186-5>
28. Geil, B.; Fujara, F.; Sillescu, H. ^2H NMR time domain analysis of ultraslow reorientations in supercooled liquids *J. Magn. Res.* **1998**, *130*, 18-26. <https://doi.org/10.1006/jmre.1997.1284>
29. Hinze, G. Geometry and time scale of the rotational dynamics in supercooled toluene. *Phys. Rev. E* **1998**, *57*, 2010-2018. <https://doi.org/10.1103/PhysRevE.57.2010>
30. Böhmer, R.; Diezemann, G.; Hinze, G.; Rössler, E. Dynamics of supercooled liquids and glassy solids. *Prog. Nucl. Magn. Reson. Spec.* **2001**, *39*, 191-267. [https://doi.org/10.1016/S0079-6565\(01\)00036-X](https://doi.org/10.1016/S0079-6565(01)00036-X)
31. Vogel, M.; Medick, P.; Rösler, E. A. Secondary Relaxation Processes in Molecular Glasses Studied by Nuclear Magnetic Resonance Spectroscopy. *Ann. Rep. NMR Spectr.* **2005**, *56*, 231-299. [https://doi.org/10.1016/S0066-4103\(05\)56005-8](https://doi.org/10.1016/S0066-4103(05)56005-8)
32. Kimmich, R.; Anzardo, E. Field-cycling NMR relaxometry. *Prog. Nucl. Magn. Reson. Spectr.* **2004**, *44*, 257-320. <https://doi.org/10.1016/j.pnmrs.2004.03.002>.
33. Kruk, D.; Herrmann, A.; Rössler, E. A. Field-cycling NMR relaxometry of viscous liquids and polymers. *Prog. Nucl. Magn. Reson. Spectr.* **2012**, *63*, 33-64. <https://doi.org/10.1016/j.pnmrs.2011.08.001>
34. Fytas, G.; Dorfmueller, T.; Wang, C. H. Pressure- and temperature-dependent homodyne photon correlation studies of liquid o-terphenyl in the supercooled state. *J. Phys. Chem.* **1983**, *87*, 5041- 5045. Doi: 10.1021/j150642a052

35. Meier, G.; Gerharz, B.; Boese, D.; Fischer, E. W. Dynamical processes in organic glass-forming van der Waals liquids. *J. Chem. Phys.* **1991**, *94*, 3050-3059. <http://dx.doi.org/10.1063/1.459828>
36. Patkowski, A.; Steffen, W.; Nilgens, H.; Fischer, E. W.; Pecora, R. Depolarized dynamic light scattering from three low molecular weight glass forming liquids: A test of the scattering mechanism. *J. Chem. Phys.* **1997**, *106*, 8401-8408. <http://dx.doi.org/10.1063/1.474117>
37. Brodin, A.; Bergman, R.; Mattsson, J.; Rössler, E. A. Light scattering and dielectric manifestations of secondary relaxations in molecular glass formers. *Euro. Phys.B.* **2003**, *36*, 349-357. <https://doi.org/10.1140/epjb/e2003-00353-6>
38. McCrum, N. G.; Read, B. E.; Williams, G. *Anelastic and Dielectric Effects in Polymer Solids*, Wiley, New York **1967**.
39. Jakobsen, B.; Niss, K.; Maggi, C.; Olsen, N. B.; Christensen, T.; Dyre, J. C. Beta relaxation in the shear mechanics of viscous liquids: Phenomenology and network modeling of the alpha-beta merging region. *J. Non-Cryst. Solids.* **2011**, *357*, 267. <https://doi.org/10.1016/j.jnoncrsol.2010.08.010>
40. Kubo, R. The fluctuation-dissipation theorem. *Rep. Prog. phys.* **1966**, *28*, 255-284.
41. Wiener, N. Generalized harmonic analysis. *Acta Mathematica*, **1930**, *55*, 117-258.
42. Khintchine, A. Korrelationtheorie der stationäre stochastischen prozesse *Mathematische Annalen.* **1934**, *109*, 604-615.
43. Böttcher, C. J. F.; Bordewijk, P. Theory of Electric Polarization, Vol. 2 ; Elsevier: Amsterdam, **1973**.
44. Kob, W.; Andersen, H.C. Testing mode-coupling theory for a supercooled binary Lennard-Jones mixture II. Intermediate scattering function and dynamic susceptibility. *Phys. Rev.E*, **1995**, *52*, 4134-4153. Doi: 10.1103/PhysRevE.52.4134
45. Kob, W.; Andersen, H.C. Testing mode-coupling theory for a supercooled binary Lennard-Jones mixture I: The van Hove correlation function. *Phys. Rev.E* **1995**, *51*, 4626-4641. <https://doi.org/10.1103/PhysRevE.51.4626>
46. Petzold, N.; Schmidtke, B.; Kahlau, R.; Bock, D.; Meier, R.; Micko, B.; Kruk, D.; Rössler, A. E. Evolution of the dynamic susceptibility in molecular glass formers: Results from light scattering, dielectric spectroscopy, and NMR. *J. Chem. Phys.* **2013**, *138*, 12A510. <http://dx.doi.org/10.1063/1.4770055>

47. Binder, K.; Kob, W. *Glassy Materials and Disordered Solids*, *World Scientific, New Jersey*, **2005**.
48. Berthier, L.; Biroli, G.; Bouchaud, J.-P. Cipelletti, L.; Saarloos W. van. *Dynamical Heterogeneities in Glasses, Colloids, and Granular Media*. *Oxford University Press, Oxford*, **2011**
49. Berthier, L.; Biroli, G. Theoretical perspective on the glass transition and amorphous materials. *Rev. Mod. Phys.* **2011**, *83*, 587–645. <https://doi.org/10.1103/RevModPhys.83.587>.
50. C.A. Angell, Strong and Fragile Liquids, in: *Relaxations in Complex Systems* (Eds K.L. Ngai, and G.B. Wright) National Technical Information Service, U.S. Department of Commerce, Springfield, VA 22161, pp. 3-11 (1985).
51. Vogel, H. The law of the relation between the viscosity of liquids and the temperature *Phys. Z.* **1921**, *22*, 645.-646.
52. Fulcher, G.S. Analysis of recent measurements of the viscosity of glasses. *J. Am. Ceram. Soc.* **1925**, *6*, 339-355. <https://doi.org/10.1111/j.1151-2916.1925.tb16731.x>
53. Tammann, G.; Hesse, W.Z. Z. Die Abhängigkeit der Viscosität von der Temperatur bei unterkühlten Flüssigkeiten, *Anorg. Allg. Chem.* **1926**, *156*, 245. <https://doi.org/10.1002/zaac.19261560121>.
54. Brodin, A.; Gainaru, C.; Porokhonsky, V.; Rössler, E. A. Evolution of dynamic susceptibility in molecular glass formers—a critical assessment. *J. Phys. Condens Matter* **2007**, *19*, 205104. <https://doi.org/10.1088/0953-8984/19/20/205104>
55. Gainaru, C.; Kahlau, R.; Rössler, E. A.; Böhmer, R. Evolution of excess wing and β -process in simple glass formers *J. Chem. Phys.* **2009**, *131*, 184510. <http://dx.doi.org/10.1063/1.3258430>.
56. Schneider, U.; Brand, R.; Lunkenheimer, P.; Loidl, A. Excess wing in the dielectric loss of glass formers: A johari-goldstein beta relaxation? *Phys. Rev. Lett.* **2000**, *84*, 5560-3. Doi: 10.1103/PhysRevLett.84.5560.
57. Casalini, R.; Roland, C. M. Excess wing in the dielectric loss spectra of propylene glycol oligomers at elevated pressure. *Phys. Rev. Lett.* **2004**, *69*, 094202. Doi: 10.1103/PhysRevB.69.094202.
58. Ngai, K. L. *Relaxation and Diffusion in Complex Systems*, Springer, New York **2011**.

59. Ngai, K. L.; Paluch, M. Classification of secondary relaxation in glass-formers based on dynamic properties. *J. Chem. Phys.* **2004**, *120*, 857-873. <http://dx.doi.org/10.1063/1.1630295>.
60. Kahlau, R.; Dörfler, T; Rössler E. A. Secondary relaxations in a series of organic phosphate glasses revealed by dielectric spectroscopy. *J. Chem. Phys.* **2013**, *139*, 134504. <https://doi.org/10.1063/1.4822002>.
61. Johari, G. P. Intrinsic mobility of molecular glasse *J. Chem. Phys.* **1973**, *58*, 1766. <https://doi.org/10.1063/1.1679421>.
62. Johari, G. P.; Goldstein, M. Viscous Liquids and the Glass Transition. II. Secondary Relaxations in Glasses of Rigid Molecules. *J. Chem. Phys.* **1970**, *53*, 2372. <http://dx.doi.org/10.1063/1.1674335>.
63. Wang, C. C.; Pecora, R. Time-correlation functions for restricted rotational diffusion *J. Chem. Phys.* **1980**, *72*, 5333. <http://dx.doi.org/10.1063/1.439024>.
64. Sitnitsky, A. E. Analytic treatment of nuclear spin-lattice relaxation for diffusion in a cone model. *J. Magn. Reson.* **2011**, *213*, 58. <https://doi.org/10.1016/j.jmr.2011.08.041>.
65. Tomalia DA, Fréchet JMJ. Introduction to the dendritic state. In: Dendrimers and other dendritic polymers. *New York: Wiley*; **2001**. Doi: 10.1002/0470845821.ch1.
66. Baschnagel, J.; Bennemann, C.; Paul, W.; Binder, K. Dynamics of a supercooled polymer melt above the mode-coupling critical temperature: cage versus polymer-specific affects. *J. Phys.: Condens. Matter* **2000**, *12*, 6365–6374. <http://iopscience.iop.org/0953-8984/12/29/308>.
67. Rouse, P.E., A Theory of the Linear Viscoelastic Properties of Dilute Solutions of Coiling Polymers. *J. Chem. Phys.* **1953**, *21*, 1272. <http://dx.doi.org/10.1063/1.1699180>
68. Stockmayer, W. H. Dielectric dispersion in solutions of flexible polymers *Pure Appl. Chem.* 1967, *15*, 539. <https://doi.org/10.1351/pac196715030539>.
69. Boese, D.; Kremer, F. Molecular Dynamics in Bulk cis-Polyisoprene as Studied by Dielectric Spectroscopy *Macromolecules* **1990**, *23*, 829-835. Doi: 10.1021/ma00205a023.
70. Adachi, K. and Kotaka, T. Dielectric Normal Mode Process in Undiluted cis-Polyisoprene *Macromolecules*, **1985**, *18*, 466-472. Doi: 10.1021/ma00145a028
71. Adachi, K. and Kotaka, T. Dielectric normal mode process in semidilute and concentrated solutions of cis-polyisoprene *Macromolecules*, **1988**, *21*, 157-164. Doi: 10.1021/ma00179a032.

72. Imanishi, Y.; Adachi, K.; Kotaka, T. Further investigation of the dielectric normal mode process in undiluted cis-polyisoprene with narrow distribution of molecular weight *J. Chem. Phys.* **1988**, *89*, 7585–7592. <http://dx.doi.org/10.1063/1.455244>.
73. Watanabe, H. Dielectric Relaxation of Type-A Polymers in Melts and Solutions. *Macromol. Rapid. Commun.* **2001**, *22*, 127-175. Doi: 10.1002/1521-3927(200102)22:3<127: AID-MARC127>3.0.CO;2-S.
74. Abou Elfadl, A.; Kahlau, R.; Herrmann, A.; Novikov, V. N.; Rössler, E. A. From Rouse to Fully Established Entanglement Dynamics: A Study of Polyisoprene by Dielectric Spectroscopy *Macromolecules* **2010**, *43*, 3340-3351. Doi: 10.1021/ma902564b.
75. de Gennes, P.G. Reptation of a polymer chain in the presence of fixed obstacles, *J. Chem. Phys.* **1971**, *55*, 572-579. doi/abs/10.1063/1.1675789.
76. Doi, M.; Edwards, S. F. *The Theory of Polymer Dynamics*; Oxford Sci. Publication, **1986**.
77. Likhtman, A.E.; McLeish, T.C.B. Quantitative Theory for Linear Dynamics of linear Entangled Polymers. *Macromolecules* **2002**, *35*, 6332-6343. Doi: 10.1021/ma0200219.
78. Colby, R. H.; Fetters, L. J.; Graessley, W. W. Melt Viscosity-Molecular Weight Relationship for Linear Polymers. *Macromolecules* **1987**, *20*, 2226-2237. Doi: 10.1021/ma00175a030.
79. Rubinstein, M.; Colby, R. H. *Polymer Physics*; Oxford University Press: Oxford, U. K., **2003**.
80. Abdel-Goad, M.; Pyckhout-Hintzen, W.; Kahle, S.; Allgaier, J.; Richter, D.; Fetters, L. J. Rheological Properties of 1,4-Polyisoprene over a Large Molecular Weight Range *Macromolecules*. **2004**, *37*, 8135- 8144. Doi: 10.1021/ma030557.
81. Unidad, H.J.; Goad, M.A.; Bras, A.R.; Zamponi, M.; Faust, R.; Allgaier, J.; Pyckhout-Hintzen, W.; Wischniewski, A.; Richter, D.; Fetters, L.J, Consequences of Increasing Packing Length on the Dynamics of Polymer Melts *Macromolecules* **2015**, *48*, 6638-6645. Doi: 10.1021/acs.macromol.5b00341.
82. Fröhlich, H. *Theory of dielectrics- Dielectric constant and loss*, Clarendon Press., Oxford, **1958**.
83. Onsager, L. Electric Moments of Molecules in Liquids. *J. Ameri. Chem. Soci.* **1936**, *58*, 1486. Doi: 10.1021/ja01299a050.
84. Blochowicz, T. Broad Band Dielectric Spectroscopy in Neat and Binary Molecular Glass Former. PhD thesis, University of Bayreuth, **2003**.

85. Kahlau, R.; Kruk, D.; Blochowicz, T.; Novikov, V. N.; Rössler, E. A. Generalization of the Cole–Davidson and Kohlrausch functions to describe the primary response of glass-forming systems. *J. Phys.: condens. matter* **2010**, *22*, 365101 Doi: 10.1088/0953-8984/22/36/365101.
86. Kremer, F., Schönhals, A. Broadband Dielectric Spectroscopy, *Springer, Berlin, Heidelberg, New York*, **2003**.
87. Kimmich, R. principals of soft matter Dynamics: Basic Theories, Non-Invasive Methods, Mesoscopic Aspects; *Springer: Dordrecht (NL)*, **2012**.
88. Ferry, D. Viscoelastic Properties of Polymers. *John Wiley & Sons*, **1980**.
89. Mohamed, F.; Flämig, M.; Hofmann, M.; Heymann, L.; Willner, L.; Fatkullin, N.; Aksel, N.; Rössler, E.A. Scaling analysis of the viscoelastic response of linear polymers, *J. Chem. Phys*, **20118** (submitted).
90. Wang, L. M.; Tian, Y.; Liu, R.; Richert, R. Structural Relaxation Dynamics in Binary Glass-Forming Molecular Liquids with Ideal and Complex Mixing Behavior *J. Phys. Chem. B* **2010**, *114*, 3618. Doi: 10.1021/jp912223j.
91. Duvvuri, K.; Richert, R.; Binary Glass-Forming Materials: Mixtures of Sorbitol and Glycerol *J. Phys. Chem. B* **2004**, *108*, 10451. Doi: 10.1021/jp031366b.
92. Wang, L. M.; Tian, Y. J.; Liu, R. P.; Ngai, K. L. Anomalous Component Dynamics of a Binary Mixture of Associating Glass-Forming Liquids. *J. Phys. Chem. B.* **2011**, *115*, 719. Doi: 10.1021/jp1101362.
93. Pizzoli, M.; Scandola, M.; Ceccorulli, G.; Molecular motions in polymer-diluent systems: Polystyrene-tritolylphosphate. *Eur. Polym. J.* **1987**, *23*, 843-846. [https://doi.org/10.1016/0014-3057\(87\)90055-3](https://doi.org/10.1016/0014-3057(87)90055-3).
94. Ceccorulli, G.; Pizzoli, M.; Scandola, M. Composition dependence of the glass transition temperature of polymer-diluent systems: 1. Experimental evidence of a dual behavior in plasticized PVC. *Polymer* **1987**, *28*, 2077-2080. [https://doi.org/10.1016/0032-3861\(87\)90044-9](https://doi.org/10.1016/0032-3861(87)90044-9).
95. Kahlau, R.; Bock, D.; Schmidtke, B.; Rössler, E. A. Dynamics of asymmetric binary glass formers. I. A dielectric and nuclear magnetic resonance spectroscopy study. *J. Chem. Phys.* **2014**, *140*, 044509. Doi: 10.1063/1.4861428
96. Blochowicz, T.; Lusceac, S.; Gutfreund, P.; Schramm, S.; Stühn, B. Two Glass Transitions and Secondary Relaxations of Methyltetrahydrofuran in a Binary Mixture *J. Phys. Chem. B.* **2011**, *115*, 1623. [dx.doi.org/10.1021/jp110506z](https://doi.org/10.1021/jp110506z).

97. Blochowicz, T.; Schramm, S.; Lusceac, S.; Vogel, M.; Stühn, B.; Gutfreund, P.; Frick, B. Signature of a Type-A Glass Transition and Intrinsic Confinement Effects in a Binary Glass-Forming System. *Phys. Rev. Lett.* **2012**, *109*, 035702. Doi: 10.1103/PhysRevLett.109.035702.
98. Bock D.; Kahlau, R.; Pötzschner, B.; Körber, T.; Wagner, E.; Rössler, E. A. Dynamics of asymmetric binary glass formers. II. Results from nuclear magnetic resonance spectroscopy *J. Chem. Phys.* **2014**, *140*, 094505. Doi: 10.1063/1.4865945.
99. Bock, D.; Petzold, N.; Kahlau, R.; Gradmann, S.; Schmidtke, B.; Benoit, N.; Rössler, E. A. Dynamic heterogeneities in glass-forming systems *J. Non-Cryst. Solids* **2015**, *407*, 88. Doi: 10.1016/j.jnoncrysol.2014.09.029.
100. Chen, S.-H.; Liu, L.; Fratini, E.; Baglioni, P.; Faraone, A.; Mamontov, E. Observation of fragile-to-strong dynamic crossover in protein hydration water. *PNAS*, **2006**, *103*, 9012. Doi: 10.1073/pnas.0602474103.
101. Laurati, M.; Sotta, P.; Long, D. R.; Fillot, L.-A.; Arbe, A.; Alegria, A.; Embs, J. P.; Unruh, T.; Schneider, G. J.; Colmenero, J. Dynamics of Water Absorbed in Polyamides *Macromolecules* **2012**, *45*, 1676. Doi: 10.1021/ma202368x.
102. Cervený, S.; Alegría, Á.; Colmenero, J. Universal features of water dynamics in solutions of hydrophilic polymers, biopolymers, and small glass-forming materials *Phys. Rev. E* **2008**, *77*, 031803. Doi: 10.1103/PhysRevE.77.031803.
103. Goracci, G.; Arbe, A.; Alegría, A.; Su, Y.; Gasser, U.; Colmenero, J. Structure and component dynamics in binary mixtures of poly(2-(dimethylamino) ethyl methacrylate) with water and tetrahydrofuran: A diffraction, calorimetric, and dielectric spectroscopy study *J. Chem. Phys.* **2016**, *45*, 1676. Doi: 10.1063/1.4946004.
104. Voigtmann, T.; Horbach, Double Transition Scenario for Anomalous Diffusion in Glass-Forming Mixtures. *J. Phys. Rev. Lett.* **2009**, *103*, 205901. Doi: 10.1103/PhysRevLett.103.205901.
105. Bosse J.; Kaneko, Y. Self-Diffusion in Supercooled Binary Liquids. *Phys. Rev. Lett.* **1995**, *74*, 4023. Doi: 10.1103/PhysRevLett.74.4023.
106. Krakoviack, V. Liquid-Glass Transition of a Fluid Confined in a Disordered Porous Matrix: A Mode-Coupling Theory. *Phys. Rev. Lett.* **2005**, *94*, 065703. Doi: 10.1103/PhysRevLett.94.065703.

107. Moreno, A. J.; Colmenero, J. Relaxation scenarios in a mixture of large and small spheres: Dependence on the size disparity *J. Chem. Phys.* **2006**, *125*, 164507. Doi: 10.1063/1.2361286.
108. Blochowicz, T.; Gainaru, C.; Medick, P.; Tschirwitz, C.; Rössler E. A. The dynamic susceptibility in glass forming molecular liquids: The search for universal relaxation patterns II. *J. Chem. Phys.* **2006**, *124*, 134503. <http://aip.scitation.org/toc/jcp/124/13>
109. Adishchev, S.; Bock, D.; Gainaru, C.; Kahlau, R.; Micko, B.; Petzold, N.; Pötzschner, B.; Rössler, E. A. Reorientational Dynamics of Organophosphate Glass Formers - a Joint Study by ^{31}P NMR, Dielectric Spectroscopy and Light Scattering. *Z. Phys. Chem.* **2012**, *226*, 1149-1168.
110. Pötzschner, B.; Mohamed, F.; Lichtinger, A.; Bock, D.; Rössler, E.A. Dynamics of asymmetric non-polymeric binary glass formers-A nuclear magnetic resonance and dielectric spectroscopy study. *J. Chem. Phys.* **2015**, *143*, 154506. <http://dx.doi.org/10.1063/1.4932981>.
111. Pötzschner, B.; Mohamed, F.; Bächer, C.; Wagner, E.; Lichtinger, A.; Minikejew, R.; Kreger, K.; Schmidt, H.-W.; Rössler, E. A. Non-polymeric asymmetric binary Glass-Formers. Part I: Main Relaxations studied by Dielectric, ^2H and ^{31}P NMR Spectroscopy. *J. Chem. Phys.* **2017**, *146*, 164503. <https://doi.org/10.1063/1.4980084>.
112. Schönhals, A.; Goering, H.; Schick, C.; Frick, B.; Mayorova, M.; Zorn, R. Segmental dynamics of poly(methyl phenyl siloxane) confined to nanoporous glasses. *Eur. Phys. J. Special Topics* **2007**, *141*, 255. Doi:10.1140/epjst/e2007-00049-3.
113. Gradmann, S.; Medick, P.; Rössler, E. A. Glassy Dynamics in Nanoconfinement as Revealed by ^{31}P NMR. *J. Phys. Chem.*, **2009**, *113*, 8443. Doi: 10.1021/jp9027518.
114. Lusceac, S.A.; Koplin, C.; Medik, P.; Vogel, M.; LeQuellec, C.; Brodie-Linder, N.; Alba-Simionesco, C.; Rössler, E. A. Type A versus Type B Glass Formers: NMR Relaxation in Bulk and Confining Geometry. *J. Phys. Chem.* **2004**, *108*, 16601. Doi: 10.1021/jp040376p.
115. Zetsche, A.; Fischer, E. W. Dielectric studies of the α -relaxation in miscible polymer blends and its relation to concentration fluctuations *Acta Polymerica*. **1994**, *45*, 168. Doi:10.1002/actp.1994.010450306.
116. Kumar, S. K.; Colby, R. H.; Anastasiadis, S. H., Fytas, G. Concentration fluctuation induced dynamic heterogeneities in polymer blends. *J. Chem. Phys.* 1996, *105*, 3777. <https://doi.org/10.1063/1.472198>.

117. Kant, R.; Kumar, S. K.; Colby, R. H. What Length Scales Control the Dynamics of Miscible Polymer Blends? *Macromolecules* **2003**, *36*, 10087. Doi: 0.1021/ma0347215.
118. Chung, G. C.; Kornfield, J. A.; Smith, S. D. Component Dynamics in Miscible Polymer Blends: A Two-Dimensional Deuteron NMR Investigation. *Macromolecules* **1994**, *27*, 964. Doi:10.1021/ma00082a013.
119. Lodge, T. P.; McLeish, T. C. B. Self-Concentrations and Effective Glass Transition Temperatures in Polymer Blends. *Macromolecules* **2000**, *33*, 5278. Doi: 10.1021/ma9921706.
120. Leroy, E.; Alegria, A.; Colmenero, J. Quantitative Study of Chain Connectivity Inducing Effective Glass Transition Temperatures in Miscible Polymer Blends. *Macromolecules* **2003**, *36*, 7280. Doi: 10.1021/ma025508w.
121. Minikejew, K.; Rössler, E.A. work in progress
122. Bock, D.; Kahlau, R.; Micko, B.; Pötzschner, B.; Schneider, G. J.; Rössler, E. A. On the cooperative nature of the β -process in neat and binary glasses: a dielectric and nuclear magnetic resonance spectroscopy study. *J. Chem. Phys.* **2013**, *139*, 064508. Doi: 10.1063/1.4816374.
123. Micko, B.; Tschirwitz, C.; Rössler, E.A. A. Secondary relaxation processes in binary glass formers: Emergence of “islands of rigidity”. *J. Chem. Phys.* **2013**, *138*, 154501 <https://doi.org/10.1063/1.4798655>.
124. Kasper, C.; Reiser, A. Variation of the secondary relaxation strength in a binary glass former *J. Chem. Phys.* **2004**, *120*, 11735581 <https://doi.org/10.1063/1.1735581>.
125. Cangialosi, D.; Alegria, A.; Colmenero, J. Dielectric relaxation of polychlorinated biphenyl/toluene mixtures: Component dynamics. *J. Chem. Phys.* **2008**, *128*, 224508. <http://dx.doi.org/10.1063/1.2937449>.
126. Sjöström, J.; Mattsson, J.; Bergman, R.; Johanson, E.; Josefsson, K.; Svantesson, D.; Swenson, J. Dielectric secondary relaxation of water in aqueous binary glass-formers. *Phys. Chem. Chem. Phys.* **2010**, *12*, 10452 Doi:10.1039/C001275K
127. Pötzschner, B.; Mohamed, F.; Bächer, C.; Wagner, E.; Lichtinger, A.; Bock, D.; Kreger, K.; Schmidt, H.-W.; Rössler, E.A. Non-polymeric asymmetric binary Glass-Formers. Part II: Secondary Relaxation studied by Dielectric, ^2H and ^{31}P NMR Spectroscopy. *J. Chem. Phys.* **2017**, *46*, 164504. <http://dx.doi.org/10.1063/1.4980085>.

128. Colmenero, J.; Arbe, A. Recent Progress on Polymer Dynamics by Neutron Scattering: From Simple Polymers to Complex Materials. *J. Polym. Sci. B.* **2013**, *51*, 87-113. Doi: 10.1002/polb.23178.
129. Wischniewski, A.; Monkenbusch, M.; Willner, L.; Richter, D.; Kali, G. Direct Observation of the Transition from Free to Constrained Single-Segment Motion in Entangled Polymer Melts. *Phys. Rev. Lett.* **2003**, *90*, 58302, Doi:10.1103/PhysRevLett.90.058302.
130. Richter, D.; Butera, R.; Fetters, L.J.; Huang, J.S.; Farago, B.; Ewen, B. Entanglement constraints in polymer melts. A neutron spin echo study. *Macromolecules*, **1992**, *25*, 6156-6164. Doi: 10.1021/ma00049a011.
131. Richter, D.; Monkenbusch, M.; Arbe, A.; Colmenero, J. "Neutron Spin Echo in Polymer Systems," *Adv. Polym. Sci.* **2005**, *174*, 1. <https://doi.org/10.1007/b106578>
132. Lozovoi, A.; Mattea, C.; Hofmann, M.; Saalwaechter, K.; Fatkullin, N.; Stapf, S. Segmental dynamics of polyethylene-alt-propylene studied by NMR spin echo techniques *J. Chem. Phys.* **2017**, *89*, 224901 <http://dx.doi.org/10.1063/1.4984265>
133. Hofmann, M.; Kresse, B.; Heymann, L.; Privalov, A.F.; Fatkullin, N.; Aksel, N.; Fujara, F.; Rössler, E.A. Dynamics of a Paradigmatic Linear Polymer: A Proton Field-Cycling NMR Relaxometry Study on Poly(ethylene-propylene), *Macromolecules* **2016**, *49*, 8622-8632. Doi: 10.1021/acs.macromol.6b01906.
134. Hofmann, M.; Herrmann, A.; Abou Elfadl, A.; Kruk, D.; Wohlfahrt, M.; Rössler, E. A. Glassy, Rouse, and Entanglement Dynamics as Revealed by Field Cycling ^1H NMR Relaxometry. *Macromolecules* **2012**, *5*, 2390–2401. Doi: 10.1021/ma202371p.
135. Herrmann, A.; Kresse, B.; Wohlfahrt, M.; Bauer, I.; Privalov, A. F.; Kruk, D.; Fatkullin, N.; Fujara, F.; Rössler, E. A. Mean Square Displacement and Reorientational Correlation Function in Entangled Polymer Melts Revealed by Field Cycling ^1H and ^2H NMR Relaxometry. *Macromolecules*, **2012**, *45*, 6516-6526 Doi: 10.1021/ma301099h.
136. Hofmann, M.; Kresse, B.; Privalov, A. F.; Heymann, L.; Willner, L.; Aksel, N.; Fatkullin, N.; Fujara, F.; Rössler, E.A. Segmental Mean Square Displacement: Field-Cycling ^1H Relaxometry vs. Neutron Scattering, *Macromolécules*, **2016**, *49*, 7945-7951. Doi: 10.1021/acs.macromol.6b01860.

137. Liu, C-Y.; Keunings, R.; Bailly, Ch. Direct Rheological Evidence of Monomer Density Reequilibration for Entangled Polymer Melts. *Macromolecules* **2007**, *40*, 2946-2954. Doi: 10.1021/ma062695f.
138. Park, S.J.; Desai, P.S.; Chen, X.; Larson, R.G. Universal Relaxation Behavior of Entangled 1,4-Polybutadiene Melts in the Transition Frequency Region. *Macromolecules* **2015**, *48*, 4122-413. DOI: 10.1021/ma5024632.
139. Fetters, L. J.; Lohse, D. J.; Richter, D.; Witten, T. A.; Zirkel, A. Connection between Polymer Molecular Weight, Density, Chain Dimensions, and Melt Viscoelastic Properties. *Macromolecules* 1994, *27*, 4639-4647. Doi: 10.1021/ma00095a001.
140. Auhl, D.; Ramirez, J.; Likhtman, A.E.; Chambon, P.; Fernyhough, Ch.; Linear and nonlinear shear flow behavior of monodisperse polyisoprene melts with a large range of molecular weights, *J. Rheol.* **2008**, *52*, 801 – 835. <https://doi.org/10.1122/1.2890780>.
141. Doi, M. Explanation for the 3.4-power law for viscosity of polymeric liquids on the basis of the tube model. *J. Polym. Sci. Phys. Ed.* **1983**, *21*, 667-684. Doi:10.1002/pol.1983.180210501.
142. Graessley, W. W. *Polymeric Liquids & Networks: Dynamics and Rheology*; Taylor and Francis: New York, **2008**.
143. Glomann, T.; Schneider, G. J.; Bras, A. R.; Pyckhout-Hintzen, W.; Wischniewski, A.; Zorn, R.; Allgaier, J.; Richter, D. Unified Description of the Viscoelastic and Dielectric Global Chain Motion in Terms of the Tube Theory. *Macromolecules* **2011**, *44* (18), 7430-7437. Doi: 10.1021/ma200674z.
144. Fox, T.; Flory, P. J. The glass temperature and related properties of polystyrene. Influence of molecular weight *J Polym. Sci.* **1954**, *14*, 315-319. Doi: 10.1002/pol.1954.120147514
145. Hintermeyer, J.; Herrmann, A.; Kahlau, R.; Goiceanu, C.; Rössler, E. A. Molecular Weight Dependence of Glassy Dynamics in Linear Polymers Revisited. *Macromolecules*, **2008**, *41*, 9335-9344. Doi: 10.1021/ma8016794
146. Kulik, A. S.; Beckham, H. W.; Schmidt-Rohr K.; Radloff, D.; Pawelzik, U.; Boeffel, C.; Spiess, H. W. Coupling of α and β Processes in Poly(ethyl methacrylate) Investigated by Multidimensional NMR. *Macromolecules* **1994**, *27*, 4746. Doi:10.1021/ma00095a015.

147. Koerber, T; Mohamed, F; Hofmann, M, Lichtinger, A; Willner, L.; Rössler, E.A. The Nature of Secondary Relaxations: The Case of Poly(ethylene-alt-propylene) Studied by Dielectric and Deuteron NMR Spectroscopy. *Macromolecules*, **2017**, *50*, 1554-1568 Doi: 10.1021/acs.macromol.6b02536.
148. Kariyo, S.; Brodin, A.; Gainaru, C.; Herrmann, A.; Schick, H.; Novikov, V. N.; Rössler, E. A. From Simple Liquid to Polymer Melt. Glassy and Polymer Dynamics Studied by Fast Field Cycling NMR Relaxometry: Low and High Molecular Weight Limit *Macromolecules* **2008**, *41*, 5313-5321. Doi: 10.1021/ma702771s.
149. Bergman, R.; Alvarez, F.; Alegria, A.; Colmenero, J. The merging of the dielectric α - and β -relaxations in poly-(methyl methacrylate). *J. Chem. Phys.* **1998**, *109*, 7546-7555. <http://dx.doi.org/10.1063/1.477376>.
150. Flämig, M.; Becher, M.; Hofmann, M.; Körber, T.; Kresse, B.; Privalov, A. F.; Willner, L.; Kruk, D.; Fujara, F.; Rössler, E. A. Perspectives of Deuteron Field-Cycling NMR Relaxometry for Probing Molecular Dynamics in Soft Matter. *J. Phys. Chem.* **2016**, *120*, 7754. Doi:10.1021/acs.jpcc.6b05109.
151. Schröter, K.; Hutcheson, S. A.; Shi, X.; Mandanici, A.; McKenna G. B. Dynamic shear modulus of glycerol: Corrections due to instrument compliance. *J. Chem. Phys.* **2006**, *125*, 214507-1-4. Doi: <http://dx.doi.org/10.1063/1.2400862>.
152. Santangelo, P. G.; Roland, C. M., Temperature Dependence of Mechanical and Dielectric Relaxation in *cis*-1,4-Polyisoprene. *Macromolecules* **1998**, *31*, 3715-3719. Doi: 10.1021/ma971663c.
153. Inoue, T.; Osaki, K. Role of Polymer Chain Flexibility on the Viscoelasticity of Amorphous Polymers around the Glass Transition Zone. *Macromolecules* **1996**, *29*, 1595-1599. Doi: 10.1021/ma950981d.
154. Plazek, D. J. Temperature Dependence of the Viscoelastic Behavior of Polystyrene. *Phys. Chem.* **1965**, *69*, 3480-3487. Doi: 10.1021/j100894a039.
155. Plazek, D. J., O'Rourke, V.M. Viscoelastic Behavior of low molecular weight Polystyrene. *J. Polym. Sci. Part A-2* **1971**, *9*, 209-243. Doi: 10.1002/pol.1971.160090202.
156. Ngai, K.L.; Plazek, D. J. Identification of Different Modes of Molecular Motion in Polymers That Cause Thermorheological Complexity. *Rubber Chem. Tech., Rubber Rev.* **1995**, *68*, 376-434. Doi: <https://doi.org/10.5254/1.3538749>.
157. Sokolov, A. P; Schweizer K.S. Resolving the Mystery of the Chain Friction Mechanism

- in Polymer Liquids. *Physc. Rev. Lett.* **2009** *102*, 248301. Doi:: 10.1103/PhysRevLett.102.248301.
158. Sokolov, A.P.; Hayashi, Y. Breakdown of Time-Temperature Superposition: From experiment to coupling model and beyond, *J. Non-Crystalline Solids* **2007**, *353*, 3838-3844. <https://doi.org/10.1016/j.jnoncrysol.2007.02.063>
 159. Ding, Y.; Sokolov, A.P. Breakdown of Time-Temperature Superposition Principle and Universality of Chain Dynamics in Polymers. *Macromolecules* **2006**, *39*, 3322-3326. DOI: 10.1021/ma052607b.
 160. Pallade, L.I.; Verney, V.; Attane, P. Time-Temperature Superposition and Linear Viscoelasticity of Polybutadienes, *Macromolecules* **1995**, *28*, 7051-7057. Doi: 10.1021/ma00125a003.
 161. Cavaille, J. Y.; Jourdan, C.; Perez, J.; Monnerie, L.; Johari, G.P. Time-Temperature Superposition and Dynamic Mechanical Behavior of Atactic Polystyrene. *J. Polym. Sci., part B: polym. Phys.* **1987**, *25*, 1235. Doi:10.1002/polb.1987.090250605.
 162. Hofman, M.; Gainaru, C.; Cetinkaya, B.; Fatkullin, N.; Rössler, E.A. Field-Cycling Relaxometry as a Molecular Rheology Technique: Common Analysis of NMR, Shear Modulus and Dielectric Loss Data of Polymers vs. Dendrimers. *Macromolecules*, **2015**, *48*, 7521-7534. Doi: 10.1021/acs.macromol.5b01805.
 163. Ramirez, J.; Likhtman, A. E. Rheology of Entangled Polymers: Toolkit for Analysis of Theory & Experiment. <http://www.reptate.com/>, Version 1.0 (April 14, **2009**)
 164. Hofmann, M. Field-Cycling NMR as a Tool of Molecular Rheology, PhD thesis, University of Bayreuth, **2016**.
 165. Flämig, M. PhD thesis, University of Bayreuth,
 166. Baumgaertel, M.; Schausberger, A.; Winter, H.H. The Relaxation of Polymers with Flexible Chain of Uniform Length. *Rheo Acta* **1990**, *29*, 400-408 Doi: 10.1007/BF01376790.
 167. Wang, M.; Joseph, R.; Bonfield, W. Hydroxyapatite-polyethylene composites for bone substitution: effects of ceramic particle size and morphology. *Biomater.* **1998**, *19*, 2357-2366 [https://doi.org/10.1016/S0142-9612\(98\)00154-9](https://doi.org/10.1016/S0142-9612(98)00154-9).
 168. Misra, S. K.; Valappil, S. P.; Roy, I.; Boccaccini, A. R. Polyhydroxyalkanoate (PHA)/Inorganic Phase Composites for Tissue Engineering Applications. *Biomacromolecules*, **2006**, *7*, 2249-2258. Doi: 10.1021/bm060317c.

169. Elimelech, M. I.; Phillip, W. A. The future of seawater desalination: energy, technology, and the environment. *Scien.* **2011**, 333, 712-7. Doi: 10.1126/science.1200488.
170. Wang, X.; Chen, X.; Yoon, K.; Fang, D.; Hsiao, B. S.; Chu, B. High Flux Filtration Medium Based on Nanofibrous Substrate with Hydrophilic Nanocomposite Coating *Environ. Sci. Technol.* **2005**, 39, 7684–7691 Doi: 10.1021/es050512j.
171. Skaff, H.; Sill, K.; Emrick, T. Quantum Dots Tailored with Poly(para-phenylene vinylene) *J. Am. Chem. Soc.*, **2004**, 126, 11322–11325. Doi: 10.1021/ja047260r.
172. Greenham, N. C.; Peng, X.; Alivisatos, A. P. Charge separation and transport in conjugated-polymer/semiconductor-nanocrystal composites studied by photoluminescence quenching and photoconductivity. *Phys. Rev. B.* **1996**, 54, 17628 <https://doi.org/10.1103/PhysRevB.54.17628>.
173. Nusser, K.; Schneider, G. J.; Richter, D. Microscopic origin of the terminal relaxation time in polymer nanocomposites: an experimental precedent. *Soft Matter* **2011**, 7, 7988-7991 Doi: 10.1039/C1SM05555K.
174. Nusser, K.; Schneider, G. J.; Richter, D. Rheology and Anomalous Flow Properties of Poly(ethylene-alt-propylene)–Silica Nanocomposites. *Macromolecules* **2013**, 46, 6263-6272. Doi: 10.1021/ma3025927.
175. Zhang; Q., Archer; L.A. *J Poly(ethylene oxide)/Silica Nanocomposites: Structure and Rheology. Langmuir.* **2002**, 18, 10435-10442. Doi: 10.1021/la026338j.
176. Anderson, B. J; Zukoski, C. F; Rheology and Microstructure of Polymer Nanocomposite Melts: Variation of Polymer Segment-Surface Interaction. *Langmuir.* **2010**, 26, 8709-8720. Doi: 10.1021/la9044573.
177. Akcora, P.; Kumar, S. K.; Moll, J.; Lewis, S.; Schadler, L.S.; Li, Y.; Benicewicz, B.C.; Sandy, A.; Narayanan, S.; Iavvasky, J.; Thiyagarajan, P.; Colby, R.H.; Douglas, J.F. “Gel-like” Mechanical Reinforcement in Polymer Nanocomposite Melts. *Macromolecules*, **2010**, 43, 1003-1010. Doi: 10.1021/ma902072d.
178. Nusser, K.; Schneider, G. J.; Pyckhout-Hintzen, W.; Richter, D., Viscosity Decrease and Reinforcement in Polymer–Silsesquioxane Composites. *Macromolecules* **2011**, 44, 7820-7830. Doi: 10.1021/ma201585v.
179. Mackay, M. E.; Dao, T.T.; Tuteja, A.; Ho, D. L.; Von Horn, B; Kim, Ho-Cheol.; Hawker, C. J. Nanoscale effects leading to non-Einstein-like decrease in viscosity *Nature Materials* **2003**, 2, 762. Doi: 10.1038/nmat999.

180. Tuteja, A.; Mackay, M. E.; Hawker, C. J.; Von Horn, B. Effect of Ideal, Organic Nanoparticles on the Flow Properties of Linear Polymers: Non-Einstein-like Behavior *Macromolecules* **2005**, *38*, 8000-8011. Doi: 10.1021/ma050974h.
181. Li, Y.; Kröger, M.; Liu, W. K. Nanoparticle Effect on the Dynamics of Polymer Chains and Their Entanglement Network. *Phys. Rev. Lett.*, **2012**, *109*, 118001. Doi: 10.1103/PhysRevLett.109.118001.
182. Karatrantos, A.; Clarke, N.; Composto, R. J.; Winey, K.I. Entanglements in polymer nanocomposites containing spherical nanoparticles *Soft Matter* **2016**, *12*, 2567-2574. Doi: 10.1039/C5SM02010G.
183. Ozmusul, M. S.; Picu, C. R.; Sternstein, S. S.; Kumar, S. K. Lattice Monte Carlo Simulations of Chain Conformations in Polymer Nanocomposites. *Macromolecules* **2005**, *38*, 4495-4500. Doi: 10.1021/ma0474731.
184. Sharaf, M. A.; Kloczkowski, A.; Sen, T. Z.; Jacob, K. I.; Mark, J. E. Filler-induced deformations of amorphous polyethylene chains. The effects of the deformations on elastomeric properties, and some comparisons with experiments. *J. Eur. Polym.* **2006**, *42*, 796–806 <https://doi.org/10.1016/j.eurpolymj.2005.10.009>.
185. Vacatello, M. Phantom Chain Simulations of Polymer-Nanofiller Systems. *Macromolecules* **2003**, *36*, 3411-3416. Doi: 10.1021/ma0217736.
186. Vacatello, M. Chain Dimensions in Filled Polymers: An Intriguing Problem. *Macromolecules* **2002**, *35*, 8191–8193. Doi 10.1021/ma020416s.
187. Zhang; Q., Archer; L.A. Monte Carlo simulation of structure and nanoscale interactions in polymer nanocomposites. *J. Chem. Phys.* **2004**, *121*, 10814-10824. <http://aip.scitation.org/toc/jcp/121/21>.
188. Smith, G. D.; Bedrov, D.; Li, L.; Bytner O. molecular dynamics simulation study of the viscoelastic properties of polymer nanocomposites *J. Chem. Phys.* **2002**, *117*, 9478-9489. <http://dx.doi.org/10.1063/1.1516589>.
189. Picu, R. C.; Ozmusul, M. S. Structure of linear polymeric chains confined between impenetrable spherical walls. *J. Chem. Phys.* **2003**, *118*, 11239–11248 <http://dx.doi.org/10.1063/1.1576216>.
190. Starr, F.W.; Douglas, J.F.; Meng, D.; Kumar, S.K. Bound Layers “Cloak” Nanoparticles in Strongly Interacting Polymer Nanocomposites *ACS Nano*, **2016**, *10*, 10960–10965. Doi: 10.1021/acsnano.6b05683.

191. Holt, A.P.; Bocharova, V.; Cheng, S.; Kisliuk, A.M.; White, B.T.; Saito, T.; Uhrig, D.; Mahalik, J. P.; Kumar, R.; Imel, A. E. Etampawala, T.; Martin, H.; Sikes, N.; Sumpter, B. G. Dadmun, M. D.; Sokolov, A. P. Controlling Interfacial Dynamics: Covalent Bonding versus Physical Adsorption in Polymer Nanocomposites. *ACS Nano* **2016**, *10*, 6843–6852. Doi: 10.1021/acsnano.6b02501.
192. Cheng, S.; Holt, A.P.; Wang, H.; Fan, F.; Bocharova, V.; Martin, H.; Etanmpawala, T.; White, T.B.; Saito, T.; Kang, N.; Dadmun, D.M.; Mays, WmJ; Sokolov, P. A. Unexpected Molecular Weight Effect in Polymer Nanocomposites. *Phys. Rev.lett.* **2016**, *116*, 038302. <http://dx.doi.org/10.1103>.
193. Kim, Y. S.; Meyer, W.H.; Saalwächter, K. Zukoski, C.F. Polymer Dynamics in PEG-Silica Nanocomposites: Effects of Polymer Molecular Weight, Temperature and Solvent Dilution. *Macromolecules*, **2012**, *45*, 4225-4237. Doi: 10.1021/ma300439k.
194. Krishnamoorti, R. Strategies for dispersing nanoparticles in polymers. *MRS Bull.***2007** *32*, 341-347.
195. De Gennes, P. G. Scaling Theory of Polymer Adsorption. *J. Phys. (Paris)* **1976**, *37*, 1445–1452. <https://doi.org/10.1051/jphys:0197600370120144500>.
196. De Gennes, P. G. Conformations of Polymers Attached to an Interface *Macromolecules* **1980**, *13*,1069-1075 Doi: 10.1021/ma60077a009.
197. Dukes, D.; Li, Y.; Lewis, S.; Benicewicz, B.; Schadler, L.; Kumar, S. K. Conformational Transitions of Spherical Polymer Brushes: Synthesis, Characterization, and Theory. *Macromolecules*, **2010**, *43*, 1564–1570. Doi: 10.1021/ma901228t.
198. Maas, J. H.; Flier, G. J.; Leemakers, F.A.M.; Cohen Stuart, M. A.; Wetting of a Polymer Brush by a Chemically Identical Polymer Melt: Phase Diagram and Film Stability. *Langmuir*, **2002**, *18*, 8871-8880. Doi: 10.1021/la020430y.
199. Glomann, T.; Hamm, A.; Allgaier, J.; Hübner, E.G.; Radulescu, A.; Farago, B.; Schneider, G. J. A microscopic view on the large scale chain dynamics in nanocomposites with attractive interactions. *Soft. Matt.* **2013**, *9*,10559-0571. Doi: 10.1039/C3SM51194D.
200. Glomann, T.; Schneider, G. J.; Allgaier, J.; Radulescu, A.; Lohstroh, W.; Farago, B.; Richter, D. Microscopic Dynamics of Polyethylene Glycol Chains Interacting with Silica Nanoparticles. *Phys. Rev. Lett.*, **2013**, *110*, 178001. Doi: 10.1103/PhysRevLett.110.178001.

201. Picu, R. C.; Rakshit, A. Dynamics of free chains in polymer nanocomposites. *J. Chem. Phys.*, **2007**, 126, 144909. <http://dx.doi.org/10.1063/1.2719196>.
202. Ehlert, S.; Taheri, S. M.; Pirner, D.; Drechsler, M.; Schmidt, H.-W.; Foerster, S. Polymer Ligand Exchange to Control Stabilization and Compatibilization of Nanocrystals. *ACS Nano* **2014**, 8, 6114-6122. Doi: 10.1021/nn5014512.
203. Pirner, D. Controlled preparation of nanoparticles and polymer core-shell structure for use in organogels and nanocomposite. PhD thesis, University of Bayreuth, **2016**.
204. Mijovic, J.; Lee, H. K.; Kenny, J.; Mays, J., Dynamics in polymer-silicate nanocomposites as studied by dielectric relaxation spectroscopy and dynamic mechanical spectroscopy. *Macromolecules* **2006**, 39 (6), Doi: 2172-2182. 10.1021/ma051995e.
205. Holt, A. P.; Sangoro, J. R.; Wang, Y.; Agapov, A. L.; Sokolov, A. P., Chain and Segmental Dynamics of Poly(2-vinylpyridine) Nanocomposites. *Macromolecules* **2013**, 46 (10), 4168-4173. Doi: 10.1021/ma400418b.
206. Kim, S. A.; Mangal, R.; Archer, L. A. Relaxation Dynamics of Nanoparticle-Tethered Polymer Chains. *Macromolecules*, **2015**, 48, 6280–6293. Doi: 10.1021/acs.macromol.5b00791.
207. Agarwal, P.; Kim, S. A.; Archer, L. A. Crowded, Confined, and Frustrated: Dynamics of Molecules Tethered to Nanoparticles. *Phys. Rev. Lett.*, **2012**, 109, 258301. Doi: 10.1103/PhysRevLett.109.258301.
208. Watanabe, H. Dielectric Relaxation of Type-A Polymers in Melts and Solutions. *Macromol. Rapid. Commun.* **2001**, 22, 127-175. Doi: 10.1002/1521-3927(200102)22:3<127::AID-MARC127>3.0.CO;2-S.
209. Boese, D.; Kremer, F.; Fetters, J. L.; Molecular Dynamics in Linear and Multiarmed Star Polymers of cis-Polyisoprene as Studied by Dielectric Spectroscopy *Macromolecules* **1990**, 23, 1826-1830. Doi: 10.1021/ma00208a045.
210. Chambon, F.; Winter, H.H. Linear Viscoelasticity at the Gel point of a crosslinking PDMS with Imbalanced Stoichiometry. *J. Rheol.* **1987**, 31, 683-697. <https://doi.org/10.1122/1.549955>
211. Anderson, B. J.; Zukoski, C. F. Rheology and Microstructure of Entangled Polymer Nanocomposite Melts. *Macromolecules*, **2009**, 42, 8370–8384 Doi: 10.1021/ma9011158.

212. Anderson, B. J.; Zukoski, C. F. Colloidal glass transition in unentangled polymer nanocomposites melts. *J. Phys.: Condens. Matter.* **2009**, *21*, 285102 tstacks.iop.org/JPhysCM/21/285102.
213. Vlassopoulos, D.; Pakula, T.; Fytas, G.; Roovers J.; Karatasos, K.; Hadjichristidis; N. Ordering and viscoelastic relaxation in multiarm star polymer melts. *Europhys. Lett.* **1997**, *39*, 617-622. <https://doi.org/10.1209/epl/i1997-00403-3>.
214. Jean M. J.; Fréchet, D. A. T., Dendrimers and Other Dendritic Polymers. *John Wiley & Sons, Ltd*: **2002**.
215. Hawker, C.J.; Fréchet MJ. Preparation of polymers with controlled molecular architecture. A new convergent approach to dendritic molecules. *J Am Chem Soc* **1990**; *112*, 7638–47. Doi: 10.1021/ja00177a027.
216. Boas, U.; Heegaard, P. M. H. Dendrimers in drug research *Chem. Soc. Rev.* **2004**, *33*, 43-63. Doi: 10.1039/b309043b.
217. Tekade, R. K.; Kumar, P. V.; Jain, N. K. Dendrimers in oncology: an expanding horizon. *Chem. Rev.* **2008**, *109*, 49-87. Doi: 10.1021/cr068212n.
218. Reek, J. N. H.; Arevalo, S.; Heerbeek, R. van.; Kamer, P. C. J.; Leeuwen, P. Van. Dendrimers in Catalysis *Adv. Catal.* **2006**, *49*, 71-151. [https://doi.org/10.1016/S0360-0564\(05\)49002-1](https://doi.org/10.1016/S0360-0564(05)49002-1).
219. Khopade, A.J.; Caruso, F.; Tripathi, P.; Nagaich, S.; Jain, N. K. Effect of dendrimer on entrapment and release of bioactive from liposomes. *Int. J. Pharm.* **2002**, *232*, 157-62. [https://doi.org/10.1016/S0378-5173\(01\)00901-2](https://doi.org/10.1016/S0378-5173(01)00901-2).
220. Zacharopoulos, N.; Economou, L. G. Morphology and Organization of Poly(propylene imine) Dendrimers in the Melt from Molecular Dynamics Simulation *Macromolecules* **2002**, *35*, 1814-1821. Doi: 10.1021/ma010953x.
221. Uppuluri, S.; Morrison, F. A.; Dvornic, P. R. Rheology of Dendrimers. 2. Bulk Polyamidoamine Dendrimers under Steady Shear, Creep, and Dynamic Oscillatory Shear. *Macromolecules* **2000**, *33*, 2551. Doi: 10.1021/ma990634u.
222. Tande, B. M.; Wagner, N. J.; Kim, Y. H. Influence of End Groups on Dendrimer Rheology and Conformation. *Macromolecules* **2003**, *36*, 4619. Doi: 10.1021/ma020801h.
223. Mijovic, J.; Ristic, S.; Kenny, J. Dynamics of Six Generations of PAMAM Dendrimers as Studied by Dielectric Relaxation Spectroscopy. *Macromolecules* **2007**, *40*, 5212. Doi: 10.1021/ma070624q

224. Markelov, D. A.; Dolgushev, M.; Gotlib, Y. Y.; Blumen, A. NMR relaxation of the orientation of single segments in semiflexible dendrimers *J. Chem. Phys.* **2014**, *140*, 244904. Doi: <http://dx.doi.org/10.1063/1.4884024>
225. Markelov, D. A.; Falkovich, S.G.; Neelov, I.M.; Illyash, M.Y.; Matveev, V.V.; Lahderanta, E.; Ingman, P.; Darinskii, A. Molecular dynamics simulation of spin-lattice NMR relaxation in poly-l-lysine dendrimers: manifestation of the semiflexibility effect *A. Phys. Chem, Chem. Phys.* **2015**, *17*, 3214-3226. Doi: 10.1039/C4CP04825.
226. Mohamed, F.; Hofmann, M.; Pötzschner, B.; Fatkullin, N.; Rössler, E.A. Dynamics of PPI Dendrimers: A Study by Dielectric and ²H NMR Spectroscopy and by Field-Cycling ¹H NMR Relaxometry. *Macromolecules*, **2015**, *48*, 3294–3302 Doi: 10.1021/acs.macromol.5b00486.
227. Garcia-Bernabe, A.; Diaz-Calleja, R.; Haag, R. Broadband Dielectric Spectroscopy Studies of Hyperbranched Polyglycerols. *Macrom. Chem. Phys.* **2006**, *207*, 970-977. Doi: 10.1002/macp.200600025.
228. Turkey, G.; Sangoro, J. R.; Rehim, M. A.; Kremer, F. Secondary relaxations and electrical conductivity in hyperbranched polyester amides. *J. Polym. Sci. Part B- Polymer Physics* **2010**, *48*, 1651-1657. Doi: 10.1002/polb.21966.
229. Sangoro, J. R.; Turkey, G.; Rehim, M. A.; Iacob, C.; Naumov, S.; Ghoneim, A.; Kaerger, J.; Kremer, F. Charge Transport and Dipolar Relaxations in Hyperbranched Polyamide Amines. *Macromolecules* **2009**, *42*, 1648-1651. Doi: 10.1021/ma8024010.1063/1.4865945.

Appendix

Parts a and b of Figure A1 show the DS spectra of the PI-58k@PbS and PI-16k@PbS (open circles) as well as the dc conductivity contribution (solid lines) and the spectra after subtracting the conductivity (filled circles), respectively.

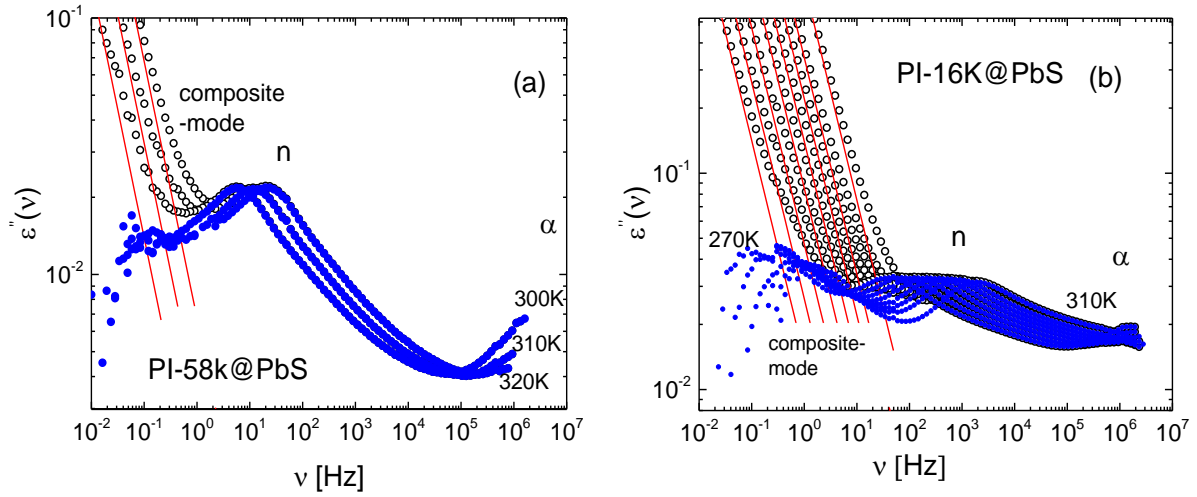


Figure A1: The dielectric spectra of the coated particles (a) PI-58@pbS and (b) PI-16k@PbS. Open circles: data as measured, solid lines: dc conductivity contribution, and filled circles: DS spectra after subtracting the dc contribution.

Figure A2 shows the $G'(\omega\tau_{a(DS)})$ (filled symbols) and $G''(\omega\tau_a)$ (open symbols) master curves for PI-5k@PbS/PI-5k.

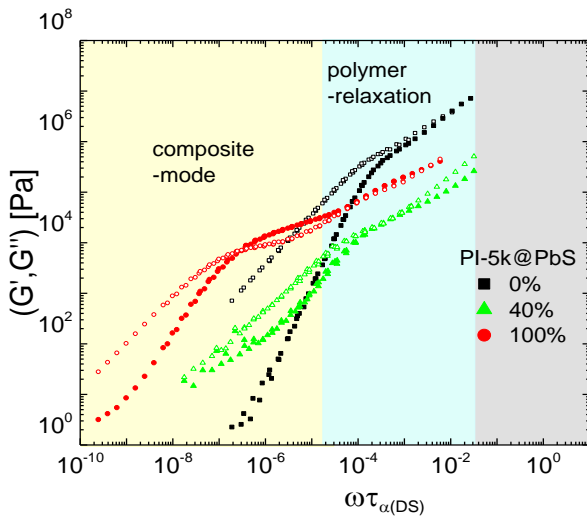


Figure A2: Master curves of (a) $G'(\omega\tau_{a(DS)})$ (filled symbols) and $G''(\omega\tau_a)$ (open symbols) for neat PI-5k@PbS particles, a mixture PI-5k@PbS/PI-5k with $w = 50\%$ and pure PI-5k.

List of Publications

- 1** Dynamics of PPI Dendrimers: A Study by Dielectric and ^2H NMR Spectroscopy and by Field-Cycling ^1H NMR Relaxometry
Mohamed, F.; Hofmann, M.; Pötzschner, B.; Fatkullin, N.; Rössler, E. A. *Macromolecules*, **2015**, 48, 3294–3302
- 2** Dynamics of asymmetric non-polymeric binary glass formers-A nuclear magnetic resonance and dielectric spectroscopy study
Pötzschner, B.; Mohamed, F.; Lichtinger, A.; Bock, D.; Rössler, E. A. *J. Chem. Phys.*, **2015**, 143, 15450
- 3** Non-polymeric asymmetric binary Glass-Formers. Part I: Main Relaxations studied by Dielectric, ^2H and ^{31}P NMR Spectroscopy
Pötzschner, B.; Mohamed, F.; Bächer, C.; Wagner, E.; Lichtinger, A.; Minikejew, R.; Kreger, K.; Schmidt, H.-W.; Rössler, E. A. *J. Chem. Phys.*, **2017**, 146, 164503.
- 4** Non-polymeric asymmetric binary Glass-Formers. Part II: Secondary Relaxation studied by Dielectric, ^2H and ^{31}P NMR Spectroscopy
Pötzschner, B.; Mohamed, F.; Bächer, C.; Wagner, E.; Lichtinger, A.; Bock, D.; Kreger, K.; Schmidt, H.-W.; Rössler, E. A. *J. Chem. Phys.*, **2017**, 46, 164504
- 5** The Nature of Secondary Relaxations: The Case of Poly(ethylene-alt-propylene) Studied by Dielectric and Deuteron NMR Spectroscopy
Koerber, T; Mohamed, F.; Hofmann, M, Lichtinger, A; Willner, L; Rössler, E. A. *Macromolecules*, **2017**, 50, 1554-1568
- 6** Scaling analysis of the viscoelastic response of linear polymers
Mohamed, F.; Flämig, M.; Hofmann, M.; Heymann, L.; Willner, L.; Fatkullin, N.; Aksel, N. E.A. Rössler *J. Chem. Phys.*, **20118** (submitted).

Acknowledgments

Here, I want to express deep gratitude to everyone who supported me in the course of my studies and my PhD work.

I would first like to thank my supervisor Prof. Ernst Rößler who offered me a position in his group. His constructive suggestions, kindness, inspirations and, his patience during the thesis preparation are fully appreciated. I can say that I have learned a great deal during the time in his group and that I have had a lot of joy.

I sincerely thank Prof. Stephan Förster and Dr. Daniela Pirner for providing us the PNCs samples. I am also indebted to Prof. Nuri Aksel for enabling me the rheological measurements in his department, and Dr. Lutz Heymann for introducing me to the rheometer and having valuable discussion.

I would like to thank my colleagues for their wonderful collaboration. You supported me greatly and were always willing to help me. I would particularly like to single out: Dr. Robert Kahlau who helped me getting started with dielectric technique, Thomas Koerber, Max Flämig and Björn Pötzschner for helping with the correction of this thesis.

Finally, I want to thank my family and, in particular, my husband Talaat who supported me a lot.

Thank you very much, everyone!